

Appendix 8.2: Seabed Survey Report



**The Recent History of the Black Sea including
Interpretation of Newly Acquired Seabed Survey Data
for the South Stream Offshore Pipeline Project**

Report to South Stream Transport B.V

DRAFT2

Report No 2013/08

August, 2013

Prepared by:
P.P.E. Weaver, D.G. Masson
Seascope Consultants Ltd.
Belbins Valley
Belbins
Romsey SO51 0PE, UK



+44 (0)1794 368245
+44 (0)7736 661009
phil.weaver@seascopeconsultants.co.uk

EXECUTIVE SUMMARY

An account is provided of the present-day oceanography and physical environment of the Black Sea, together with an account of its recent history. This has been compiled from published literature and reports supplied by South Stream Transport. This information is used as a background to set in context new information derived from an investigation of the geophysical data collected along the Black Sea pipeline route for the South Stream project.

The new data has been analysed to identify seabed features including biological features. Data sets included swath bathymetry, sidescan sonar, video and still photography. A small amount of sub-bottom profile data was also examined. Features of interest have been mapped in GIS format and are described in this report. The main conclusions are:

1. The Russian slope is a challenging environment with rocks and boulders on steep slopes. Geohazard analysis was not part of this report.
2. The Bulgarian slope has been affected by multiple landslide events.
3. On both the upper part of the Russian slope and the Bulgarian slope carbonate mounds occur between water depths of 110 and 140 m.
4. Fluid seeps are present on the outer Bulgarian shelf edge with associated bacterial activity. Mussels are present in this area (probably *Modiolus phaseolinus* or *Mytilus galloprovincialis*) but these are unlikely to be chemosynthetic mussels.
5. Most of the survey area is located on the abyssal plain. No features were identified on the abyssal plain that are likely to have an impact on the proposed pipeline route. Nearly all of the area is covered by a soft, sometimes jelly-like, layer of organic detritus. Some pockmarks were identified as well as other features that are likely to be due to fluid escape at the seabed.
6. Organic life is limited to bacteria in waters deeper than 150-200 m. No significant bacterial communities, such as cold seep communities with associated macrofauna, were encountered along the pipeline route.
7. The outer part of the Danube Fan lies within the surveyed area and some fan channels are evident. These appear to be inactive at the present time.
8. A large number of objects are found on the seafloor of the abyssal plain and most of these have been revealed as trees by video survey. Shipwrecks and man-made rubbish have also been identified.
9. Extensive fine-scale lineations and irregular patterns seen on sidescan sonar data appear to reflect buried features related to past periods of bottom current activity. Many of these are aligned in a fan shape with the apex focussed on the Bosphorus. They may have been formed when there was a rapid inflow to the Black Sea from the Mediterranean.
10. The western part of the abyssal plain has a large area of sand waves built by turbidity currents. These appear to post-date both the linear features and the major slide scar.
11. A N-S striking fault zone, crossing the proposed pipeline route, was identified in the Bulgarian Abyssal Plain.

CONTENTS

EXECUTIVE SUMMARY	1
CONTENTS	2
1. INTRODUCTION AND BACKGROUND	3
2. GEOMORPHOLOGY OF THE BLACK SEA	3
3. HISTORY OF THE BLACK SEA SINCE THE LAST GLACIATION	4
4. SEDIMENTARY PROCESSES IN THE BLACK SEA	5
5. PRESENT DAY OCEANOGRAPHY	6
6. BIOGEOCHEMISTRY	7
7. BIOLOGY	8
SOFT SEDIMENT	9
GAS SEEPS	10
MUD VOLCANOES.....	10
8. OVERVIEW OF MAIN FEATURES ALONG THE PIPELINE ROUTE	11
DATA	11
RUSSIAN MARGIN	11
<i>Background</i>	11
<i>Upper Russian slope</i>	12
<i>Lower Russian slope</i>	13
<i>Russian Abyssal Plain</i>	14
TURKISH ABYSSAL PLAIN.....	14
<i>Bulgarian Abyssal Plain</i>	15
<i>Bulgarian continental margin</i>	16
9. DISCUSSION OF SPECIFIC FEATURES	17
<i>a) Features related to probable and possible fluid escape</i>	17
<i>b) Lineations and irregular fine scale patterns</i>	19
<i>c) Point targets on sidescan sonar data</i>	20
<i>d) Flocculated organic matter</i>	20
<i>e) Bottom currents</i>	21
<i>f) Cables</i>	21
10. LIST OF FIGURES	22
11. REFERENCES	25
12. FIGURES	30

1. INTRODUCTION AND BACKGROUND

South Stream Transport B.V (hereafter South Stream Transport) proposes to construct an offshore pipeline (consisting of four adjacent pipelines) that will extend approximately 930 km across the Black Sea from the Russian coast near Anapa, through the Russian, Turkish, and Bulgarian Exclusive Economic Zones (EEZ), to the Bulgarian coast near Varna (Figure 1). The South Stream Offshore Pipeline is the offshore component of the South Stream Pipeline System that will transport natural gas from Russia to countries of Central and South-Eastern Europe.

Seascope Consultants was contracted by URS Ltd, on behalf of South Stream Transport, to examine the seabed geophysical survey data and interpret any biological features of significance. A large amount of data was provided including bathymetry, sidescan sonar, sub-bottom profiles, videos and photographs. The aim of the study was to examine each of the datasets (primarily bathymetry, sidescan and video) and to integrate the interpretations to understand the seafloor processes that had caused them. The seabed features vary from ones that are well known to enigmatic features, such as linear and irregular fine-scale markings, that have no published explanations. This report offers some possible explanations for these features.

Seascope Consultants were further asked to provide an account of relevant background information on the Black Sea, taking into account a number of previous reports that had been produced for the South Stream Offshore Pipeline. This report includes the full description of the features identified along the pipeline route and sets this information in the wider context.

2. GEOMORPHOLOGY OF THE BLACK SEA

The Black Sea covers an area of 432,000 km² and is the largest anoxic basin in the world. The central area is represented by a flat abyssal plain with a water depth of about 2000 m, and a maximum depth 2.212 m (Figure 2). The published literature describes the area of the abyssal plain to represent 12.2% of the total area of the Black Sea (e.g. Panin, 2008), but this appears to be a considerable underestimate. The Black Sea has an extremely large drainage basin of more than two million km², collecting the water from almost all the European countries, except the westernmost ones. The Black Sea has a volume of about 534,000 km³ (Panin, 2008). The Black Sea is divided into two sub-basins by a deep structural ridge extending south from the Crimean Peninsula although there is little surface expression of this (Figure 2). The northwestern part of the basin receives input from some of the largest European rivers including the Danube, Dniepr, Dniestr and the Southern Bug. This area features the Danube and Dniepr/Dniestr deep-sea fans which extend from the shelf break zone, at approximately 200 m isobath, for about 150 km downslope reaching a depth of about 2200 m within the abyssal plain (Figure 3). The surface of the Danube Fan is covered by a network of meandering channels with stacked channel levee systems intercalated with mass transport deposits in the subsurface (Lericolais et al., 2013). To the south the Anatolian rivers deliver more than 33% of the total sediment input to the Black Sea but account for only 8% of the river discharge (Panin, 2008). The southern margin of the Black Sea around Turkey, and the western edge around Georgia and Russia, are typified by narrow shelves that rarely exceed 20 km in width and steep aprons with numerous submarine canyons. The Bosphorus

Strait connects the Black Sea to the Marmara Sea and the strait of the Dardanelles connects the Sea of Marmara to the Mediterranean.

3. HISTORY OF THE BLACK SEA SINCE THE LAST GLACIATION

The water level in the Black Sea has oscillated with time both due to global sea level fluctuations and due to changes in river input related to dry-wet cycles in Eurasia. During sealevel lowstands the Black Sea was an isolated basin, separated from the Mediterranean, in which the absence of seawater input combined with freshwater input from rivers turned the Black Sea into a fresh to brackish lake (Soulet, et al., 2010). During intervals when the Black Sea is connected to the Mediterranean a strong pycnocline develops with salty water forming the lower layer and a fresher water layer above. This stratification prevents deep circulation and consequently the deep waters of the Black Sea become anoxic during high sea levels when it is connected to the Mediterranean.

There has been considerable scientific debate about the timing and process of the transition from the Black Sea lake at the end of the last ice age to its present mode. The debate was fired by the hypothesis that the level of the Black Sea was 100 m below the level of the Mediterranean at the end of the last ice age and the Bosphorus strait was catastrophically breached at 7,200 years BP, allowing salt water from the Mediterranean to rapidly fill the basin (Ryan et al., 1997). The timing of the Black Sea/Mediterranean reconnection is now relatively well constrained with a revised age of 9,000 years BP (Soulet et al., 2011). The magnitude of the difference in sealevel height before the reconnection has been disputed (e.g. Giosan et al., 2009), who suggested a 30 m difference. Lericolais et al., (2009) provided evidence of varying sealevel heights over the last 30,000 years caused by periods of low river input during cold periods and major river inflow during periods of ice melt (Figure 4). The rapidity of the inflow from the Mediterranean to refill the Black Sea has also been disputed, with suggestions that this was catastrophic (Ryan et al., 2003) or gradual (Hiscott et al., 2007). The most recent estimates from Bahr et al., (2008) suggest the refilling took about 100 years – rapid but not catastrophic.

The transition from freshwater to marine conditions caused a complete replacement of the fauna in the Black Sea and this took about 900 years beginning with the deepest water. The transition was complete by ~7,700 years BP at mid water depths and by about 7,200 years BP on the shelves (Soulet et al., 2011) (Figure 5). The loss of lacustrine species was associated with the development of stratification and onset of anoxia. This led to the deposition of a sapropel layer across most of the basin, at least in waters deeper than approximately 200 m (Jones and Gagnon, 1994; Soulet et al., 2011). A sapropel is a sediment layer with a very high level of organic material, which in the Black Sea can exceed 20% (Bahr et al., 2008). It is produced when high levels of surface water productivity deposit into oxygen depleted bottom waters where the organic matter cannot be consumed. The sapropel is recorded in cores from the western basin (Lericolais et al, 2013) to the Russian slope in the eastern basin (Woodside et al., 1997). Sapropelic deposits continued to be deposited until ~2700 years BP (Jones and Gagnon, 1994), following which coccolith-bearing, organic-rich and varve-laminated sediments have been deposited. This latter unit has two to six % organic matter with a higher proportion of calcareous material than the sapropel (Calvert and Karlin, 1998). The calcareous material is derived from marine coccolithophore

Emiliania huxleyi, which have formed part of the Black Sea plankton since 2700 years BP. Blooms of *E. huxleyi* still occur in the Black Sea during late spring and summer each year.

In summary the most recent pelagic sediment layers in the Black Sea can be divided into:

- Unit I, the top approximately 30 cm, is a micro-laminated sediment, rich in plankton-derived carbonates, with relatively low levels of organic carbon. This unit was deposited in oxygen depleted bottom waters.
- Unit II sediment (ca. 30 to 70 cm below the surface) is a micro-laminated sapropel deposited under anoxic marine conditions between approximately 2,700 and 7 to 7,700 years ago. The onset of Unit II is characterized by the occurrence of thinly laminated layers rich in aragonite crystals (e.g. Ross and Degens, 1974; Soulet et al., 2011) and by a sharp increase in Total Organic Carbon (Bahr et al., 2008) (Fig. 5).
- Transitional unit, marking the transition from lacustrine to marine conditions. This unit varies across the basin and includes salinity tolerant molluscs on the shelf (hash layer) whilst appearing as an authigenic carbonate layer in deeper water (“seekreide” of Ryan et al., 2003).
- Unit III sediment, below approximately 70 cm, is older than 7,000 years and was deposited when the Black Sea was an oxic freshwater lake, and are characterised by mix of organic-poor clays and silts (Izdar & Ergün, 1991; Hay *et al.*, 1991). Unit III sediments have organic contents <1%.

Above Unit I sediments lies a discrete proto-white lamina layer (about two cm thick), and above this lies a discrete benthic flocculant layer, or the “fluff layer”, also about two cm thick (Figure 6; Pilskaln & Pike, 2001). The fluff layer has been observed to be largely composed of lithogenic material derived from the surrounding rivers (47%), carbonates derived from coccolithophirid blooms (31%) with the remains of diatom and silicoflagellate blooms (7%) and particulate organic carbon, e.g. faecal pellets (6%) (Pilskaln & Pike, 2001). The proto-white laminae layer is composed of coccolithophorid blooms (46%), lithogenic material (33%), the remains of diatom and silicoflagellate blooms (4%) and particulate organic carbon (7%).

4. SEDIMENTARY PROCESSES IN THE BLACK SEA

The main sedimentary processes are associated with the deep-sea fans located off the major rivers, with downslope sediment transport by turbidity currents through canyon systems, with landslides on the continental margins and with the development of mud volcanoes.

In the northwest, the large Danube and Dniepr/Dniestr fans have actively transported sediments from the shelf to the deep sea via submarine channels and levee complexes (Popescu et al., 2001; Lericolais et al, 2009, 2013) (Figure 3).

These systems were very active during the last glacial period when the rivers extended to the shelf edge. The sediment supply via the Danube and Dniepr/Dniestr fan systems increased significantly during the melting of European ice sheets at the end of the last glaciation, but came to an end when sealevel rose following the reconnection with the Mediterranean at 9,000 years BP (Lericolais, et al., 2013). The deep-sea fan systems have remained inactive since that time.

In the south, on the eastern Turkish margin, there is significant transport of sediment along the shelf in an eastwards direction (Duman et al., 2006), but this sediment is intercepted by the canyons and transferred from the continent to the deep sea either by turbidity currents or landslides (Lericolais et al., 2013). This process has continued intermittently from the glacial period to the present day with the landslide events probably triggered by earthquakes on the North Anatolian fault.

There is very little other published literature on turbidity current activity in the Black Sea, but the presence of numerous canyons around the margin suggests it is a common process. Whether these canyons are actively transporting sediment during the current sea level highstand is not clear. In many other areas canyons are more active during sea level lowstands (glacial periods) (Weaver et al., 2000).

Other notable sedimentary features in the Black Sea are mud volcanoes. Two main types of mud volcano are found in the Black Sea (Kruglyakova et al., 2004): (1) those along the periphery of the basin (Bulgaria, Kerch-Taman region), and (2) those associated with fluidized sediment flow connected to ruptures on domes of gently sloping symmetrical anticlines in the central part of the Black Sea (Figure 7). Dimitrov (2002) describes a group of mud volcanoes in the west Black Sea Basin, south of the Crimean Peninsula. These mud volcanoes occur at about 2000 m water depth and have a mushroom or cone-like shape with diameters of one to three km and rising 20 to 150 m above the seafloor. They are formed by the expulsion of mud, rock fragments and fluids (high in methane) from depth, with the oldest rock fragments coming from the Maikopian Formation (Lower Miocene in geologic age). Dimitrov (2002) suggests that mud volcanoes are present in this area due to the presence of an ophiolite structure, identified on the basis of a magnetic anomaly. This domes up the Maikopian clays bringing them closer to the seafloor, forcing their overpressure and creating tensional faults above and around them. Several of the known mud volcanoes in this area appear to be inactive today, although others such as the Dvurechenskii mud volcano (Lichtschlag et al., 2010) and the Tredmar mud volcano (Ivanov, 1996) are active. One of the volcanoes (Goncharov Volcano) is within about 15 km off the pipeline route at KP 430. Although it is close to the route, it should have little significance because the erupted materials rarely spread more than two to three km from mud volcanoes and new mud volcanoes are unlikely to appear along the pipeline route because their origin appears to be tied to the area of the domed ocean crust (Dimitrov, 2002).

The occurrence of gas hydrates in the Black sea has been discussed by Vassilev and Dimitrov, (2002), who indicate that they are likely to be very common in water depths below 620 m. Vassilev and Dimitrov, (2002) also report that they have been identified in shallower areas than this (e.g. at 380 m by Ginsburg and Soloviev, 1994). Thus the areas where gas hydrates occur may be much more extensive than shown in Figure 7.

5. PRESENT DAY OCEANOGRAPHY

The Black Sea is the World's largest meromictic basin where the deep-waters and surface waters do not mix. Freshwater is supplied by rivers, particularly those in the northwest - the Danube River with a mean water discharge of about 200 km³/yr and the Ukrainian rivers Dniepr, Southern Bug and Dniestr contributing with about 65 km³/yr (Panin, 2008). These inputs plus those from smaller rivers such as from the north Turkish margin create a surface

low salinity layer across the whole of the Black Sea. The net freshwater input to the Black Sea is about $300 \text{ km}^3 \text{ y}^{-1}$ and derives from the river input plus precipitation.

The low salinity surface water flows out of the Black Sea through the Bosphorus Strait and from there through the Sea of Marmara to the Dardanelles Strait and into the Mediterranean. It is replaced by a deeper water inflow of saline water from the Mediterranean through the Bosphorus Strait. About $600 \text{ km}^3 \text{ y}^{-1}$ of low salinity water flows out of the Bosphorus as a surface outflow (Murray et al., 2007). This outflow is compensated by about $300 \text{ km}^3 \text{ y}^{-1}$ of higher salinity water that flows into the Black Sea through the Bosphorus as a deep inflow (Murray et al., 2007).

The contrast of the low salinity surface layer with the denser and more saline lower layer gives rise to a strong salinity gradient as seen in ARGO float profile data (Figure 8). The steep gradient in salinity (pycnocline) is seen at around 50-150 m with a gradual increase with depth below to about 200 m.

During winter the relatively fresh water of the NW shelf becomes cold and forms the Cold Intermediate Layer (CIL) that lies between the saltier water below the pycnocline and the summer river input at the surface. In colder winters more CIL water is formed. The inflow from the Bosphorus mixes with the CIL water mainly before it reaches the shelf break north of the Bosphorus. The resultant Bosphorus plume is mixed downwards to form the deep water (Oguz, 2009).

Today the surface water circulation in the Black Sea consists of two large cyclonic (counterclockwise) central gyres that define the eastern and western basins (Figure 9). The gyres are bounded by the wind-driven rim current that flows along the edge of the continental shelf and above the continental slope around the whole basin (Oguz, 2009). Data from autonomous profiling floats has shown currents typically have a velocity of 15 cm s^{-1} at 200 m depth along the Rim Current jet around the basin (Korotaev et al., 2006). At depths of 750 m and 1500 m current velocities of 5 cm s^{-1} have been recorded with the deeper current closely following the topography along the southern margin of the Black Sea (Korotaev et al., 2006) (Figure 10). Outside the Rim Current, numerous quasi-permanent coastal eddies are formed as a result of upwelling around the coastal apron and 'wind curl' mechanisms.

6. BIOGEOCHEMISTRY

The strong vertical stratification severely reduces the replenishment of waters deeper than a few tens of metres and thus all oxygen in the deep Black Sea is consumed by respiration of organic matter, leading to anoxic conditions and the build up of sulphide (Murray et al., 2007). The sulphide values increase with depth to a value of $380 \mu\text{M}$ by 2,200 m (Murray et al., 2007). These strong biogeochemical changes in the upper part of the Black Sea give rise to four distinct biogeochemical layers (Figures 11 and 12). The uppermost layer (euphotic zone) extends to the depth of the 1% light level at around 50 m and has high oxygen concentrations ($\sim 300 \mu\text{M}$) with seasonally varying nutrient and organic material concentrations supplied laterally from rivers and coastal zones and vertically from sub-surface levels through vertical mixing. This layer has active biological processes including plankton grazing, nutrient uptake, microbial loop etc. The second layer is the oxycline, which is characterised by steep gradients in chemical properties, where particle remineralisation causes strong reductions in oxygen concentration from ~ 300 to $10 \mu\text{M}$, whereas nitrite concentration increases to around six to

nine μM (Codispoti et al., 1991). This layer is 20-30 m thick and overlies the suboxic zone, which is about 20-40 m thick and within which nitrate concentrations decrease to trace values at the base of the zone due to the consumption of organic matter (Murray et al., 1989). The deepest zone, which begins at about 90-100 m depth, is the anoxic layer in which sulphate is used to decompose organic matter, and hydrogen sulphide is produced as a byproduct. The interface between the suboxic and anoxic zones involves a series of complicated bacterially-mediated redox reactions including nitrification and denitrification, that control the downward transport of nitrate and the upward transport of ammonium and sulphide.

The Black Sea is considered a classic marine anoxic basin (Murray et al., 2007) where an oxygenated surface layer overlies an anoxic deeper layer with elevated H_2S concentrations up to $380 \mu\text{M}$ (Murray et al., 2007). Other naturally occurring anoxic marine systems are rare, but include the Cariaco basin in the Gulf of Mexico and some fjords in Norway (e.g. Framvaren); these are considerably smaller than the Black Sea (Kononov et al., 2005).

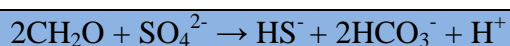
The anoxic state of the deep Black Sea is due to the presence of the permanent pycnocline, a stable density gradient, which restricts the downward flux of oxygen (Kononov et al., 2005; Oguz et al., 2005). The pycnocline ensures that the Black Sea's oxic layer is vertically decoupled from the anoxic layer. However, in some locations the anoxic and oxic layers are linked by lateral processes; for example, the Bosphorus plume (Kononov & Murray, 2001; Kononov et al., 2003). Oguz et al., (2005) describe the deepest part of the Black Sea's waters (below 1,700 m) as being a "vertically homogeneous and horizontally uniform water mass". Murray (1991) suggested that water masses below the halocline (100-150 m) possess near uniform vertical characteristics with temperatures averaging 9°C and salinities averaging 22 ppt.

7. BIOLOGY

The strong stratification and anoxic conditions in much of the Black Sea have profound effects on marine life, with aerobic processes limited to the top 90 to 180 m of the water column, depending on location. Microbial anaerobic processes dominate below the oxygenated layer. This means that macrofauna such as fish and other common marine life are confined to the oxic layer of the Black Sea, whilst the deeper layers are completely dominated by microbial anaerobic processes.

Within the anoxic layer the most common microbially driven chemosynthetic pathways are sulphate reduction and methanogenesis, and the most common chemosynthetic environments are the reduced, marine soft sediments, cold seeps and mud volcanoes. The cold-seep communities of macrofauna that develop in association with mud volcanoes and cold-seeps in oxic oceans are never developed in the Black Sea.

In soft sediment ecosystems below the chemocline (approximately 150 m water depth), oxygen, nitrate and most of the reactive iron and manganese oxides are depleted (Lichtschlag et al., 2010). The primary metabolic pathway is a reaction where sulphate acts as the principal electron acceptor in the mineralisation of organic matter by anaerobic sulphate-reducing bacteria (Eqn. 1). This can lead to sulphide concentrations of up to $380 \mu\text{M}$ (Murray et al., 2007).



Equation 1: Equation showing organic matter mineralisation occurring in the sediment resulting in a hydrosulphide ion, two bicarbonate ions and a hydrogen ion (Lichtsclag *et al.*, 2010).

A second metabolic pathway (Eqn. 2) is also common in the Black Sea sediments, primarily where methane seepage occurs, e.g. the Dvurechenskii mud volcano, and at methane seeps off Crimea (Lichtsclag *et al.*, 2010; Bohrmann *et al.*, 2003; Kruglyakova *et al.*, 2002; Michealis *et al.*, 2002). At these sites, sulphate reduction is coupled to anaerobic oxidation of methane by methane-oxidizing Archea and sulphate-reducing bacteria; this reaction also produces large amounts of sulphide (Hinrichs *et al.*, 1999; Boetius *et al.*, 2000).



Equation 2: Equation showing sulphate reacting with methane, releasing a hydrosulphide ion, a bicarbonate ion and water, that occurs in methane seeps (Hinrichs & Boetius, 2002).

Although both metabolic pathways may function in all anoxic Black Sea sediments, methane availability tends to be higher at gas seeps and mud volcanoes, and therefore the methane pathway (Eqn 2) is more prevalent in this localised environments.

Soft Sediment

The energy sources used by soft sediment microbes in the anoxic zone of the Black Sea are identical to those at gas seeps and mud volcanoes, i.e. both Eqns 1 & 2 can function although Eqn 2 is likely to be more dominant at gas seeps and mud volcanoes due to the higher concentrations of methane in those environments. Biodiversity and microbial community structure, as well as metabolic pathways in deep Black Sea soft sediments, are poorly studied and understood. However, it is thought that deep Black Sea sediment bacterial communities are not as diverse as those in typical deep-sea sediments due to the absence of oxygen and nitrate (Leloup *et al.*, 2007). Organic matter is mineralised by methanogenic archaea and sulphate-reducing bacteria (SRB) in the upper two to four m of sediment¹ (known as the “sulphate zone”); below this layer, in the “methane zone”, only methanogenesis occurs (Jørgensen *et al.* 2004; Leloup *et al.*, 2007). The SRBs *Desulfosarcina*, *Desulfobotulus*, *Desulfobulbus* and *Desulfobacterium* are characteristic operational taxonomic units (OTUs)² of the sulphate zone and the transitional area between the sulphate zone and the methane zone (LeLoup *et al.*, 2007). The numbers of SRB taxonomical units in the *Desulfococcus* group were found to increase with depth (ranging from 90 to 2,200 m) across seven sample sites in the Black Sea sediments (Ince *et al.*, 2006). Methanogenic microbes are dominated by archaea in the ANME-1 group (Michaelis *et al.*, 2002). Archaeal groups similar to *Methanococcales*, *Methanobacteriales* and *Methanogenium* dominate methanogenic microbes in benthic sediments below 2,000 m (Ince *et al.*, 2006).

¹ depth can vary among sites, cf. Schippers *et al.* 2012

² operational taxonomic units – means of categorising unidentified organisms

Gas Seeps

Gas seeps are a form of cold seep, but with visible gas flares. More than 3,000 individual gas seeps (Fig. 7) have been documented in the Black Sea (Egorov *et al.*, 2011). Many more are likely to exist, as much of the Black Sea has not been surveyed in detail (Starostenko *et al.*, 2010). Gas seeps are characterised by the release of gas bubbles/flares (largely methane). Some of the larger seeps have flare heights reaching 500 m from the seafloor, but the majority are non-intensive seeps, with flares between 50 – 130 m high (Starostenko *et al.*, 2010). The majority of gas seeps occur along the shelf break, especially where there are shallow subsurface faults (Kruglakova *et al.*, 2004).

Gas seeps are often associated with an accumulation of carbonates, formed by anaerobic methane oxidation by archaea in syntrophy (symbioses between single celled organisms) with sulphate-reducing bacteria (Egorov *et al.*, 2011). The principle biogeochemical process forming the concretionary carbonates is the sulphate-dependent anaerobic oxidation of methane (Eqn. 2) (Reitner *et al.*, 2005). The oldest carbonate structures have been located on the deepest seafloor (Guilin *et al.*, 2003; Egorov *et al.*, 2011).

At certain sites on the north-west Black Sea shelf, carbonate accumulation has formed tower-like reef structures that can reach several metres in height (Michaelis *et al.*, 2002; Reitner *et al.*, 2005). These towers may release methane bubbles so that they superficially resemble hydrothermal vent chimneys found on tectonic margins (Fig. 13). The chimneys are characterised by the presence of morphologically and phylogenetically distinct unicellular communities (Reitner *et al.*, 2005). Studies have shown that Black Sea cold seep communities are dominated by the ANME-2 group of archaea in consortia with sulphate-reducing bacteria similar to *Desulfosarcina*, *Desulfococcus* (Pimenov *et al.*, 1997; Boetius *et al.*, 2000; Thiell *et al.*, 2001; Michaelis *et al.*, 2002; Tourova *et al.*, 2002; Blumberg *et al.*, 2004; Reitner *et al.*, 2005). Archaea in the ANME-1 group (distantly related to *Methansarcinales*) and Crenarchaeota are also characteristic microbial operational taxonomic units (OTUs) (Michaelis *et al.*, 2002). Carbonate concretions are often surrounded by bacterial mats characterised by greigite-forming (an iron sulphide mineral) sulphate-reducing bacteria which may indicate iron cycling as a process in the anaerobic oxidation of methane (Reitner *et al.*, 2005). The diversity of metabolic pathways in Black Sea cold-seep communities is not fully understood, but is probably more complex than the currently accepted model dominated by archaea in syntrophy with sulphate-reducing bacteria (Kube *et al.*, 2005).

Mud Volcanoes

Mud volcanoes are geological features occurring worldwide where mud and fluids emanate or erupt from the subsurface through the seafloor (*sensu* Kopf, 2002); the locations of known mud volcanoes in the Black Sea are indicated on Figure 7. Mud volcanism does not refer to a single process like hydrothermal venting, rather the driving forces (e.g. activity, size, materials and morphology) which varies between sites (Milkov, 2000; Dimitrov, 2002; Kopf, 2002; Huguenot *et al.*, 2004; Huseynov & Guliyev, 2004). Mud volcanoes are a poorly understood phenomenon whereby overpressured, fine-grained sediments extrude to the surface from depths of up to several km. They are often clustered around tectonically active areas where compressive forces act on the sediments at depth.

Although mud volcanoes are orders of magnitude larger than gas seeps, the microbes at both sites use the same metabolic pathways (cf. Eqns 1 and 2). For instance, one of the many deep-sea mud volcanoes in the Black Sea, the Dvurechenskii mud volcano in the Sorokin Trough, south of the Crimea (Figure 7), is an elliptical mound 1,200 by 800 m in diameter rising to 80 m above the seabed, with gas flares rising to up to 1,300 m from the seafloor (Bohrmann *et al.*, 2003; Greinert *et al.*, 2006; Lichtschlag *et al.*, 2010). Most studies of Black Sea mud volcanoes involve sites situated in the central abyssal plain and the Sorokin Trough Area (Fig. 7) (Woodside *et al.*, 1997; Bouriak & Akhmetjanov, 1998; Ivanov *et al.*, 1998; Kenyon *et al.*, 2002; Bohrmann *et al.*, 2003; Greinert *et al.*, 2006; Lichtschlag *et al.*, 2010). Similar to the Black Sea gas vents, the microbial community at Black Sea mud volcanoes are characterised by archaea in the ANME-1 group which were in syntrophy with sulphate-reducing bacteria within the *Desulfobacteraceae* family (e.g. *Desulfosarcina*, *Desulfococcus*) (Stadnitskaia *et al.*, 2005)

8. OVERVIEW OF MAIN FEATURES ALONG THE PIPELINE ROUTE

The following account draws on background information where available from published literature and reports, and uses information from interpretations of the geophysical data collected in the route surveys.

Data

The data consisted of sidescan sonar, multibeam bathymetry and sub-bottom profiler (SBP) data acquired using an AUV, and video data collected using an ROV. Sidescan sonar and SBP data were acquired using an Edgetec FS-AU system (100 KHz sidescan and 2-16 kHz profiler). Multibeam data was acquired using a 200 kHz Simrad EM2000 system. Sediment core data was not considered.

Sidescan sonar and video data are the best tools for examining processes that are active at, or have recently modified, the present day seafloor. Thus these were the primary datasets in the present analysis. Bathymetry and profile data were used to support the interpretation where necessary.

The key findings are summarised in a series of nine interpretation maps located on Figure 14 (Figures 15-23).

Russian margin

Background

There are very few publications on seabed features on the Russian/Georgian margins. Some data has been collected on the Russian margin in the Training Through Research project (Woodside *et al.*, 1997; Akhmetzhanov *et al.*, 2007). Further information is available in the

d'Appolonia report (2013) and in the Intecsea report (2013) from which the following account was taken.

On the Russian margin sediment transport via turbidity currents and debris flows was common during the last glacial, but has been much reduced during the last 9,000 years. The main sources of sediment for the Anapa shelf are the Don and Kuban Rivers, which currently discharge through the Kerch Strait from the Sea of Azov. Secondary sources are the small rivers flowing from the southern slopes of the Greater Caucasus. Due to the absence of major rivers in the coastal area, there is currently minor mass sediment transportation onto the shelf. Nevertheless, autumn and spring river surges are reported to have initiated submarine debris flows farther to the southeast where the Blue Stream project was constructed (Delft Hydraulics, 1998). Strong currents flow parallel to the depth contours towards the west, following the characteristic circulation pattern of the Black Sea. Longshore currents tend to flow towards the east. These two factors of low sediment discharge and high current flow combine to greatly restrict the expected volume of sediment deposited over the shelf area. It should, however, be noted that high point sources of sediment can be introduced locally onto the shelf by large collapses of the coastal hills.

The shape of the continental slope off Anapa is controlled by bedrock, comprised primarily of the Mesozoic and Neogene Flysch, which is also observed along the present coast. Bedrock is at or close to the surface in parallel ridges aligned along the slope. The presence of bedrock is the main reason why the continental slope is exceptionally steep. Gradients reach in excess of 30° at the shelf break and gradually decrease moving down the slope. The morphology of the continental slope is characterized by a highly dissected, dendritic canyon system cut into the Flysch bedrock. The slope has concave morphological characteristics, in which gradients becomes progressively gentler as they are traced towards the foot of the slope. Gradients decrease from 30° to less than 5°. This morphology is the result of cycles of erosion, which caused parallel retreat of the slope and the development of a random network of dendritic valleys.

The Russian continental slope has numerous mass wasting features including submarine landslides (including tension cracking associated with imminent failures at the shelf break), individual boulder falls, debris flows, and density currents. The continental slope is typically rocky in the upper part and transitions into a boulder 'scree' slope in the lower part.

Upper Russian slope

The upper Russian slope is characterised by steep slopes, an erosional gullied terrain and extremely rugged topography (Figure 24). The gullies have a strongly dendritic pattern (Figures 25 and 27). Overall, they can be grouped into two gully/canyon systems, divided by a central ridge (Figures 24 and 25). The numerous gullies of both systems merge downslope between 1,000 and 1,500 m to form two broad valleys. The sidescan sonar data typically show relatively high backscatter in the gully axis, indicative of coarser sediment (Figures 26-27). High backscatter also occurs on some steep gully walls, where backscatter patterns also clearly show bedded rock at outcrop (Figure 28). ROV photographs from the upper slope show frequent large angular boulders or rock at outcrop, as well as the sharp edges of some gullies (Figure 29). Gully-system heads form a characteristic 'cauliflower' shape (Figure 27). Upslope, most gullies gradually shallow and die out just below the continental shelf edge in water depths of 100 to 130 m. However, some terminate in a distinct headwall scarp that suggests that gullies can propagate upslope by headward erosion (Figure 27).

Downslope, the broad valleys formed from the merged gully systems have steep downslope gradients (8 to 10°), although they have relatively smooth floors (Figures 24 and 25). The valley floors are characterised by high backscatter and by sediment waves oriented across the slope (Figures 24 and 30). ROV photographs show frequent large boulders, covered by only a thin intermittent sediment drape (Figure 31). The valley floors are best described as an area of talus slope, the extent of which is best defined by the high backscatter area on the sidescan sonar data (Figures 23 and 25).

Some slope gullies begin at an intermittent scarp that occurs along or immediately below the continental shelf edge at a depth of 90 to 100 m (Figure 32). This feature does not appear to be directly related to the gullies. Its origin is unclear, but it may be related to a period when relative sea level was lower in the Black Sea.

Small carbonate mounds related to fluid seepage can be identified at a few locations along the Russian shelf edge (Figures 23 and 33). These are discussed in more detail in Section 9. Other than these mounds, only one small aggregation of possible seep-related features was identified on the Russian slope (Figure 23). We note that this aggregation of features occurs in an area of bedrock outcrop, rather than sediment accumulation, casting some doubt on their identification. However, seepage from bedrock (e.g. groundwater seepage) cannot be ruled out. Overall, it should also be kept in mind that the rough terrain and varied backscatter character of the rough slope region might make identification of seeps difficult.

A narrow linear backscatter anomaly crossing the Russian shelf edge is identified as a possible submarine cable trench (Figure 34). However, extensive gradiometer surveys of this feature failed to detect any cable. Three cables were identified on video footage crossing the upper Russian slope (Figure 35). Cables are in places suspended above the seafloor as they cross the rough terrain, while in other places they are completely buried by sediment. A jumble of cable, tangled around some large boulders, was found at a depth of 905 m (Figure 35). This is probably cable destroyed by a landslide or sediment flow.

Lower Russian slope

The lower Russian continental slope, extending from 1,500 m to about 2,080 m, is generally relatively smooth with a gradient that gradually decreases until the slope merges with the abyssal plain. There is no clear gradient break that can be used to define the base of slope. The one exception to the smooth slope is a marked incision where the Anapa Canyon cuts across the slope at about 1,650 m water depth (Figure 23). This creates a series of scarps, in total nearly 100 m high, crossing a significant part of the survey corridor (Figure 36). The pipeline route is due to cross the Anapa Channel, which is connected to the Anapa Canyon and thus any activity in the channel could be important. Woodside et al., (1997) suggested on the basis of sidescan sonar and profiler data that the Anapa Canyon is covered by soft sediment, suggesting that it is not an active conduit for turbidity currents at the present time. This suggestion has been verified by d'Appolonia (2013) who examined sub-bottom profiles in relation to the South Stream project and confirmed that the modern channel is covered by a sedimentary drape about one to two m thick. The d'Appolonia report also mentions core samples that confirm the presence of stratified clay in this area, and states that one to two m of sedimentary drape is also present in the Anapa channel and across turbidity wave deposits from the channel. Thus the canyon/channel does not appear to have been active for the last few thousand years.

Downslope from the canyon, the slope is characterised by landslide scars and depositional debris lobes (Figure 22). The landslide scars are all low relief features, with slide scarps

typically only a few metres high. Some scarps, however, have a relatively fresh appearance, with backscatter contrasts between slide scar and the adjacent seafloor, possibly indicating a relatively recent landslide (Figure 38). The debris flow lobes are characterised by low backscatter and a typical frond-like margin (Figure 39). However, they have barely discernible relief on profile data.

Russian Abyssal Plain

The pipeline route extends for about 110 km across the Russian sector of the abyssal plain in water depths from about 2,080 to 2,170 m. As discussed above, there is no clear slope break marking the boundary between the lower slope and abyssal plain. The seafloor is essentially smooth and almost featureless across the entire area. The only features noted on sidescan sonar are faint high backscatter lineations and irregular marks. The main lineation trend is WNW, approximately parallel to the contours.

Turkish Abyssal Plain

In general the abyssal plain is characterized by flat well-stratified sediments, although irregular rough seafloor was observed in limited areas along the pipeline route. D'Appolonia (2013) report that seismic sections that pass through these areas of bottom roughness show numerous diffractions that appear to be related to disturbance of sediment due to the movement of Maikopean (Lower Miocene) mud associated with the nearby field of mud volcanoes (Dimitrov, 2002; Kruglyakova et al., 2004). Other areas of disrupted seafloor interpreted to be related to mud/gas upwelling are concentrated in the area of the lower Danube fan system.

The proposed pipeline route extends for some 460 km across the Turkish sector of the abyssal plain. Water depth varies from 2,025 to 2,199 m across the area (Figure 40). The eastern part of the abyssal plain is the deepest and is essentially flat. The western part has more irregular topography, resulting from a complex of channel levee systems that crosses the area. This forms an elevated ridge that rises about 50 m above the main abyssal plain (Figure 40) and represents the distal part of the Danube Fan (Lericolais, et al., 2013)

The main features of the Turkish sector of the abyssal plain are shown on maps three to seven (Figures 17-21). The deepest, eastern part of the abyssal plain (east of -69,0000) lacks any large-scale features. However, sidescan sonar data shows abundant linear and irregular fine-scale markings (Figure 41), interpreted as tool marks caused by objects carried along by bottom currents. They mainly trend NE-SW, tending to become more NNE-SSW towards the west. They are discussed in detail in section 9. Sidescan sonar data also show numerous small high backscatter targets that are typically scattered randomly but can on occasion form aggregated groups (Figure 42). These are also discussed in detail in section 9.

West of easting -69,000, the seafloor rises gently onto the flank of the channel levee area. Sidescan sonar data show the lower part of the levee complex flank to be covered by sediment waves (Figures 18 and 19). These are oriented approximately E-W, perpendicular to the adjacent channels and to the levee slope (Figure 43). They are interpreted as sediment waves built by unconfined turbidity currents. Their location is consistent with turbidity flows moving south in the deep to the east of the levee, but pinned against the levee flank by coriolis force. This interpretation is also supported by the occurrence of backscatter banding,

oriented almost N-S, that is the typical signature of sediment deposited by turbidity currents (Figure 44).

Six channels crossing the pipeline can be identified in bathymetry data within the channel levee complex (Figures 17 to 19). Most of these have rather indistinct signatures on sidescan sonar data and are clearly partly buried. They can thus be inferred to be inactive (not subject to sediment flows, turbidity currents, moving through the canyon), although this needs to be confirmed by analysis of sediment cores. The easternmost channel, however, has a relatively sharp appearance on both bathymetry and sidescan sonar data, as well as a clear backscatter contrast between channel floor and flanking levee (Figure 45). It is thus inferred to be the youngest channel in the overall channel levee complex, although recent activity cannot be confirmed or ruled out. Again, analysis of core data is required to date the youngest turbidites associated with this channel. This channel shows flanking features that could be interpreted either as terraces, or as channel wall failures (Figure 46). However, the position of these features, just downstream of bends in the channel and on the inside channel wall, supports their interpretation as terraces.

Linear and irregular fine-scale markings cover the sidescan sonar data from the top of the levee, with similar densities of markings as seen further east (compare Figures 41 and 47). At least some lineations cross the channels (Figure 45). It thus appears that the lineations post-date levee formation.

In sidescan sonar data, the Turkish Abyssal Plain between eastings -227,654 and -263150 is marked by numerous small hard targets arranged in linear chains or irregular aggregates (Figures 48 to 52). The areas in which these features occur also show roughness at a scale of a few metres, contrasting with the adjacent smooth seafloor (Figure 53). Many of the groups of hard targets are surrounded by diffuse high backscatter halos (e.g. Figures 48 and 51). Many, but not all, are also located in relative bathymetric lows, although these are typically only a metre or two deep. These features may be related to fluid seepage from the sub-seafloor. They are discussed in detail in Section 9.

Bulgarian Abyssal Plain

The proposed pipeline route crosses about 120 km of the Bulgarian Abyssal Plain, seaward of a sharp slope break that occurs at 1,950 m water depth at the base of the Bulgarian continental slope. Much of this area is characterised by smooth seafloor, marked only by abundant linear and irregular fine-scale markings (Figures 54 and 55). Lineations trend NNE-SSW, tending to become N-S towards the west.

In the eastern Bulgarian Abyssal Plain, around easting -298,180, a small but complex channel levee system, including a number of abandoned meander loops, crosses the pipeline route. Although a clear bathymetric feature, this channel is poorly defined in sidescan sonar data, indicating it is partially buried and inactive. A small extremely strong backscatter target occurs on the eastern flank of the channel system (Figure 56). It has dimensions of some 50 x 25 m. Possible interpretations include a shipwreck or a mud volcano. If a ship, the size indicates a modern vessel and its identity may be available from databases such as Lloyds register. Its location is well away from the proposed pipeline route.

The proposed pipeline route also crosses an area of rough topography, related to a fault zone, around easting -356,000. The sidescan sonar and bathymetry data show a complex series of *en echelon* fault scarps, some of which are very sharply defined, suggesting recent

activity (Figure 57). Video data from this region shows areas of unusual fractured seafloor sediment, which may be indicative of active pockmarks (Figure 58). These are discussed in section 9.

Sediment waves cover a significant part of the western Bulgarian abyssal plain, adjacent to the base of the continental slope (Figures 15-16). The waves are oriented approximately N-S, parallel to the contours on the slope, indicating that they were most likely formed by turbidity currents flowing down the slope (Figure 59). This is supported by the occurrence of extensive sediment waves on the slope (Figure 60). The sediment waves on the abyssal plain appear to overprint the linear and irregular fine-scale markings that occur in the same area (Figure 59). Note that the lineations were formed by a N-S current, perpendicular to the E-W current that formed the sediment waves.

Bulgarian continental margin

There appear to be no published accounts of recent sedimentary processes on the Bulgarian margin. The report by d'Appolonia (2013) contains the following interpretation of geophysical data collected during the South Stream Offshore Pipeline . The Bulgarian continental slope exhibits numerous large submarine slope failures originating from the edge of the continental shelf and continuing down the continental slope. Failures appear to have initiated from the headscarps along the edge of the continental shelf. The main scarp is covered by about 1.5-2 m of sediments representing deposition over the past 7,500 – 10,000 years. Farther downslope the sedimentary drape is thinner and almost absent where active washout phenomenon appear to affect the seafloor. Another area characterized by steep slopes is the shelf break. The break at the shelf is covered by about two to five m of drape, but at a short distance downslope, hummocky bedforms related to modern slope debris are observed. Unusual sediment ridges, interpreted to be formed by downslope movement of sediments, are present along the Bulgarian slope. These ridges are typically about 20 to 50 m wide and can be as long as about 300 m. They are typically one to two m thick, but can be as thick as about 5 m. Because they appear to form slowly and may be inactive, they appear unlikely to be a significant geohazard.

Much of the area of the Bulgarian slope crossed by the proposed pipeline route has been affected by landsliding (Figure 15). A large landslide complex as well as several smaller discrete landslides are imaged on bathymetry and sidescan sonar data (Figures 15 and 61 to 62). A detailed analysis of landslide activity has not been attempted, since this was not part of the remit of this report. However, backscatter contrasts within the large landslide complex suggest that it has experienced several (many?) periods of landslide activity (Figure 61). A large proportion of the failed sediment from the large landslide complex has been entirely removed from the continental slope, either in the form of debris flows, or flows that transformed into turbidity currents. No morphological evidence for any landslide debris was found on the adjacent abyssal plain floor, indicating either that this is deeply buried, or that the material has been spread widely across the basin by turbidity currents. The occurrence of extensive sediment wave fields within the landslide scar (Figures 15 and 60), probably created by turbidity currents, might indicate that at least some of the later landslide phases (e.g. headwall collapses) did indeed transform to turbidity currents.

In contrast to the large landslide complex, the failed material from some smaller landslides, in the form of blocky landslide debris, was deposited locally on the continental slope (Figure 62).

Linear and irregular fine-scale markings are abundant on the lowermost Bulgarian slope, where they trend approximately N-S (Figure 55). These types of feature also occur further upslope, but in the latter area they are much less abundant and the dominant trend is NNE-SSW, parallel to the contours (Figure 15).

The relative ages of landslides, sediment waves and lineations can be determined by their relative superposition. Extensive N-S lineations cut the lower part of the main landslide scar (Figure 15), indicating that most of the landslide activity pre-dates the event that formed the lineations. As already noted, the sediment waves overprint the lineations, indicating that they are younger (Figure 59). Thus the likely sequence of events is (i) the major landslide phase, (ii) the lineation generating event and (iii) sediment wave generation by turbidity currents, either as a result of later small landslides or of sediment transport off the Bulgarian shelf.

The uppermost Bulgarian slope is marked by several fields of furrows (Figures 63 to 64). Some furrows appear to emanate from small block like features on the seafloor, suggesting that they were caused by erosion behind the block, or have aligned blocks running along their length. These are clearly erosional features created by alongslope currents. Bathymetry data show that they can be up to a metre in depth (Figure 64). However, video data from this area show the seafloor to be covered by a thick blanket of organic material, suggesting a lack of recent current activity. The organic material, commonly referred to as flocs, is discussed in section 9. Thus erosion by alongslope currents would not appear to be an active process.

Small carbonate mounds occur along the Bulgarian shelf edge (Figures 65 and 66). Their identity is confirmed by video observation, which also shows evidence of active seepage associated with some mounds (Figures 67 and 68). This is discussed in more detail in section 9.

9. DISCUSSION OF SPECIFIC FEATURES

a) Features related to probable and possible fluid escape

Identification of features related to fluid seepage, such as mud volcanoes, pockmarks or carbonate mounds, was one of the main objectives of this study. However, large mud volcanoes similar to those identified at many locations around the Black Sea (e.g. Lericolais, 2006) do not appear to be present along the proposed pipeline routes. Similarly, carbonate mounds only occur in extremely localised areas.

The following features that relate to, or might relate to fluid escape, were identified:

(i) Carbonate mounds

Carbonate mounds were identified on sidescan sonar data from just below the continental shelf edge on both the Russian and Bulgarian slopes. On sidescan data, they are hard targets with a typical irregular 'knobbly' appearance (Figures 33, 65 and 66). Most cannot be identified on bathymetric data, partly because they are small, low relief features, but also because their occurrence is masked by the typically steep terrain in which they occur. ROV

video data from mounds on the upper Bulgarian slope confirm the identity of these features (Figures 67 and 68). These data also show evidence for active seepage in the form of localised patches of discoloured seafloor associated with the carbonate buildups.

On both slopes carbonate mounds occur in the same relatively narrow depth band between about 110 and 140 m. This suggests that in addition to fluid seepage, the location of these features is constrained by other factors, most likely the level of oxygen in the stratified water column.

(ii) Other possible 'carbonate' features

Other than the relatively obvious carbonate mounds identified along the shelf edge, no other positive identification of carbonate buildups have been made from the available dataset. A few unexplained targets seen on video data from the abyssal plain floor could potentially be low relief carbonate chimneys or blocks, but most are covered with organic floc material and no positive identification is possible (Figure 68, lower panel).

(iii) Pockmarks

Possible active pockmarks were identified on a number of ROV videos from the Bulgarian and Turkish Abyssal Plains and from the Bulgarian continental slope (Figures 58, 69 and 70). These features are typically shallow depressions a few metres across with evidence for disrupted sediment layers around their margins. The lack of accumulation of floc material in the depressions might suggest that they are being kept clear by active fluid flow, although no direct evidence of such flow was seen.

It has not, to date, proved possible to correlate video and sidescan evidence from known pockmarks. This is a consequence of the small number of examples of pockmarks identified on video, the lack of systematic video survey, and small discrepancies (up to 10 m) between ROV and sidescan navigation (inferred from clearly identified targets, such as trees or shipwrecks). It is also possible that many targets identified on sidescan sonar data are obscured by a layer of organic flocs. However, given several pockmarks have been identified from the small number of ROV dives along the survey route, it is likely that these features may be widespread.

(iv) Linear groups or clusters of small hard targets seen on sidescan data.

Linear groups or clusters of small, hard targets were seen predominantly in one area of the Turkish sector of the abyssal plain (Figure 17). Individual targets within the groups are typically five m or less across, although most appear elongated along the sidescan track, suggesting an element of artificial elongation related to data acquisition (Figure 48). Thus most are probably smaller than five m in diameter. Many of the groups of hard targets are surrounded by a diffuse high backscatter halo (Figures 48 and 51).

The linear/clustered targets often occur preferentially in bathymetric lows, although this is not a clear-cut relationship in every case (Figures 48, 50 to 52). No video data is available to allow identification of these targets. One possible explanation is that they are related to fluid seepage from the seafloor, and that the bathymetric lows in which they occur are pockmarks. Additional systematic video surveys of these features are required to confirm their identification.

(v) Small randomly scattered sidescan sonar targets.

Small randomly scattered targets occur across wide areas of the abyssal seafloor (Figures 42 and 56). Individual targets are only a few metres across. Their distribution, and complete absence from some areas, indicates that they are real features rather than acoustic artefacts related to data acquisition. Video evidence is insufficient to confirm their identification. The small size of the features, lack of systematic video survey and the positional uncertainty of the ROV make positive correlation between seabed features and sidescan targets difficult. Many may also be buried beneath a layer of organic flocs. Systematic video surveys of area(s) with several random targets of this type are required to confirm the identification of these features.

(vi) Seeps on the Bulgarian shelf

Abundant small-scale fluid seepage, evidenced through patchy orange, black and white discolouration of the seafloor, can be seen on video data collected while tracking submarine telephone cables on the Bulgarian shelf (Figures 71 and 72). The coloured areas are likely to represent areas of chemosynthetic bacterial activity. Some of these patches have aggregations of mussels, possibly *Modiolus phaseolinus* or *Mytilus galloprovincialis* (Begun et al., 2010) distributed adjacent to but not within the possible bacterial areas. These species are not chemosynthetic species, but do require a hard substrate for attachment. We speculate that seepage may generate this hard substrate through cementation of surface sediment or deposition of carbonate.

b) Lineations and irregular fine scale patterns

All of the sidescan sonar data from the abyssal plain area, and to a lesser extent from the Russian and Bulgarian slopes, are extensively marked by lineations and marks displaying relatively high backscatter. Forms include continuous lines, discontinuous 'dashed' or 'dotted' lines and many forms of irregular, usually short, and often curved lines, although the last are also often arranged in linear trains that parallel the trend of the more simple linear features (Figures 41, 47, 54 and 55). Individual features range from a metre or so in width to (rarely) 20 m or more. Many can be traced for several km, across the entire survey corridor. Only very few of the lineations have any measurable bathymetric expression, although a vague bathymetric fabric parallel to the lineations can be seen in some areas, and some point features on discontinuous lines have relief of a few tens of cm (Figure 73).

The trends of the linear features were plotted across the abyssal plain region (Figure 74). The majority of features (90%+) conform to a clear pattern, trending near N-S at the base of the Bulgarian slope and progressively more NE/SW towards the east. Viewed in the context of the entire Black Sea, the lineations form a fan shaped pattern, with the apex of the fan located in the region where the Bosphorus connects to the Black Sea.

Coherent patterns of linear features covering large areas of seafloor, especially in deep water, are almost exclusively related to erosion or deposition by persistent bottom currents. In this case, the pattern of the lineations and their relationship to the Bosphorus clearly suggests that they are related to the inflow of dense Mediterranean water into the Black Sea. Today this sinks and then disperses across the abyssal seafloor. The lineations must post-date the reconnection of the Black and Mediterranean Seas that occurred around 8,400 years ago

(Ryan et al., 1997; Lericolais, 2009). The lack of topographic relief on the lineations suggests that the process that created them is not currently active. An initial inspection of a few high-resolution seismic lines from the Black Sea abyssal plain suggests that the surface into which the lineations are cut is buried beneath at least one m of acoustically transparent sediment, indicating that the creation of these features occurred several thousand years ago. This leads us to speculate that the lineations were created during the flooding event that occurred after the reconnection of the Black and Mediterranean Seas.

Linear features formed by deep-water thermohaline ocean currents are normally simple linear furrows and ridges. The more irregular features, even where clearly aligned, suggest a more complex formation mechanism. We suggest that they are a form of 'tool mark', created where objects carried by the bottom water currents impacted the seabed. The most likely objects are the numerous trees and tree branches observed on video transects across the seafloor (Figures 75 and 76). Small pieces of modern debris, such as plastic bags, provide a modern analogue for the tool mark hypothesis. These objects create furrows or trails of pits as they are carried across the soft organic rich seabed surface layer by bottom currents (Figures 77 and 78).

The small number of lineations that do not conform to the dominant trend do not have a secondary coherent trend, although they do tend to be perpendicular or parallel to the local contours. This suggests that they relate to downslope settling of near neutrally buoyant objects or to neutrally buoyant objects being carried along slope by contour currents, with trees again being the most likely such objects.

c) Point targets on sidescan sonar data.

The sidescan sonar data show a number of scattered, relatively strong acoustic 'targets' that occur randomly throughout the area. They typically range from a few metres to about 20 m (rarely 50 m) in length or diameter (Figures 56 and 66). Only the larger of these can be identified on the basis of the sidescan data alone (e.g. Figure 66, where a strong target about 15 m in length clearly corresponds to a ship). The majority of targets appear as a few pixels of contrasting backscatter with the number of pixels being too small to define the object shape. Positive identification of such targets requires video surveys. Only a limited number of video surveys, biased towards the larger, stronger targets, are currently available. This evidence base suggests that targets most commonly correspond to trees (Figures 66 and 67). Anthropogenic objects such as sunken ships (Figures 79 and 80), or other man-made detritus (e.g. a large fender made of car tyres and possible aircraft debris, Figures 81 and 82) are also relatively common. None of the targets of this type examined during video surveys had a geological origin.

d) Flocculated organic matter

A layer of flocculated organic matter, hereafter referred to as flocs, is seen on ROV video data covering almost all of the seafloor in the study area, apart from the Bulgarian shelf, uppermost part of the Bulgarian slope, and the steeper parts of the upper Russian slope (Figures 83 to 85). On the abyssal plain, the most recent flocs form black, mat-like aggregations, sometimes with an outer lighter-coloured rim, that collect in subtle bathymetric lows (Figures 83 and 84). This material is extremely soft and easily stirred up by the wash of the ROV. At shallower water depth on the Bulgarian slope, a patchy layer of olive-brown flocs

overlies areas of both dark and light coloured flocs (Figure 85). The different colour of the flocs probably relates to their composition with the white colour being composed of coccolith (calcareous plankton) debris and the darker flocs being composed of other plankton such as diatoms, dinoflagellates etc. The flocs occur when particles and plankton aggregate into clumps in the surface ocean. These clumps or flocs are then able to sink to the seabed, where under normal conditions, they would be consumed by benthic organisms. In the anoxic Black Sea, where benthic organisms are absent, they remain as flocs.

In the area of the fault zone on the Bulgarian abyssal plain, ROV images from the 'Caucasus' cable survey show that the cable has cut or worn a trench (at least 15 to 20 cm) into the seabed, suggesting that the soft organic layer is here up to 20 cm or more thick (Figure 86). The edges of the trenches cut into the seabed can clearly be seen to move when the bow wave of the ROV passes, suggesting that the layer has a jelly-like consistency. Previous scientific reports have noted floc layer thicknesses up to seven cm (Lichtschlag et al., 2010). Such a layer is likely to be 'transparent' to the acoustic frequencies used in sidescan sonar and bathymetry data collection, with the sidescan picking up reflectors in the subsurface. This potentially explains why many sidescan targets are not seen on ROV video data.

e) Bottom currents

Bottom currents are noticeably absent on almost all of the ROV videos, except for those on the Bulgarian shelf. In most cases, flocs disturbed from the seabed simply hang in the water column without appreciable movement. However, evidence for past bottom currents is clearly visible, even on 'recent' time scales.

Firstly, items of anthropogenic rubbish, such as plastic bags, show evidence, in the form of furrows cut into the soft floc layer, of having been moved across the seafloor (Figure 77). Similarly, plastic rubbish tends to collect on objects such as trees, suggesting that it has been swept there by currents (Figure 75).

Secondly, features such as furrows and sediment waves indicate stronger currents that have occurred on recent geological timescales. These currents include downslope turbidity currents and dense saline flows that enter the Black Sea from the Mediterranean Sea and flow downslope into the deep basin.

f) Cables

Submarine telephone cables were observed on a number of ROV dives (Figures 58, 86 and 87). Two trenches or plough marks where cables have been buried on the continental shelf were also seen in sidescan sonar data (Figures 34 and 88).

10. LIST OF FIGURES

- Figure 1. Location map showing pipeline route.
- Figure 2. GEBCO bathymetry map of the Black Sea.
- Figure 3. Location of deep-sea fans in the western Black Sea.
- Figure 4. Sealevel fluctuations in the Black Sea since the last glaciation.
- Figure 5. History of the marine reconnection with the Mediterranean.
- Figure 6. Image of the seabed showing floc layers
- Figure 7. Location of the mud volcanoes gas seeps and gas hydrates in the Black Sea.
- Figure 8. Salinity profile for the upper approximately 500 metres of the Black Sea.
- Figure 9. Surface water circulation in the Black Sea.
- Figure 10. Trajectory of ARGO float 6900804 from March 2011 to May 2013
- Figure 11. Biochemical changes in the upper water layers of the Black Sea.
- Figure 12. Vertical biogeochemical structure of the Black Sea
- Figure 13. Image of a microbial tower (reef) structure
- Figure 14. Location of survey area, pipeline routes and interpretation maps 1-9.
- Figure 15. Map 1: Bulgarian slope.
- Figure 16. Map 2: Bulgarian Abyssal Plain.
- Figure 17. Map 3: western Turkish Abyssal Plain.
- Figure 18. Map 4: western Turkish Abyssal Plain.
- Figure 19. Map 5: central Turkish Abyssal Plain.
- Figure 20. Map 6: eastern Turkish Abyssal Plain.
- Figure 21. Map 7: eastern Turkish Abyssal Plain and Russian Abyssal Plain.
- Figure 22. Map 8: lower Russian slope.
- Figure 23. Map 9: upper Russian slope.
- Figure 24. 3D representation of the upper Russian continental slope.
- Figure 25. Overview of sidescan sonar data from the upper Russian continental slope.
- Figure 26. Dendritic canyons on the upper Russian continental slope.
- Figure 27. Detail of dendritic canyon heads on the upper Russian continental slope.
- Figure 28. Bedded rock outcrop on gully flanks on the upper Russian continental slope
- Figure 29. ROV photographs of boulders and a gully edge on the Russian slope
- Figure 30. Sidescan sonar image of gravel waves and boulders on the Russian slope.
- Figure 31. ROV photographs of boulders on the floors of valleys on the Russian slope.

Figure 32. Intermittent scarp along Russian shelf edge

Figure 33. Carbonate mounds along the Russian shelf edge.

Figure 34. Possible cable trench at the Russian shelf edge.

Figure 35. ROV photographs of cables on the Russian slope.

Figure 36. 3D image of Anapa Canyon.

Figure 37. Overview of sidescan sonar data from the lower Russian slope.

Figure 38. Slide scar on the lower Russian slope.

Figure 39. Debris lobes on the lower Russian slope.

Figure 40. Topographic profile along the Turkish Abyssal Plain.

Figure 41. Lineations on the eastern Turkish Abyssal Plain.

Figure 42. Possible randomly spaced seeps on the eastern Turkish Abyssal Plain.

Figure 43. Turbidity current sediment waves on the flank of the channel levee complex.

Figure 44. Backscatter patterns typical of sediment deposition by turbidity currents.

Figure 45. Sidescan sonar and bathymetry data from the easternmost channel levee complex.

Figure 46. 3D representation of the easternmost channel showing terraces on the channel flanks.

Figure 47. Lineations in the central Turkish Abyssal Plain, near the levee crest.

Figure 48. A cluster of seeps in a shallow depression; note high backscatter.

Figure 49. Loose cluster of seeps with no backscatter anomaly.

Figure 50. Linear seep chains on a gentle sloping seabed.

Figure 51. Clustered seeps with weak relationship to bathymetric lows.

Figure 52. Linear seeps chains, primarily in bathymetric lows.

Figure 53. Contrast between rough seafloor with linear seep chains and adjacent smooth seafloor.

Figure 54. Lineations in the Bulgarian Abyssal Plain.

Figure 55. Lineations at the Bulgarian Abyssal Plain and the continental slope boundary.

Figure 56. High backscatter target, eastern Bulgarian Abyssal Plain

Figure 57. Fault zone in the Bulgarian Abyssal Plain.

Figure 58. ROV photographs of possible pockmarks in the Fault zone area.

Figure 59. Sediment waves in the western Bulgarian Abyssal Plain.

Figure 60. Sediment waves on the Bulgarian slope.

Figure 61. Sidescan sonar data of part of the slide scar on the Bulgarian slope.

Figure 62. Sidescan sonar showing blocky landslide debris on the Bulgarian slope.

Figure 63. Erosional furrows on the upper Bulgarian slope.

Figure 64. Erosional furrows with bathymetry superimposed on the upper Bulgarian slope.

- Figure 65. Sidescan sonar image of carbonate mounds on the upper Bulgarian slope.
- Figure 66. Sidescan image of carbonate mounds and a shipwreck on upper Bulgarian slope.
- Figure 67. ROV photographs of carbonate mounds showing active seepage.
- Figure 68. ROV photographs of carbonate mounds showing active seepage.
- Figure 69. ROV photographs of pockmarks on the Turkish Abyssal Plain.
- Figure 70. ROV photographs of pockmarks on the Bulgarian slope.
- Figure 71. ROV photographs of seepage sites on the Bulgarian shelf.
- Figure 72. ROV photographs of seepage sites on the Bulgarian shelf.
- Figure 73. ROV photographs of possible toolmarks (or sediment wave in second case)
- Figure 74. Summary of fine-scale lineation trends
- Figure 75. ROV photographs of trees.
- Figure 76. ROV photographs of trees.
- Figure 77. ROV photographs of modern toolmarks created by rubbish moving across seafloor.
- Figure 78. ROV photographs of modern furrows and pits on the seabed.
- Figure 79. ROV photographs of wooden shipwrecks
- Figure 80. ROV photographs of wooden shipwrecks
- Figure 81. ROV photographs of anthropogenic rubbish.
- Figure 82. ROV photographs of anthropogenic rubbish.
- Figure 83. ROV photographs of flocs.
- Figure 84. ROV photographs of flocs.
- Figure 85. ROV photographs of flocs.
- Figure 86. ROV photographs of submarine cables.
- Figure 87. ROV photographs of submarine cables.
- Figure 88. sidescan sonar image of the KAFOS cable trench on the Bulgarian shelf.

11. REFERENCES

- Akhmetzhanov, A.M., Ivanov, M.K., Kenyon, N.H., Mazzini, A. 2007. Deep-water cold seeps, sedimentary environments and ecosystems of the Black and Tyrrhenian Seas and Gulf of Cadiz. IOC Technical Series No. 72, UNESCO
- Bahr, A., Lamy, F., Arz, H.W., Major, C., Kwiecień, O., Wefer, G., 2008. Abrupt changes of temperature and water chemistry in the late Pleistocene and early Holocene Black Sea. *Geochemistry Geophysics Geosystems* 9. (Q01004), 1–16
- Begun, T., Teaca, A., Gomoiu, M-T. 2010. State of macrobenthos within *Modiolus phaseolinus* biocoenosis from Romanian Black Sea continental shelf. *GEO-ECO-MARINA* 16, 5-18.
- Blumenberg M., Seifert R., Reitner J., Pape T., Michaelis W. 2004. Membrane lipid patterns typify distinct anaerobic methanotrophic consortia. *Proceedings of the National Academy of Sciences, USA*. 101: 11111-11116.
- Bohrmann G, Ivanov M, Foucher JP, Spiess V, Bialas J, Greinert J, Weinrebe W, Abegg F, Aloisi G, Artemov Y, Blinova V, Drews M, Heidersdorf F, Krabbenhoft A, Klauke I, Krastel S, Leder T, Polikarpov I, Saburova M, Schmale O, Seifert R, Volkonskaya A, Zillmer M 2003. Mud volcanoes and gas hydrates in the Black Sea: New data from Dvurechenskii and Odessa mud volcanoes. *Geo-Marine Letters*. 23: 239-249.
- Boetius A., Ravenschlag K., Schubert C.J., Rickert D., Widdel F., Gieseke A., Amann R., Jørgensen B.B., Witte U., Pfannkuche O. 2000. A marine microbial consortium apparently mediating anaerobic oxidation of methane. *Nature*. 407: 623-626.
- Bouriaik S.V., Akhmetzhanov A.M. 1998. Origin of gas hydrate accumulation on the continental slope of the Crimea from geophysical studies. In: Henriot J-P, Mienert J (eds.) Gas hydrates: relevance to world margin stability and climatic change. The Geological Society, London. pp 215–222.
- Calvert, S. E. and Karlin, R.E. 1998. Organic carbon accumulation in the Holocene sapropel of the Black Sea. *Geology*, v. 26, p. 107-110
- Çifçi G, Dondurur D., Ergün M. 2002. Sonar and high resolution seismic studies in the eastern Black Sea. *Turkish Journal of Earth Sciences*. 11: 61-81
- Codispoti, L.A., Friederich G.E., Murray J.W. and Sakamoto C.M., 1991. Chemical variability in the Black Sea: implications of continuous vertical profiles that penetrated the oxic/anoxic interface. *Deep-Sea Res.* 38, Suppl.2A, S691-S710.
- d'Appolonia 2013 South Stream project Black Sea: Geohazard summary report for design basis. Report to Intecsea Doc. No. 12-244-H2
- Delft Hydraulics, 1998, Report "Geohazard Study Black Sea Pipeline; Phase 1", Reference: Order No. 008.009/074.
- Dimitrov, L., 2002. Mud volcanoes – the most important pathway for degassing deeply buried sediments. *Earth Science Reviews* 59, 49-76
- Duman, M., Duman, S., Lyons, T.W, Avci, M., Izdar, E., Demirkurt, E., 2006. Geochemistry and sedimentology of shelf and upper slope sediments of the south-central Black Sea. *Marine Geology* 227 (1–2), 51–65.
- Egorov V.N., Artemov Y.G., Guilin S.B., Polikarpov G.G. 2011. Methane seeps in the Black Sea: discovery, quantification and environmental assessment. *Journal of Black Sea/Mediterranean Environment*. 17: 171-185.

- Ginsburg, G., and V. Soloviev, 1994. *Submarine Gas Hydrates* [in Russian], 216 pp., VNIIOkeangeologia, St. Petersburg.
- Giosan, L., Filip. F. and Constantinescu, S. 2009. Was the Black Sea catastrophically flooded in the early Holocene?. *Quaternary Science Reviews*, 26, pp. 1-6,
- Greinert J., Artemov Y., Egorov V., De Batist M., McGinnis D., 2006. 1300-m-high rising bubbles from mud volcanoes at 2080m in the Black Sea: Hydroacoustic characteristics and temporal variability. *Earth Planetary Science Letters*. 244: 1-15.
- Gulin S.B., Polikarpov G.G., Egorov V.N. 2003. The age of microbial carbonate structures grown at methane seeps in the Black Sea with an implication of dating of the seeping methane. *Marine Chemistry* 84: 67-72.
- Hay B.J., Arthur M.A., Dean W.E., Neff E.D., Honjo S. 1991. Sediment deposition in the Late Holocene Abyssal Black-Sea with Climatic and chronological implications. *Deep-Sea Research*. 38: 1211–1235.
- Hinrichs K.U., Hayes J.M., Sylva S.P., Brewer PG, DeLong EF 1999. Methane-consuming archaeobacteria in marine sediments. *Nature*. 398: 802-805.
- Hinrichs, K.U., Boetius, A., 2002. The anaerobic oxidation of methane: new insights in microbial ecology and biogeochemistry. In: Wefer, G., Billett, D., Hebbeln, D., Jørgensen, B.B., Schlüter, M., Van Weering, T. (Eds.), *Ocean Margin Systems*. Springer- Verlag, Berlin-Heidelberg, pp. 457–477.
- Hiscott, R. N., Aksu, A.E., Mudie, P.J., Marret, F., Abrajano, T., Kaminski, M.A., Evans, J., Çakiroglu, A.I., Yasar, D., 2007. A gradual drowning of the southwestern Black Sea shelf: evidence for a progressive rather than abrupt Holocene reconnection with the eastern Mediterranean Sea through the Marmara Sea Gateway. *Quaternary International* 167-168, 19-34.
- Huguen C., Mascle J., Chaumillon E., Kopf A., Woodside J., Zitter T. 2004. Structural setting and tectonic control of mud volcanoes from the Central Mediterranean Ridge (Eastern Mediterranean). *Marine Geology*. 209: 245-263.
- Huseynov D.A., Guliyev I.S. 2004. Mud volcanic natural phenomena in the South Caspian Basin: geology, fluid dynamics and environmental impact. *Environmental Geology*. 46: 1012-1023.
- Ince B.K., Usenti I., Ryigor A., Oz N.A., Kolukirik, M., Ince O. 2006. Analysis of methanogenic archaean and sulphate reducing bacterial populations in deep sediments of the Black Sea. *Geomicrobiology Journal*. 23: 1-8.
- Intecsea 2013. South Stream offshore Pipeline FEED; Geohazard Summary Report 31pp plus appendixes.
- Ivanov, M.K., Limonov, A.F., vanWeering, Tj.C.E., 1996. Comparative characteristics of the Black Sea and Mediterranean Ridge mud volcanoes. *Mar. Geol.* 132, 253-271.
- Ivanov M., Limonov A.M., Woodside J.M. 1998. Extensive deep fluid flux through the sea floor on the Crimean continental margin (Black Sea). In: Henriot J-P, Mienert J (eds.) *Gas hydrates: relevance to world margin stability and climatic change*. The Geological Society, London. pp 195-214.
- Izdar E, Ergün M 1991. Recent geological evolution of the Black Sea: an overview. In: Izdar, E. Murray JW (Eds.). *Black Sea Oceanography*, Kluwer Academic Publishers, NATO ASI Series, Series C: *Mathematical and Physical Sciences*. 351: 379-387.
- Jones, G.A., Gagnon, A.R., 1994. Radiocarbon chronology of Black Sea sediments. *Deep-Sea Research Part 1* 41 (3), 531–557.
- Jørgensen B.B., Böttcher M.E., Lüschen H., Neretin L., and Volkov I.I. 2004. Anaerobic methane oxidation and a deep H₂S sink generate isotopically heavy sulfides in Black Sea sediments. *Geochimica et Cosmochimica Acta*. 68: 2095-2118.

- Kenyon N.H., Ivanov M.K., Akhmetzhanov A.M., Akhmanov G.G. 2002. Interdisciplinary study of geological processes in the Mediterranean and Black Seas and North East Atlantic. UNESCO, Paris.
- Konovalov SK, Murray JW 2001. Variations in the chemistry of the Black Sea on a time scale of decades (1960-1995). *Journal of Marine Systems*. 31: 217-243.
- Konovalov S.K., Murray J.W., Luther G.W., Buesseler K.O., Friederich G., Tebo B.M., Samodurov A.S., Gregoire M., Ivanov L.I., Romanov A.S., Clement B., Murray K. 2003. Oxygen fluxes, redox processes and the suboxic zone in the Black Sea. Oceanography of the Eastern Mediterranean and Black Sea: Similarities and differences of two interconnected basins. In: Yilmazz A (ed) Proceedings on the second international conference on oceanography of the Eastern Mediterranean and Black Sea. Athens, Greece, 1999. TUBITAK publishers Ankara Turkey. Pp 566-577.
- Konovalov S.K., Murray J.W., Luther G.W. 2005. Basic processes of Black Sea biogeochemistry. *Oceanography*. 18: 24-35.
- KOPF, A.J. 2002. Significance of mud volcanism, *Rev. Geophys.*, **40** (2), pp. 52,
- Korotaev, G., Oguz, T., Riser, S. 2006. Intermediate and deep currents of the Black Sea obtained from autonomous profiling floats. *Deep Sea Res. II*, 53, 1901-1910.
- Kruglyakova R, Gubanov Y, Kruglyakov V, Prokoptsev G 2002. Assessment of technogenic and natural hydrocarbon supply into the Black Sea and seabed sediments. *Continental Shelf Research*. 22: 2395-2407.
- Kruglyakova, R. P., Y. A. Byakov, M. V. Kruglyakova, L. A. Chalenko, and N. T. Shevtsova, 2004, Natural oil and gas seeps on the Black Sea floor, *Geo-Mar. Lett.*, 24: 150–162,
- Kube M., Beck A., Meyerdierks A., Amann R., Reinhardt R., Rabus R. 2005. A catabolic gene cluster for anaerobic benzoate degradation in methanotrophic microbial Black Sea mats. *Systematic and applied microbiology*. 28: 287-294.
- Leloup J., Loy A., Knab N.J., Borowski C., Wagner M., Jørgensen B.B. 2007. Diversity and abundance of sulphate reducing microorganisms in the sulphate and methane zones of marine sediment, black Sea. *Environmental Microbiology*. 9: 131-142.
- Lericolais, G., and Assemblage partners, 2006. Assemblage deliverable 16: Report on velocity analysis and on core information about methane release: European Community, Energy, Environment and Sustainable Development, Deliverables of the EVK3-CT-2002-00090 European project; 42pp.
- Lericolais, G., Bourget, J., Popescu, I., Jermannaud, P., Mulder, T., Jorry, S., Panin, N. 2013. Late Quaternary deep-sea sedimentation in the western Black Sea: New insights from recent coring and seismic data in the deep basin. *Global and Planetary Change*, 103, p. 232-247.
- Lericolais, G., Bulois, C., Gillet, H., Guichard, F., 2009. High frequency sea level fluctuations recorded in the Black Sea since the LGM. *Global and Planetary Change* 66, (1–2), 65–75.
- Lichtschlag A, Felden J, Wenzhöfer F, Schubotz F, Ertefai TF, Boetius A, de Beer D 2010. Methane and sulfide fluxes in permanent anoxia: In situ studies at the Dvurechenskii mud volcano (Sorokin Trough, Black Sea). *Geochimica et Cosmochimica Acta*.74: 5002-5018.
- Michaelis W, Seifert R, Nauhaus K, Treude T, Thiel V, Blumenberg M, Knittel K, Gieseke A, Peterknecht K, Pape T, Boetius A, Amann R, Jorgensen BB, Widdel F, Peckmann J, Pimenov NV, Gulin MB 2002. Microbial reefs in the Black Sea fuelled by anaerobic oxidation of methane. *Science*. 299: 1013-1015.
- Milkov A.V. 2000. Worldwide distribution of submarine mud volcanoes and associated gas hydrates. *Marine Geology*. 167: 29-42.
- Murray J.W. 1991. the 1988. Black Sea Oceanographic Expedition: Overview and new discoveries. *Oceanography*. 2: 15-21.

- Murray, J.W., Jannash H.W., Honjo S., Anderson R.F., Reeburgh W.S., Top Z., Friederich G.E., Codispoti L.A. and Izdar E., 1989. Unexpected changes in the oxic/anoxic interface in the Black Sea. *Nature*, 338, 411–413.
- Murray, J.W., Stewart, K., Kassakian, S., Krynytzky, M., and Di-Julio, D. 2007. Oxic, Suboxic and Anoxic Conditions in the Black Sea, in: *The Black Sea Food Question: Changes in Coastline, Climate and Human Settlement*, edited by: Yanko-Hombach, V., Gilbert, A.S., Panin, N., and Dolukhanov, P.M., Springer, 1–22.
- Oguz T., Tugrul S., Kideys A.E., Ediger V., Kubilay N. 2005. Physical and biogeochemical characteristics of the Black Sea. *The Sea 14*: 1331 –1369. Chapter 33.
- Oguz T. 2009. Chapter 1. General oceanographic properties: physicochemical and climatic features. In : *State of the Environment of the Black Sea (2001-2006/7)*. Edited by T.Oguz. Publications of the Commission on the Protection of the Black Sea Against Pollution (BSC), Istanbul, Turkey, 421 pp.
- Panin N. 2008. Chapter 1b General Oceanographic Properties: Geography, Geology and Geochemistry. In: *BSC, 2008 –State of the Environment of the Black Sea (2001–2006/7)*. Edited by Temel Oguz. Publications of the Commission on the Protection of the Black Sea against Pollution (BSC) 2008-3, Istanbul, Turkey, 448 pp
- Pilskaln C.H., Pike J. 2001. Formation of Holocene sedimentary laminae in the Black Sea and the role of the benthic flocculent layer. *Paleoceanography*. 16: 1-19.
- Pimenov N.V., Rusanov I.I., Poglazova M.N., Mityushina L.L., Sorokin D.Y., Khmelenina V.N., Trotsenko Y.A. 1997. Bacterial mats on coral-like structures at methane seeps in the Black Sea. *Microbiology* (translated from *Mikrobiologiya*) 66: 354-360.
- Popescu, I., Lericolais, G., Panin, N., Wong, H.K., Droz, L., 2001. Late Quaternary channel avulsions on the Danube Deep-Sea Fan. *Marine Geology* 179 (1–2), 25–37.
- Reitner J., Peckmann J., Reimer A., Schumann G., Thiel V. 2005. Methane-derived carbonate build-ups and associated microbial communities at cold seeps on the lower Crimean shelf (Black Sea). *Facies*. 511: 66-79.
- Ross, D.A., and Degens, E.T., 1974. Recent sediments of the Black Sea, in Degens, E.T., and Ross, D.A., eds., *Black Sea–Geology, Chemistry, and Biology*: American Association of Petroleum Geologists, Memoir 20, p. 183–199.
- Ryan, W.B.F., Major, C.O., Lericolais, G., Goldstein, S.L., 2003. Catastrophic flooding of the Black Sea. *Annual Review Earth and Planetary Sciences* 31, 525–554.
- Ryan, W.B.F., Pitman III, W.C., Major, C.O., Shimkus, K., Moskalenko, V., Jones, G., Dimitrov, P., Gorur, N., Sakinc, M., Yuce, H., 1997. An abrupt drowning of the Black Sea shelf. *Marine Geology* 138, 119–126.
- Seascope 2013. Interpretation of Seabed Survey Data for the South Stream offshore pipeline project. Report No 2013/07.
- Schippers A., Kock D., Höft C., Köweker G., Siegert M. 2012. Quantification of Microbial Communities in Subsurface Marine Sediments of the Black Sea and off Namibia. *Frontiers in Microbiology*. 3: 16. Schubotz F, Wakeham SG, Lipp JS, Fredricks HF, Hinrichs K-W (2009) Detection of microbial biomass by intact polar membrane lipid analysis in the water column and surface sediments of the Black Sea. *Environmental Microbiology*. 11: 2720-2734.
- Soulet, G., Delaygue, G., Vallet-Coulomb, C., Böttcher, M.E., Sonzogni, C., Lericolais, G., Bard, E., 2010. Glacial hydrologic conditions in the Black Sea reconstructed using geochemical pore water profiles. *Earth and Planetary Science Letters* 296 (1–2), 57–66.
- Soulet, G., Ménot G., Lericolais, G., Bard, E. 2011. A revised calendar age for the last reconnection of the Black Sea to the global ocean. *Quaternary Science Reviews* 30, 1019–1026.

- Stadnitskaia, A., Muyzera, T.G., Abbasa, B., Coolena, M.J.L, Hopmansa, N.C., Baasa, M., van Weeringa, T.C.E., Ivanov, M.K., Poludetkina, E., Sinninghe Damste, J.S. 2005. Biomarker and 16S rDNA evidence for anaerobic oxidation of methane and related carbonate precipitation in deep-sea mud volcanoes of the Sorokin Trough, Black Sea, *Mar. Geol.* 217, 67–96.
- Starostenko V.I., Rusakov O.M., Shnyukov E.F., Kobolev V.P., Kutas R.I. 2010. Methane in the Northern Black Sea: characterisation of its geomorphological and geological environments. In Sosson M, Kaymakci N, Stephenson RA, Bergerat F, Starostenk C (eds) *Sedimentary basin tectonics from the Black Sea and the Caucasus to the Arabian Platform. Geological Society, London, Special publications.* 340: 57-75.
- Thiel V., Peckmann J., Richnow H.H., Luth U., Reitner J., Michaelis W. 2001. Molecular signals for anaerobic methane oxidation in Black Sea seep carbonates and a microbial mat. *Marine Chemistry.*73: 97-112.
- Tourova T.P., Kolganova T.P., Kusnetsov K.B., Pimenov N. 2002. Phylogenetic diversity of the archaean component of bacterial mats on coral-like structures in zones of methane seeps in the Black Sea. *Microbiology* (translated from *Mikrobiologiya*) 71: 196-201.
- Vassilev, A. and Dimitrov, L.: Spatial and quantity evaluation of the Black Sea gas hydrates, *Russian Geology and Geophysics*, 43, 637–649, 2002.
- Weaver, P.P.E. Wynn, R.B., Kenyon, N.H. and Evans, J.M. 2000 Continental margin sedimentation, with special reference to the north-east Atlantic margin. *Sedimentology* 47, 1-17.
- Woodside, J.M., Ivanov, M.K., Limonov, A.F. 1997. Neotectonics and fluid flow through seafloor sediments in the Eastern Mediterranean and Black Seas. IOC Technical Series No. 48, UNESCO

12. FIGURES

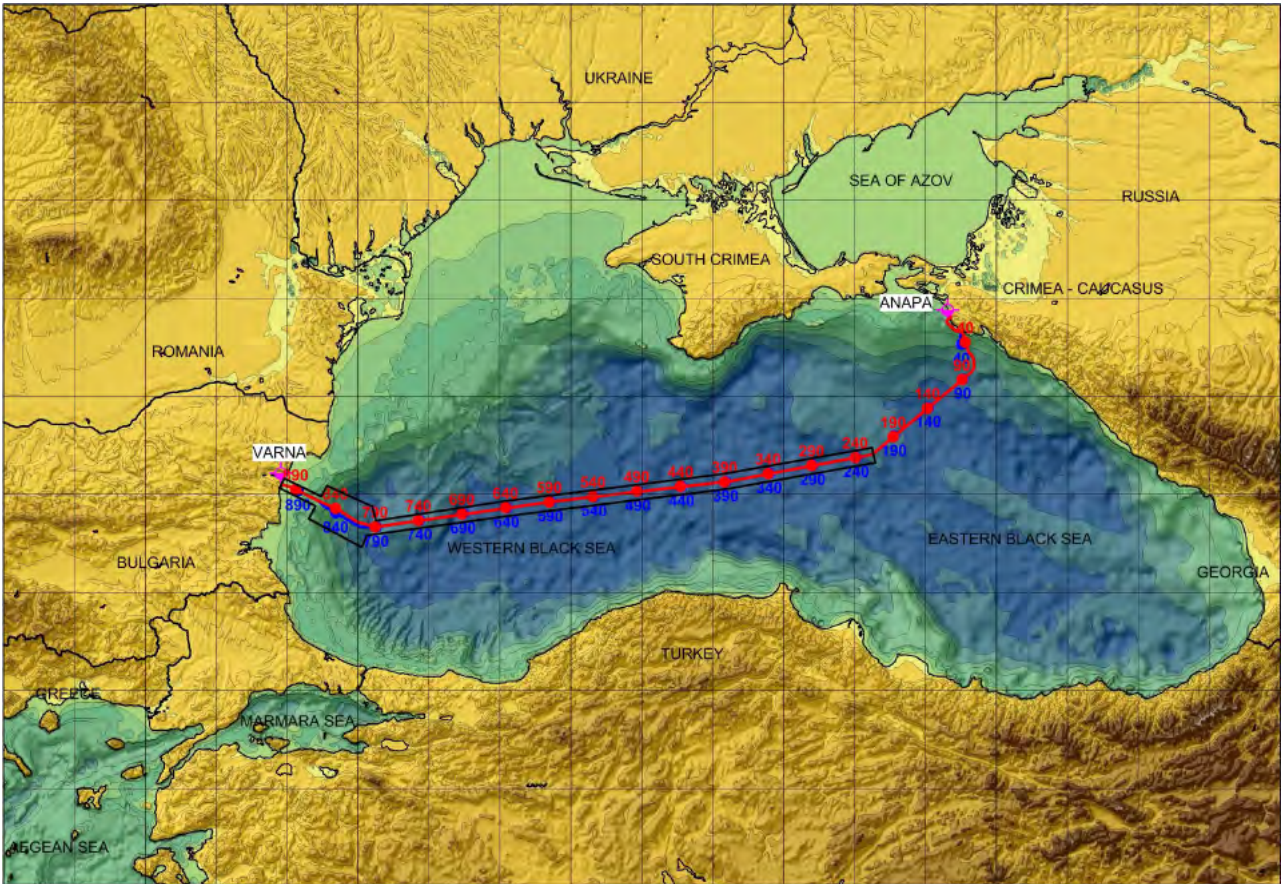


Figure 1. Map of Black Sea showing pipeline route. (from d'Appolonia, 2013)

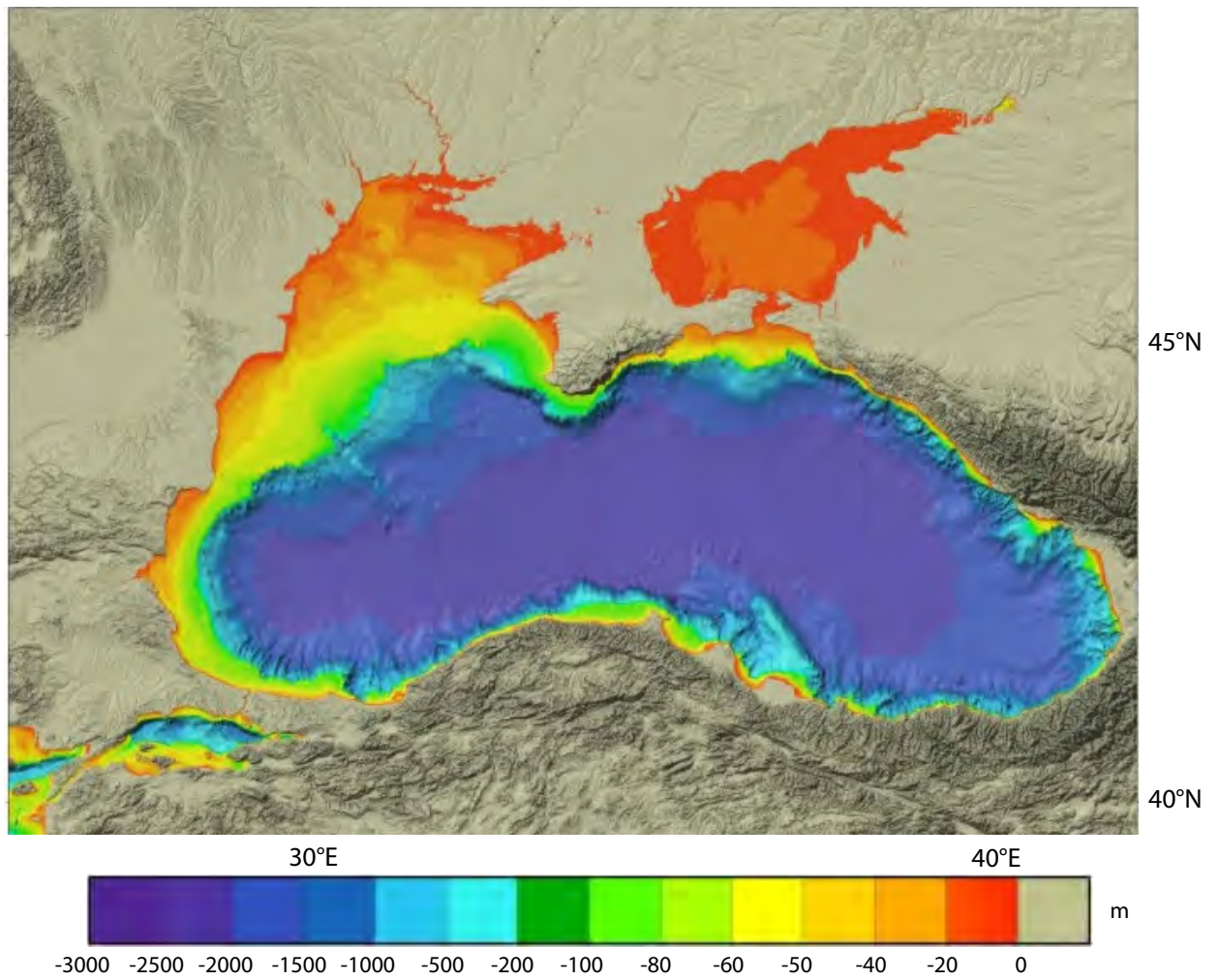


Figure 2. Bathymetric chart of the Black Sea from GEBCO (including 2010 updates) (http://www.gebco.net/data_and_products/gridded_bathymetry_data/gebco_08_update_history/version_20100927/#black_sea).

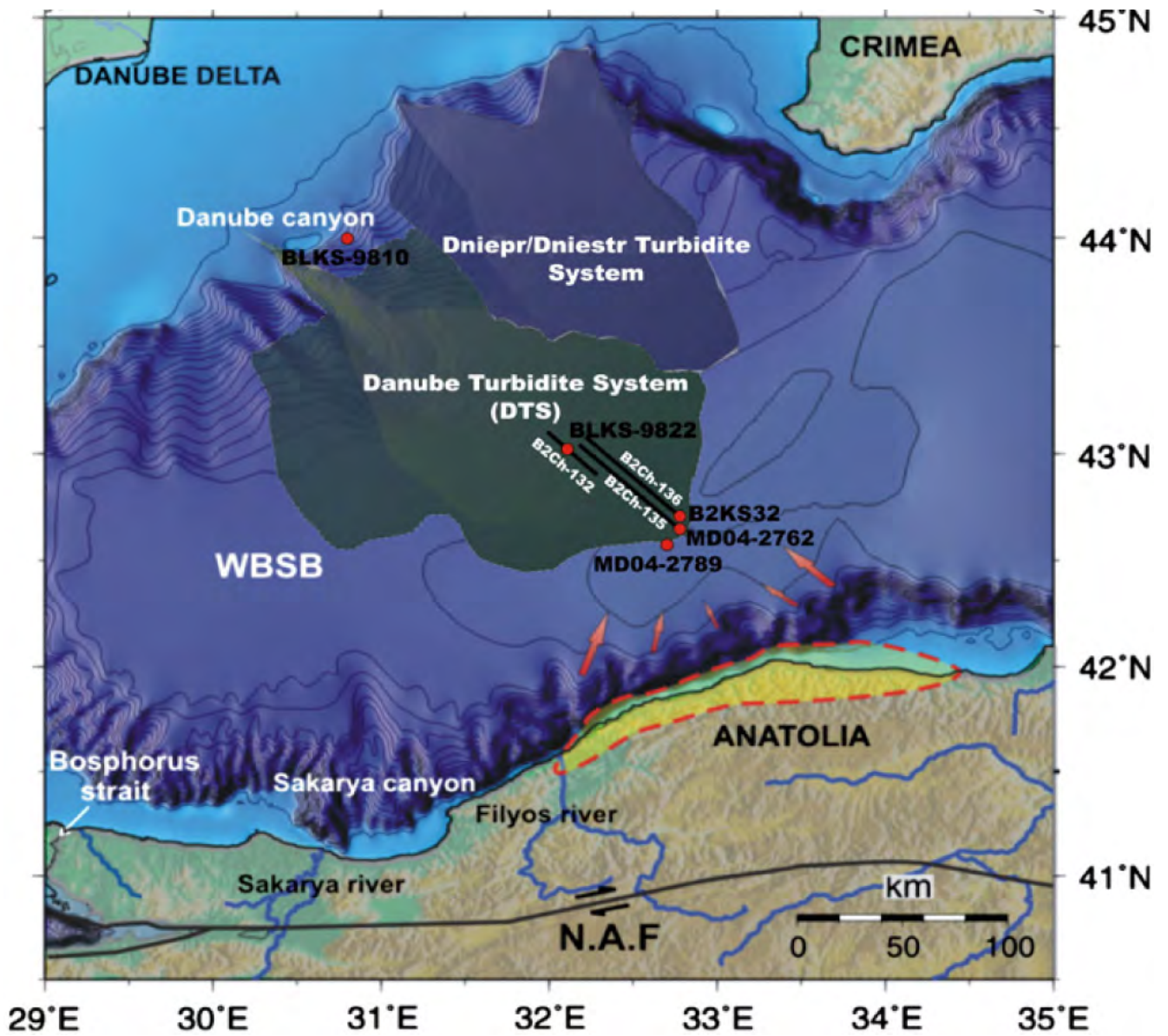


Figure 3. Extent of the Danube Turbidite System (DTS) and the Dniepr Turbidite System in the western Black Sea basin (From Lericolais et al, 2013, also includes locations of seismic lines and core positions from that paper).

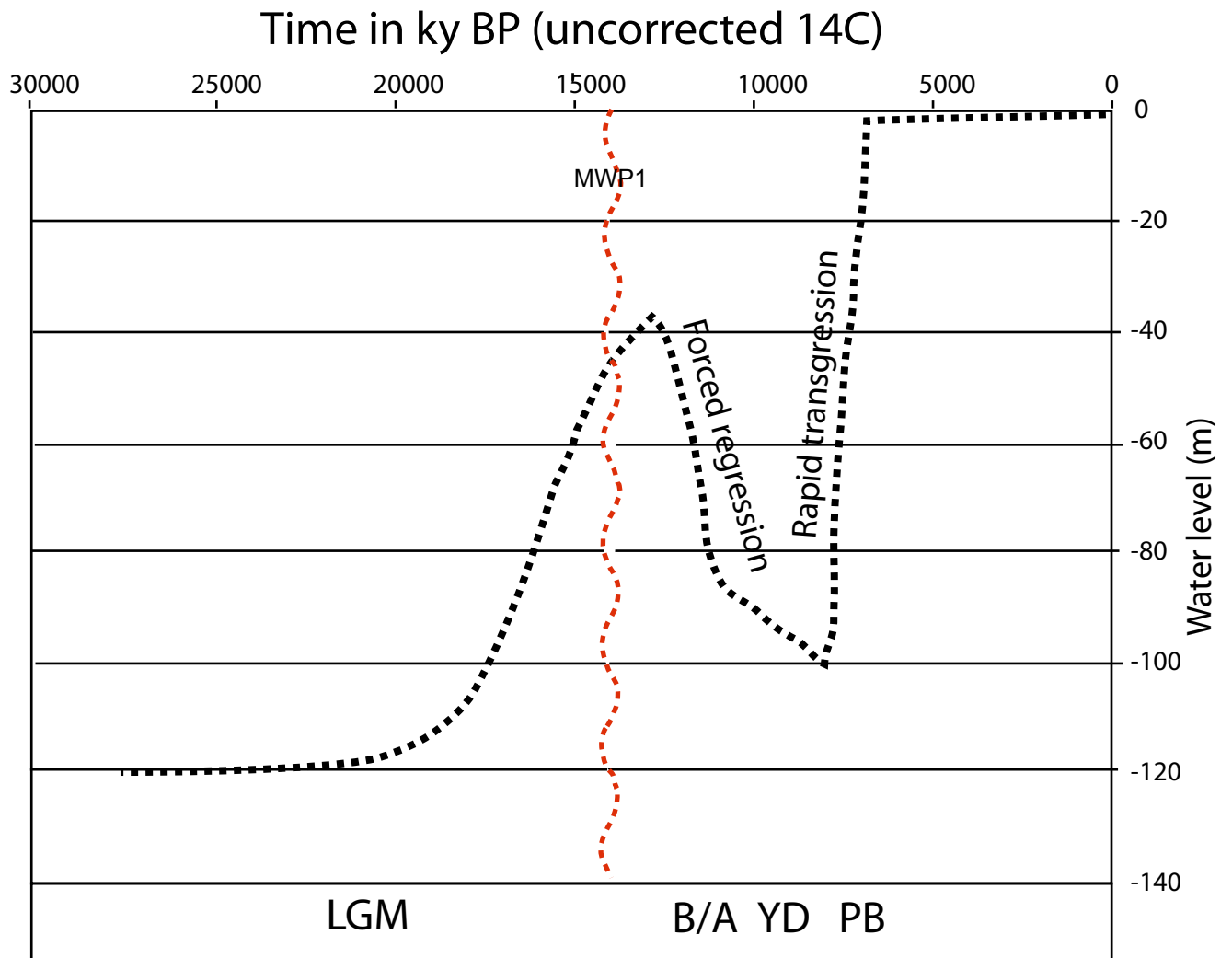


Figure 4. Water level fluctuation in the Black Sea since the Last Glacial maximum deduced from the observations recovered on the Northwestern Black Sea shelf. LGM=Last Glacial Maximum, B/A=Bølling-Allerød, MWP1=Melt Water Pulse 1a, YD=Younger Dryas, PB=PreBoreal. (After Lericolais et al., 2009).

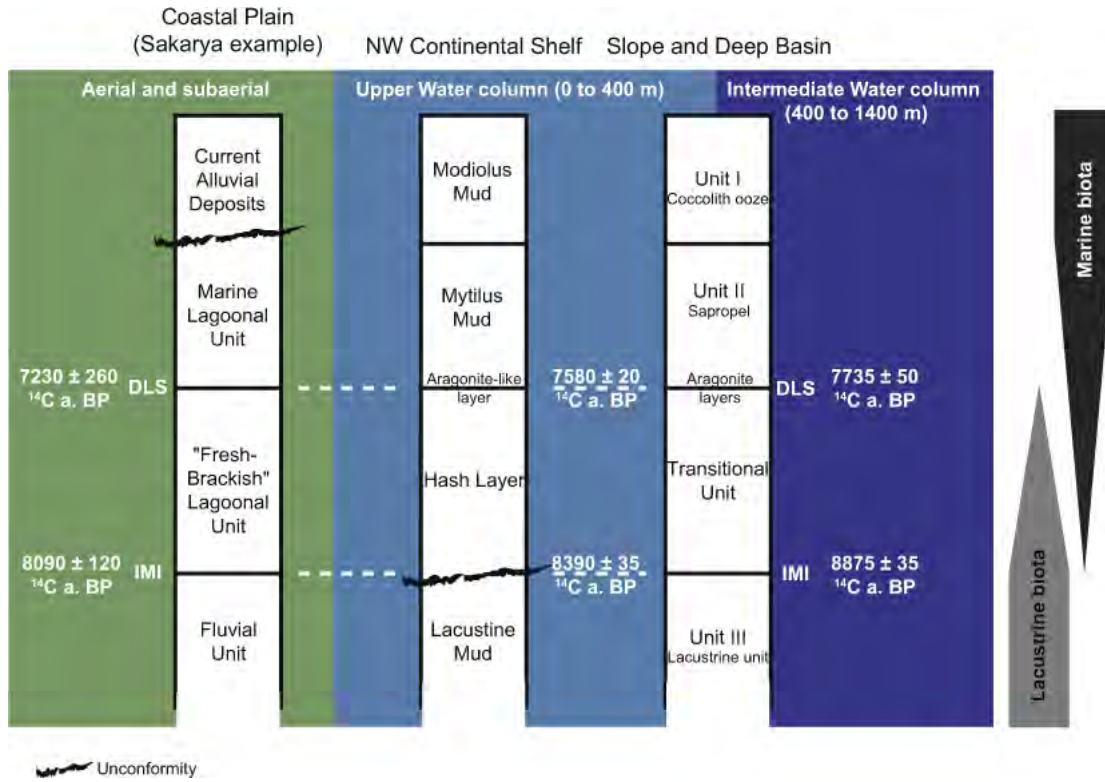


Figure 5. A synthesis of the sedimentary expressions and radiocarbon ages of the Initial Marine Inflow (IMI) and the Disappearance of Lacustrine Species (DLS) boundaries following Black Sea geomorphologic environments and water depths. (From Soulet et al., 2011).



Figure 6. Photo from South Stream dive No.122 showing the vertical distribution of sediments in the deep black sea: although often accumulated in hollows on the seabed, the proto-white laminae layer (creamy-white material) overlies the pale brown seafloor sediment, and is itself overlain by the dark area of flocs.

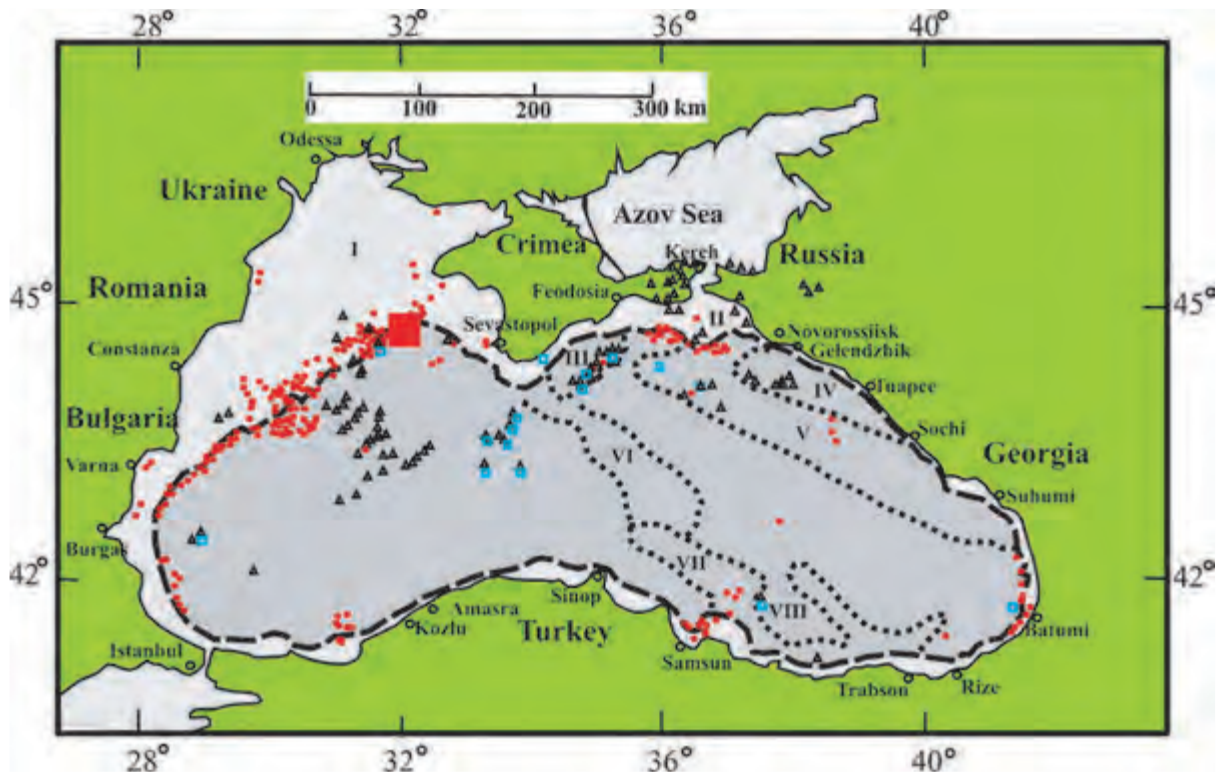


Figure 7. Location of the mud volcanoes gas seeps and gas hydrates in the Black Sea . (Adapted from Starostenko et al., 2010).

Figure key:

- Triangles in black: mud volcanoes
- Circles in red: gas seeps
- Squares in ice blue: gas hydrate
- Bold dashed lines in black: shelf edge
- Bold squared lines: boundaries of tectonic units
- Filled rectangular in red: Dnipro palaeo-delta area

- I: NW Shelf
- II: Kerch-Taman trough
- III: Sorokin trough
- IV: Tuapse trough
- V: Shatsky ridge
- VI: Andrusov ridge
- VII: Arkhangelsky ridge
- VIII: Giresuan basin

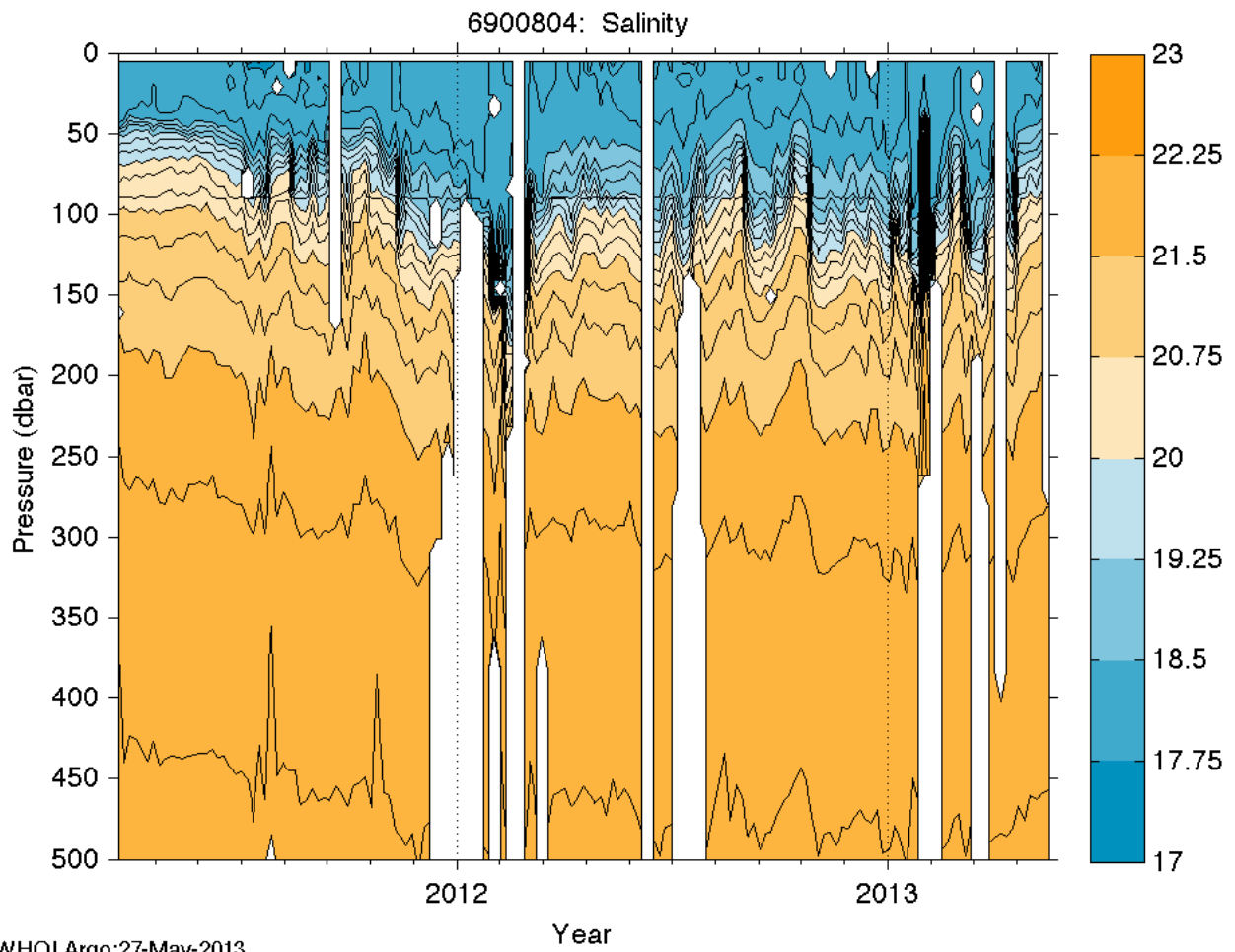
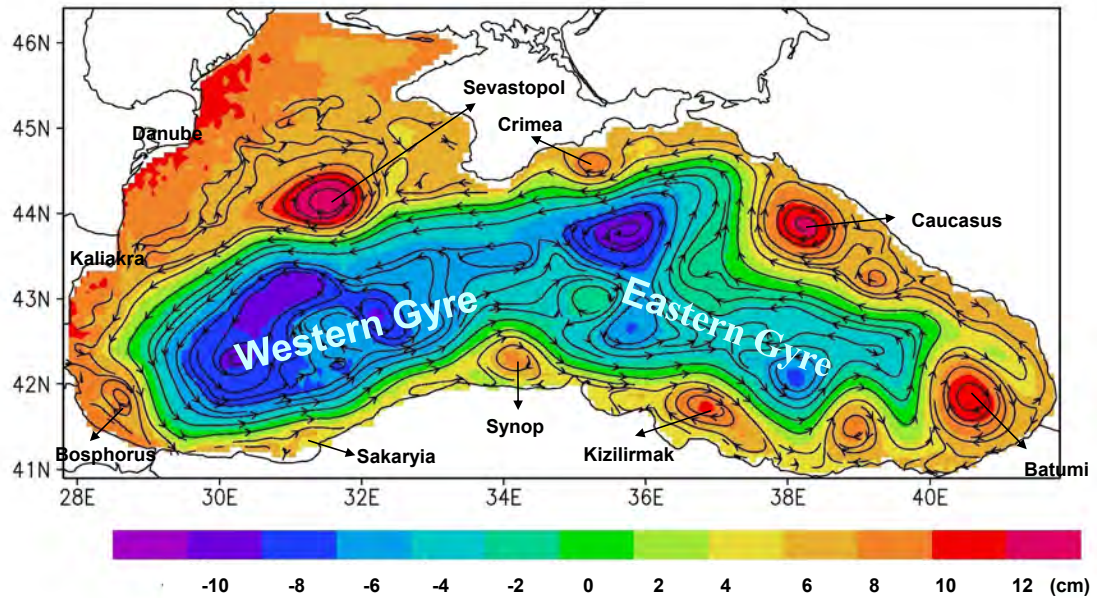


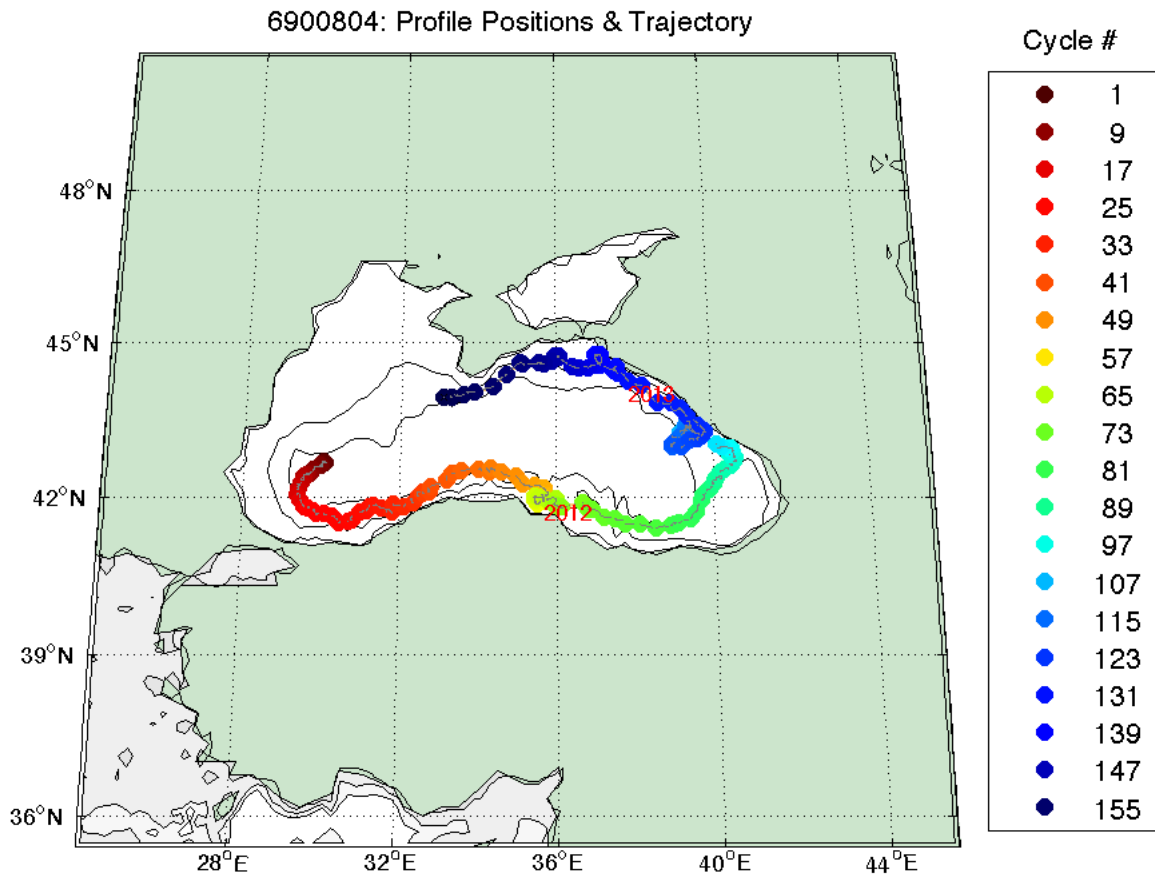
Figure 8 Salinity profile for the upper ~500 metres of the Black Sea as derived from ARGO float No 6900804 that has been traversing the Black Sea since 2011.

Two-gyre circulation plus anticyclonic coastal circulation



Seasonal amplitude of sea level: ~10 cm,
winter intensification of circulation

Figure 9. Surface water circulation in the Black Sea. Note Rim Current that circulates around the combined eastern and western gyres and the coastal eddies. (From Stanev and Grayek - presentation made to 2nd COSS-TT International Coordination Workshop 04-07 February 2013, Lecce, Italy).



WHOI Argo:27-May-2013

Figure 10. Trajectory of ARGO float 6900804 from March 2011 to May 2013

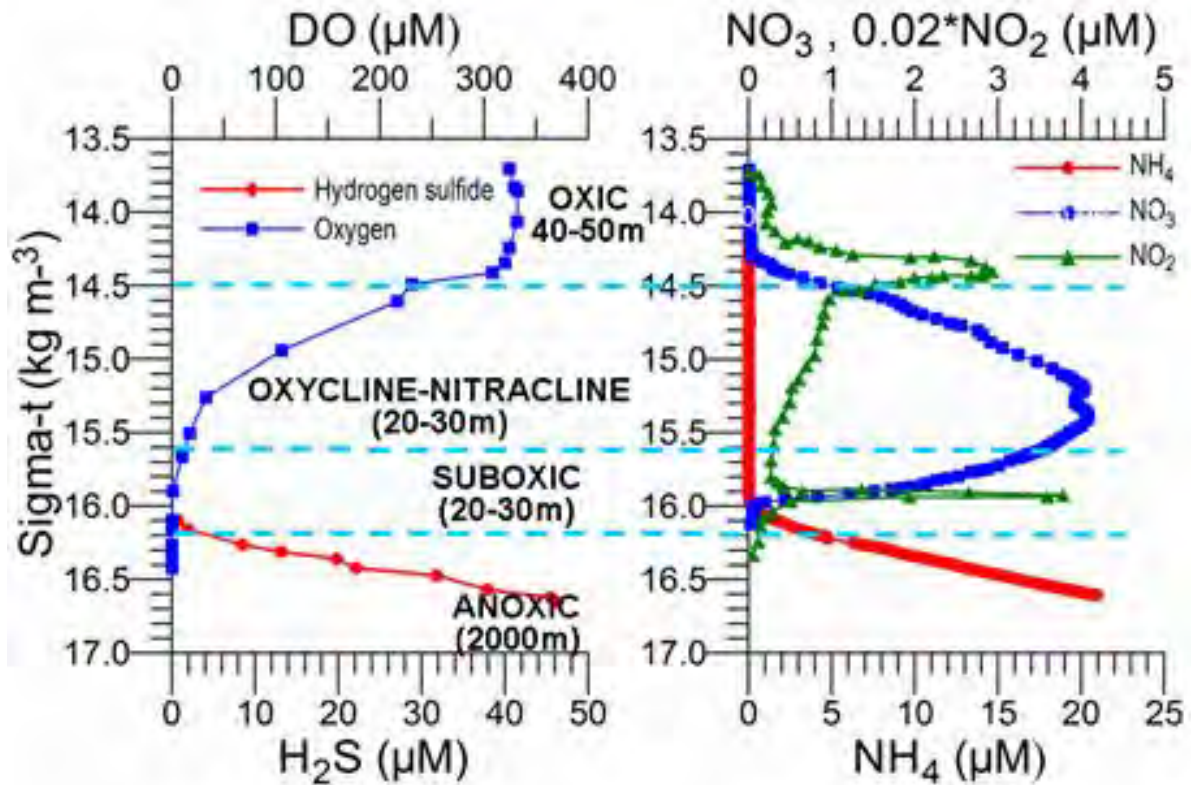


Figure 11. Oxygen and Hydrogen sulphide profiles (left) and NO_3 , NO_2 and NH_4 profiles (right) versus density expressed in $\sigma\text{-t}$ (kg m^{-3}) in the center of the eastern gyre of the Black Sea during May 2003. ($\sigma\text{-t}$ = density of seawater at a given temperature. $\sigma\text{-t}$ is defined as $\rho(\text{S},\text{T}) - 1000 \text{ kg m}^{-3}$, where $\rho(\text{S},\text{T})$ is the density of a sample of seawater at temperature T and salinity S, measured in kg m^{-3} , at standard atmospheric pressure). Approximate thicknesses of each layer are given in the figure. (From Orguz, 2009)

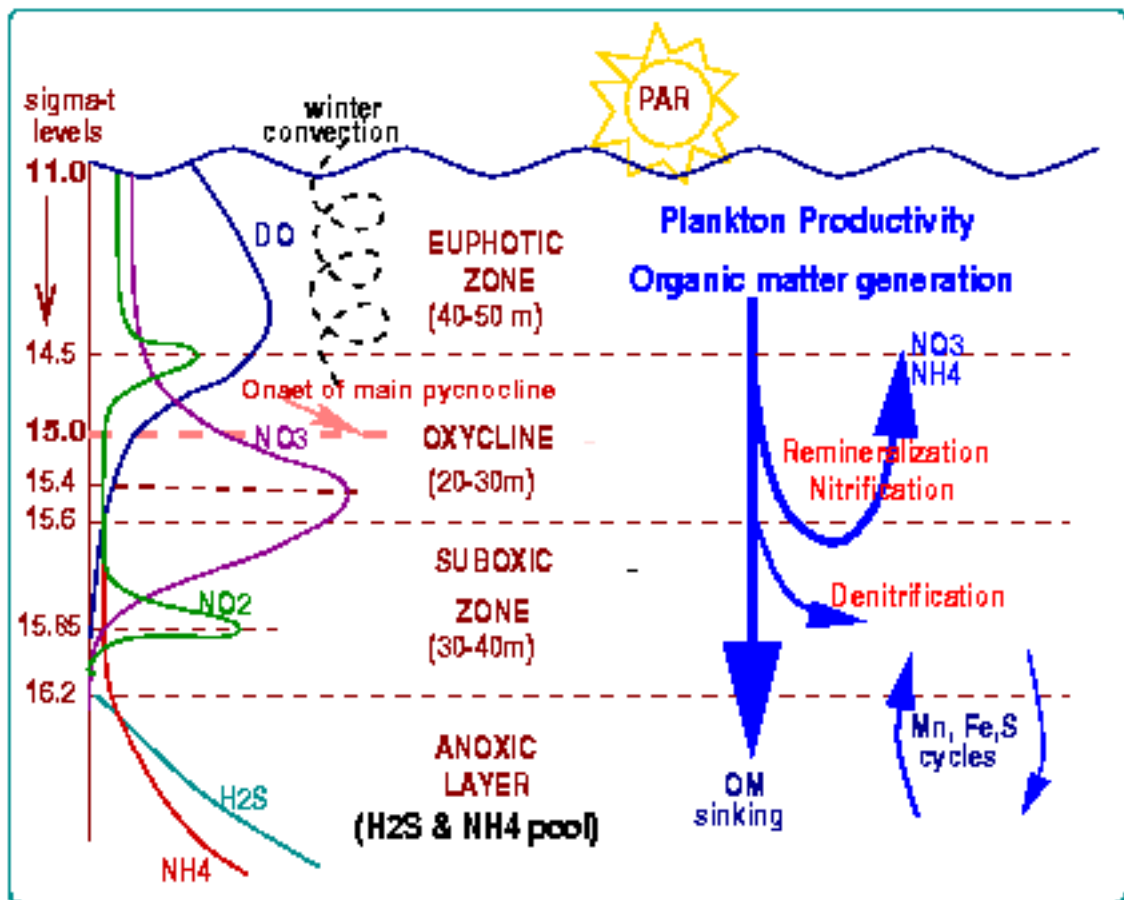


Figure 12. Vertical biogeochemical structure of the Black Sea. (From <http://www.ims.metu.edu.tr/cv/oguz/bio-pump.htm>. Accessed 09/08/2013)



Figure 13. Image of a microbial tower (reef) structure. Methane gas bubbles seeping from a microbial reef at 250 m depth in the northwest Black Sea. ©MARUM – Center for Marine Environmental Sciences, University of Bremen.

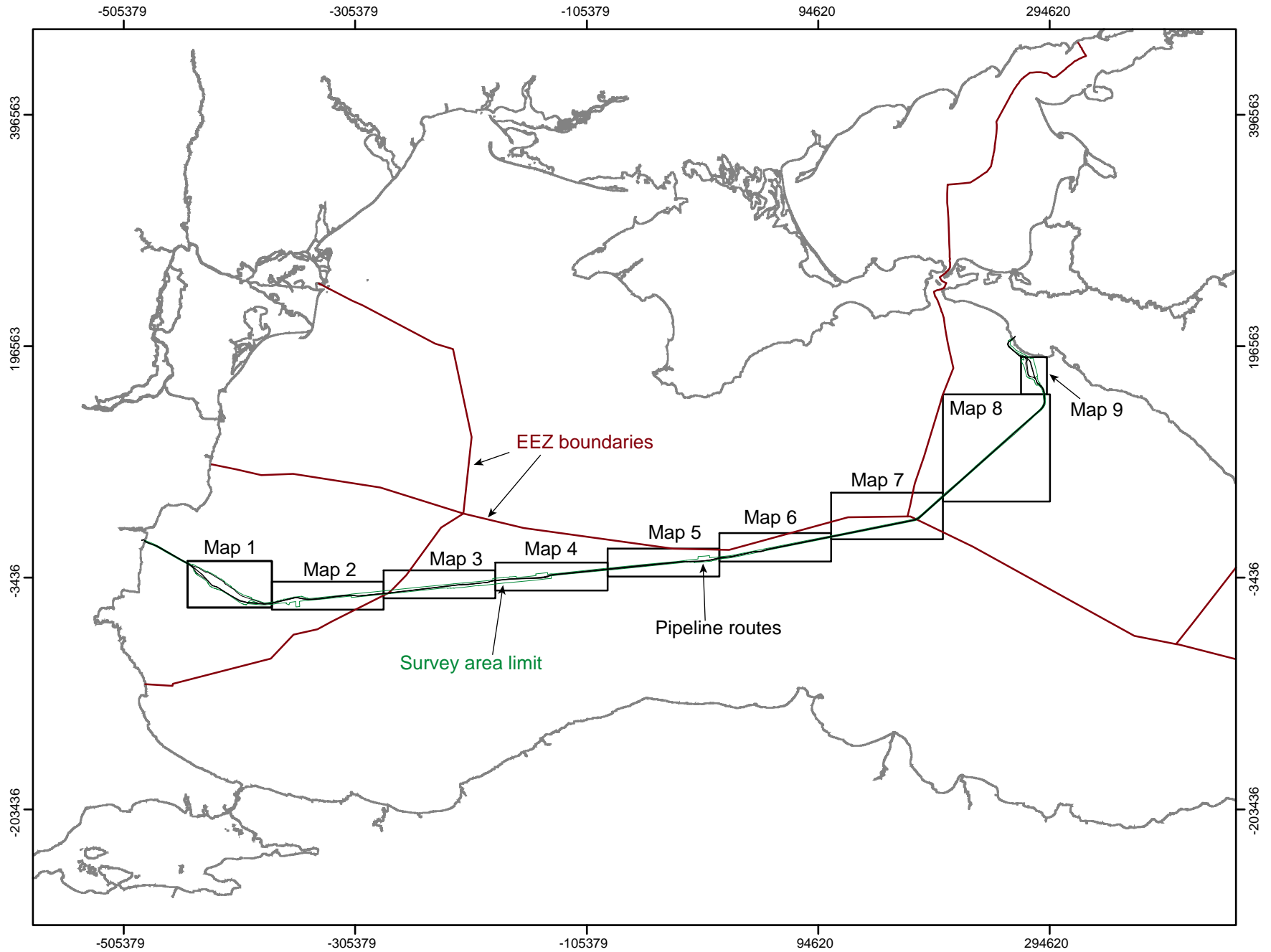


Fig. 14. Map showing location of pipeline route, EEZ boundaries and locations of interpretative maps shown in figures 15-23.

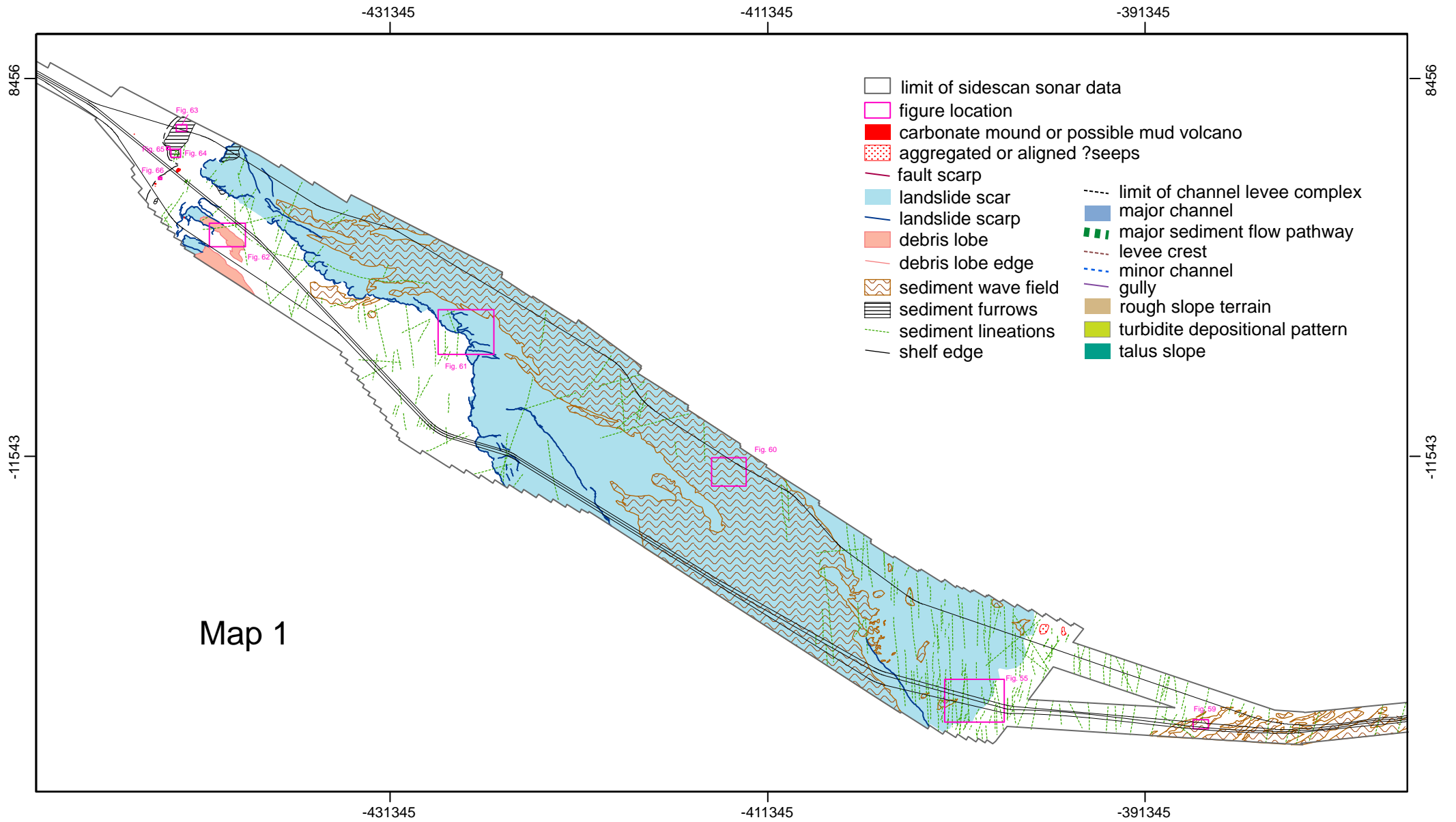
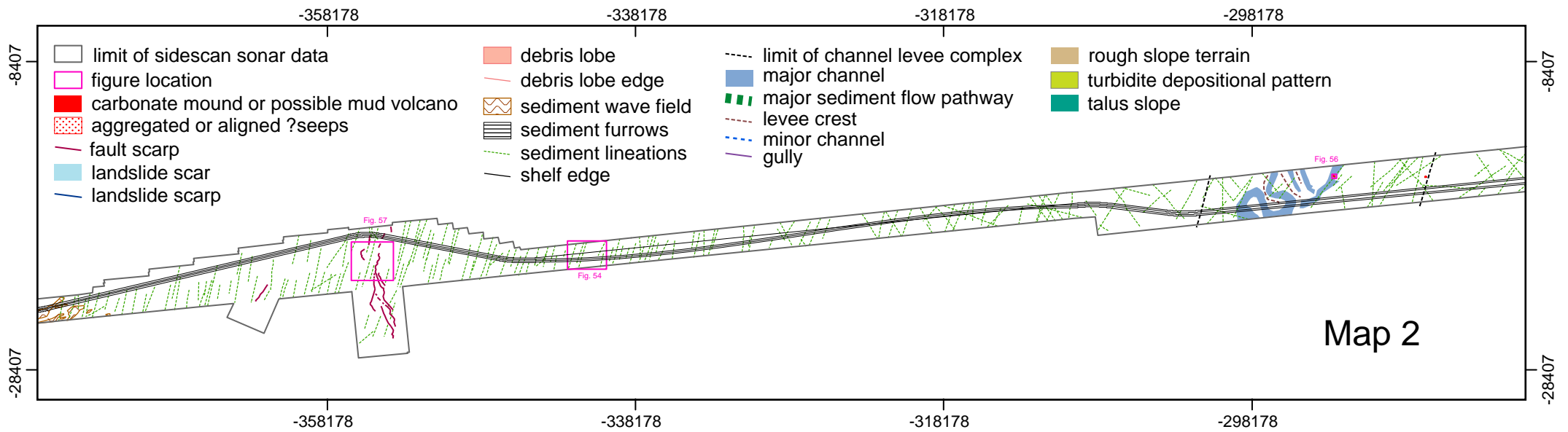


Figure 15. Summary interpretation of features on the Bulgarian slope. For location see figure 14.



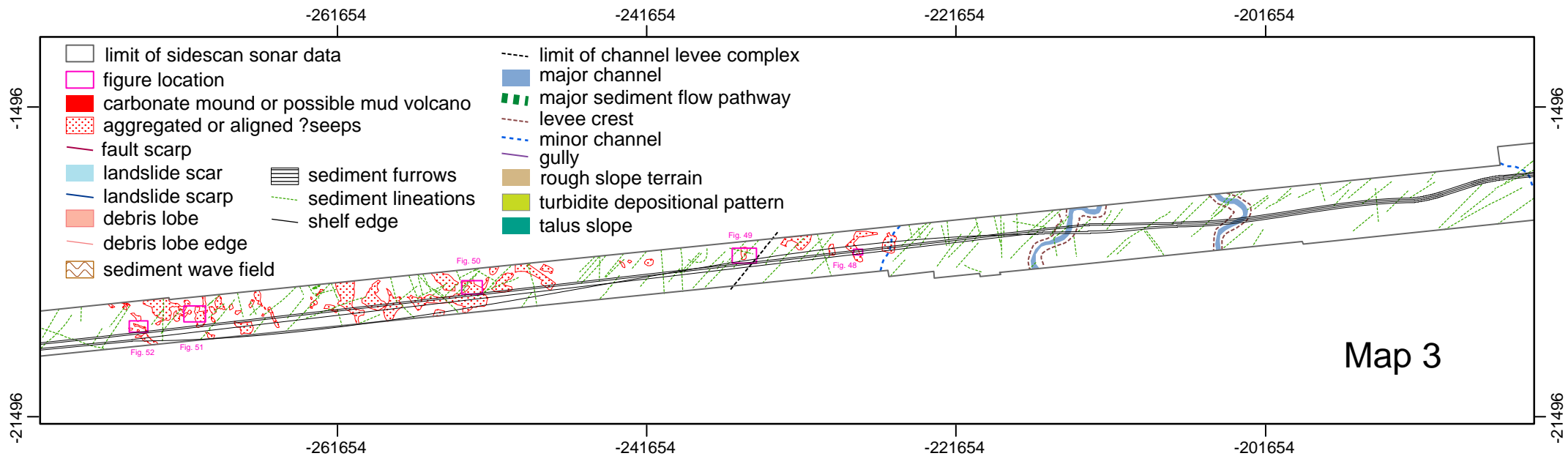


Figure 17. Summary interpretation of features on the western Turkish Abyssal Plain. For location see figure 14.

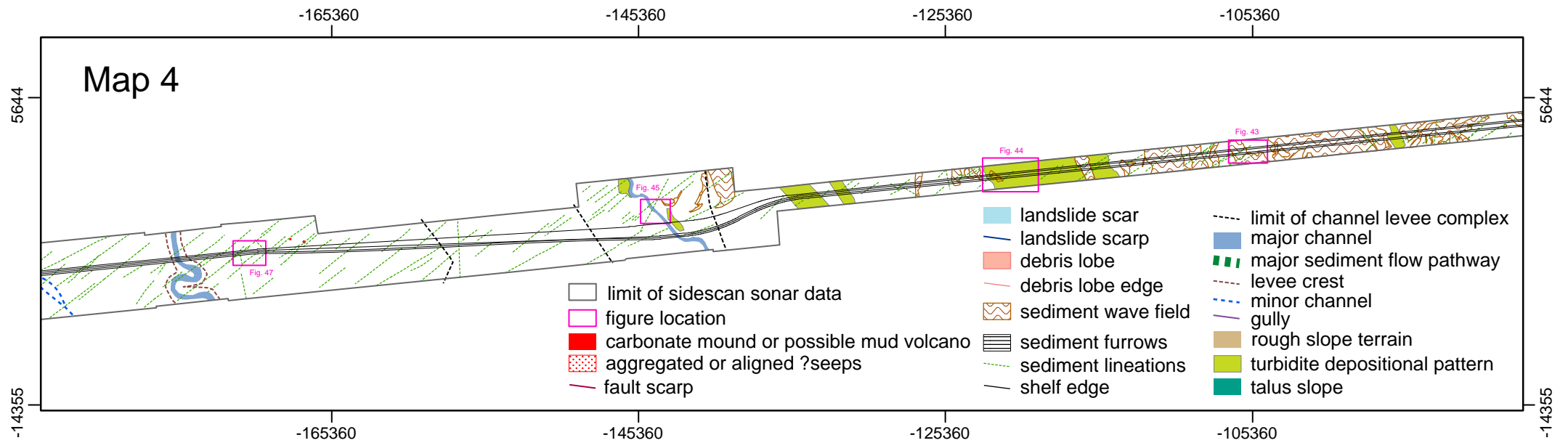


Figure 18. Summary interpretation of features on the central Turkish Abyssal Plain. For location see figure 14.

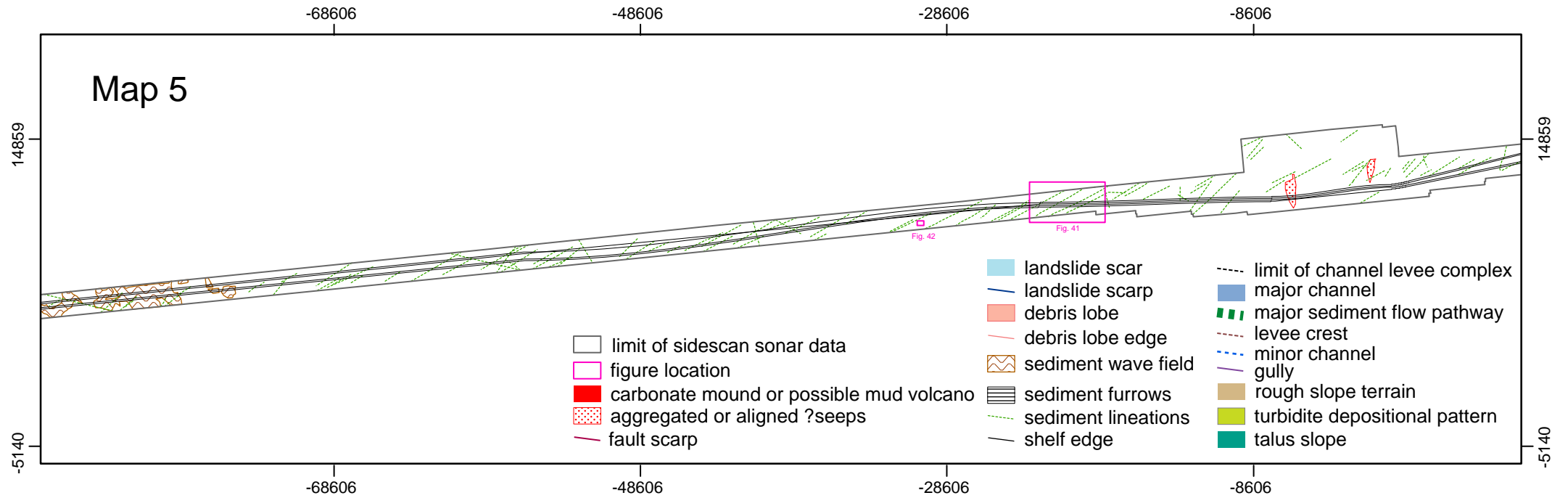


Figure 19. Summary interpretaion of features on the eastern Turkish Abyssal Plain. For location see figure 14.

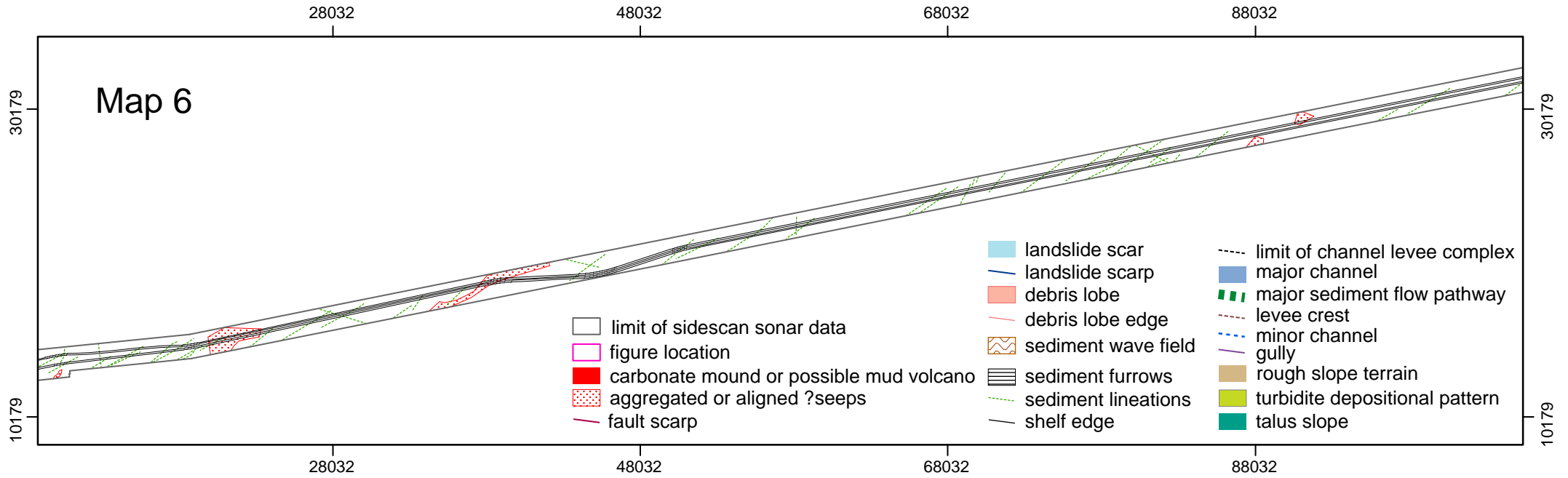


Figure 20. Summary interpretaion of features on the eastern Turkish Abyssal Plain. For location see figure 14.

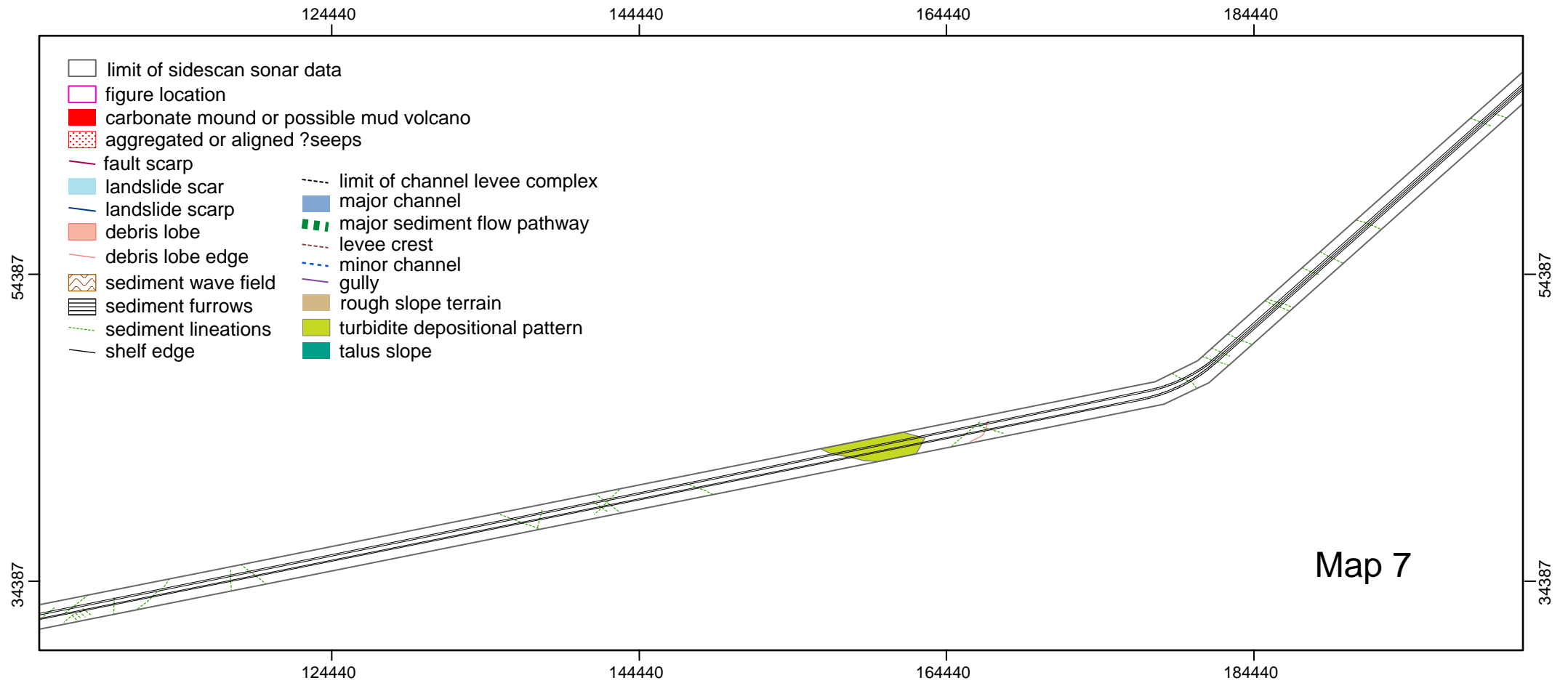
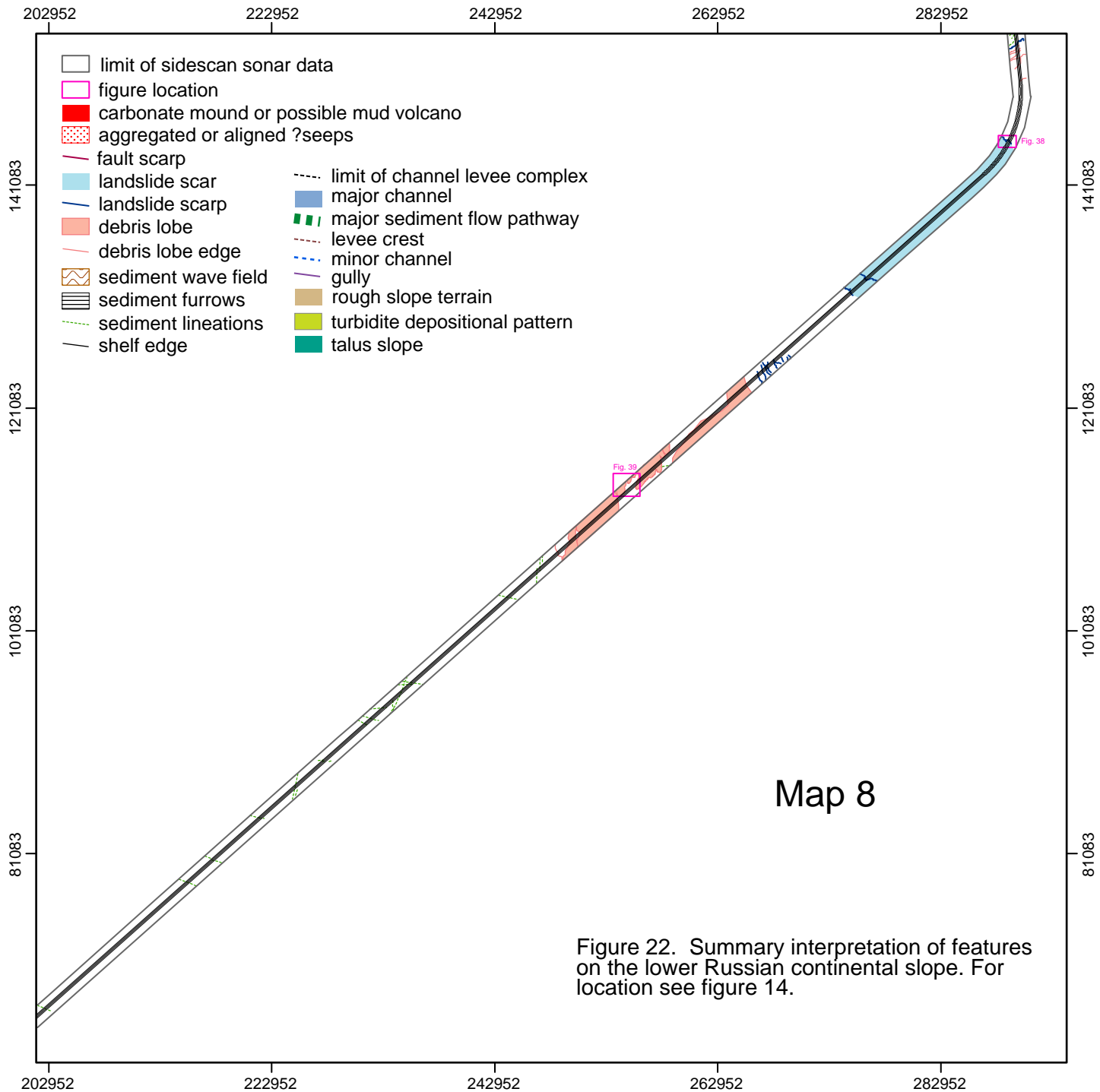


Figure 21. Summary interpretation of features on the eastern part of the Turkish Abyssal Plain and the Russian Abyssal Plain. For location see figure 14.



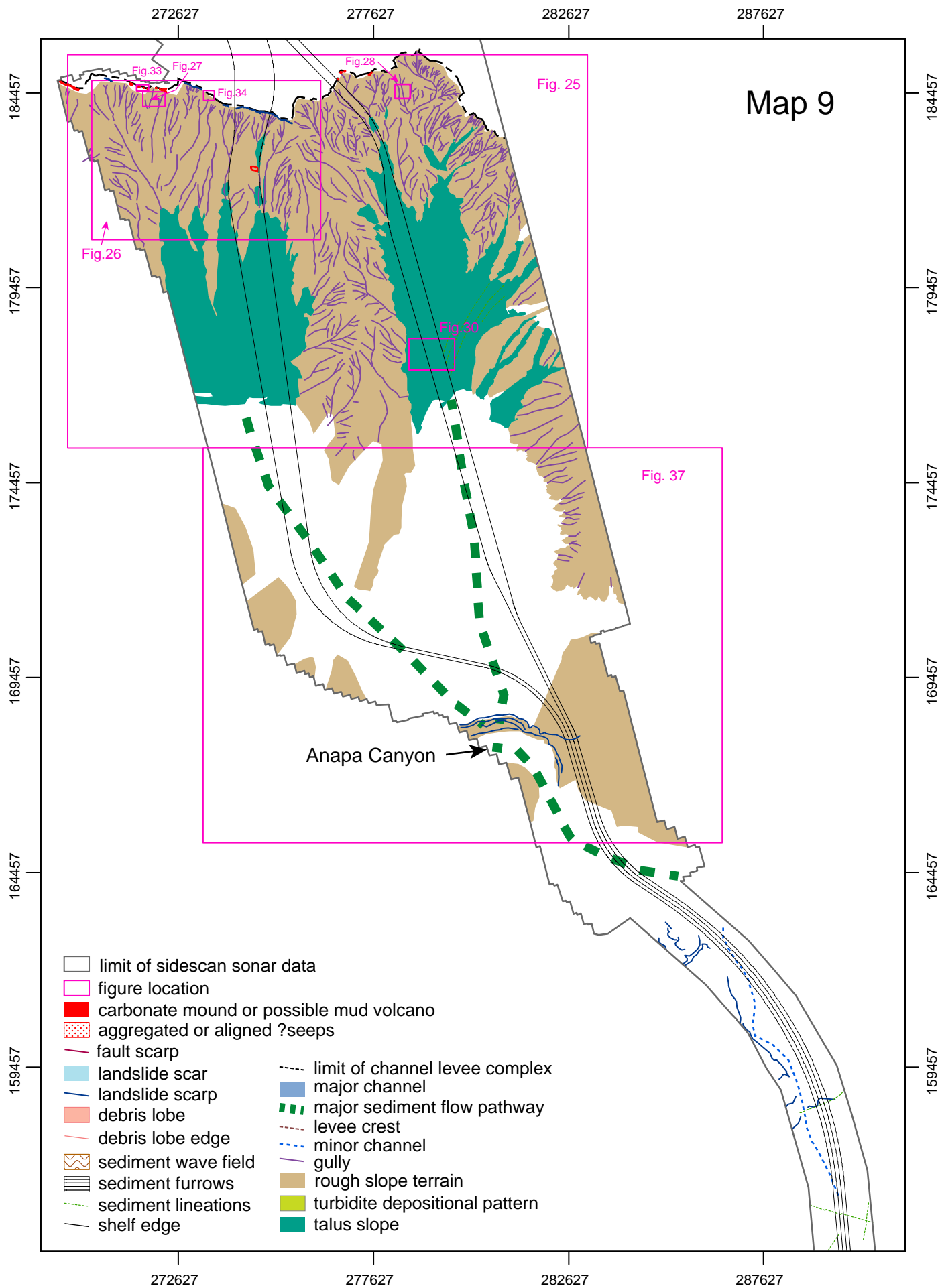


Figure 23. Summary interpretation of features on the upper Russian slope. For location see figure 14.

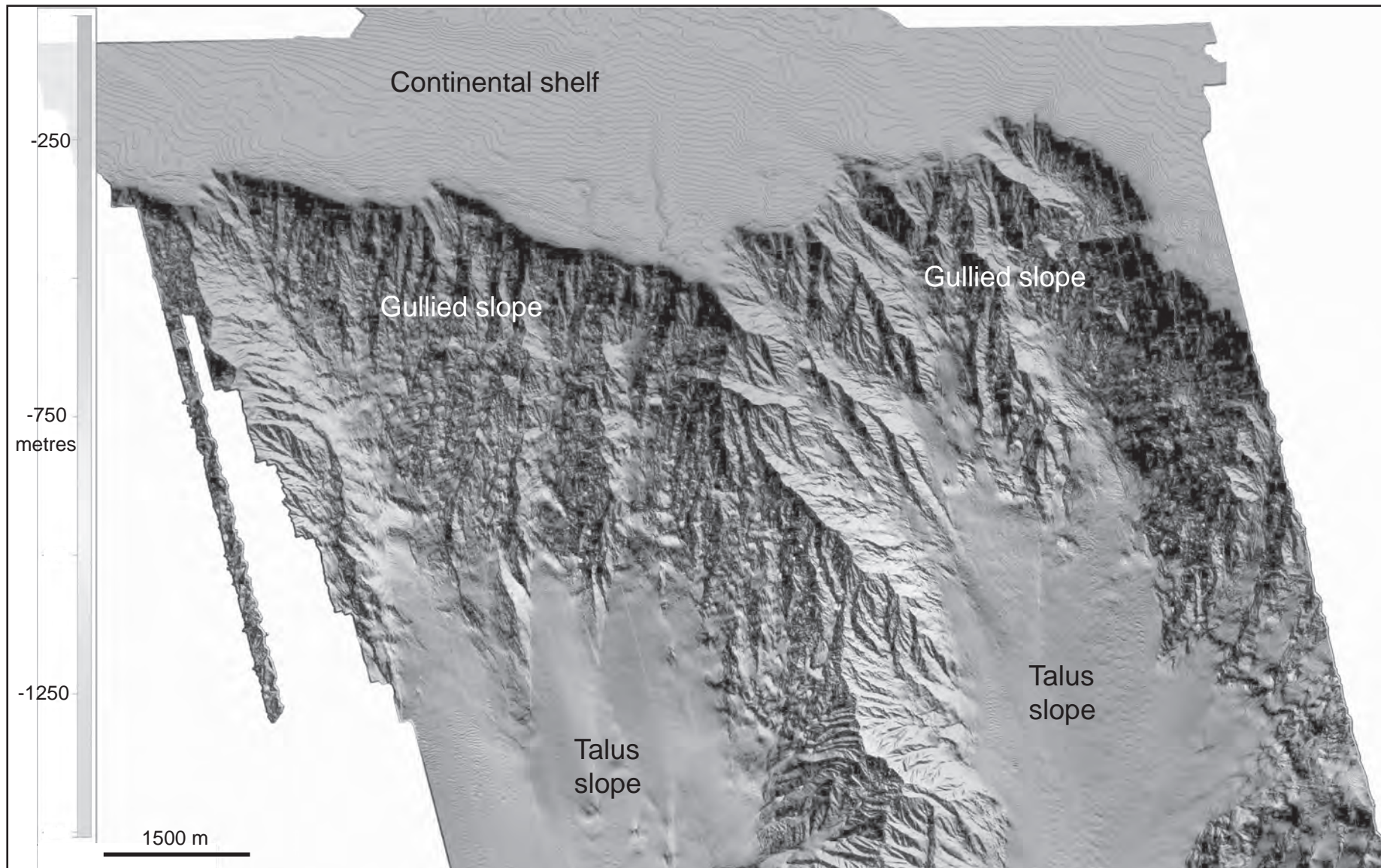


Figure 24. 3D representation of the upper Russian slope showing the rugged gullied topography feeding downslope into steep talus fans. For location see figure 23.

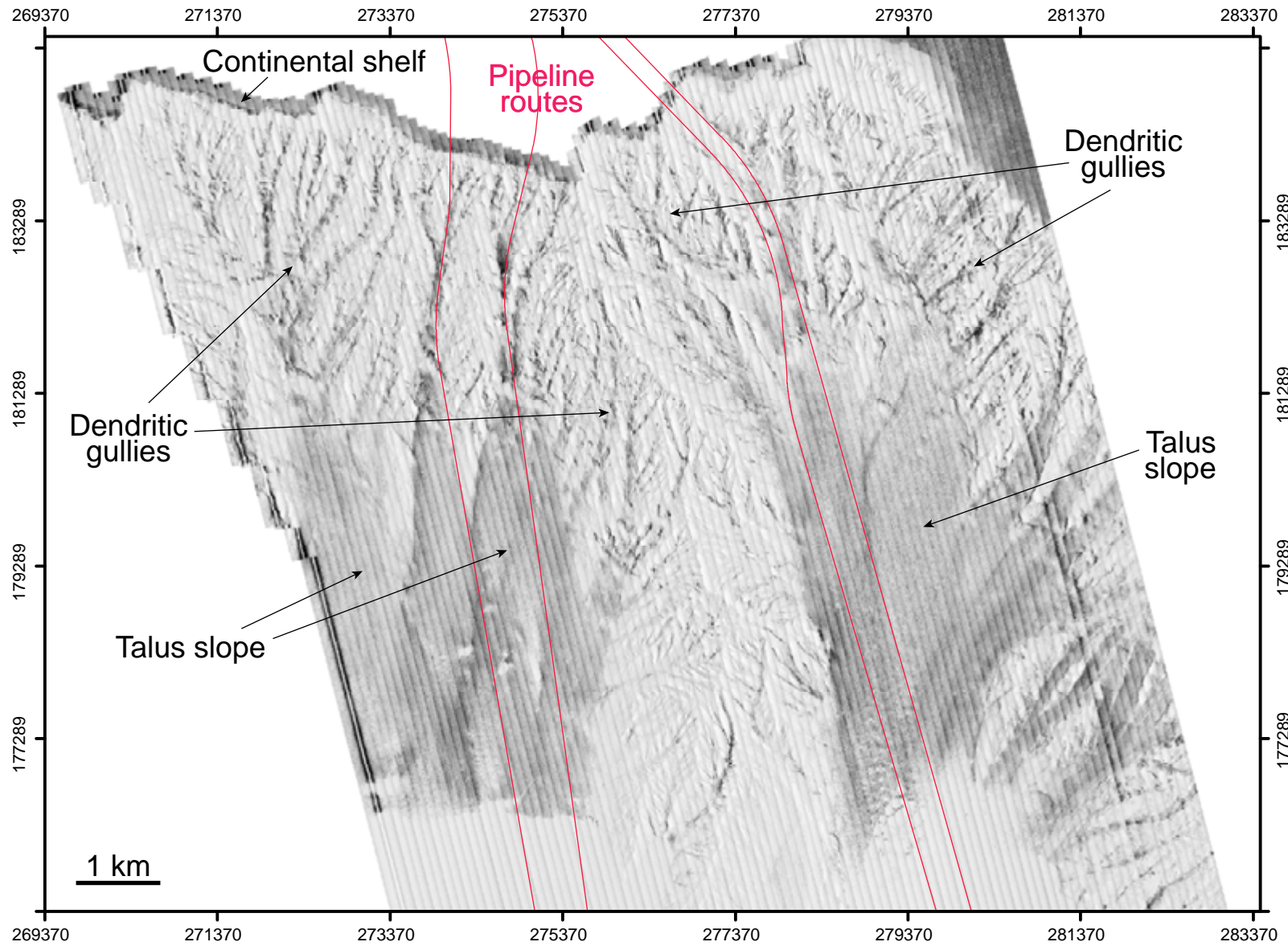


Figure 25. Overview of sidescan sonar data from the upper Russian continental slope showing the dendritic gully systems and talus slopes, the latter picked out by high (dark) backscatter. For location see figure 23.

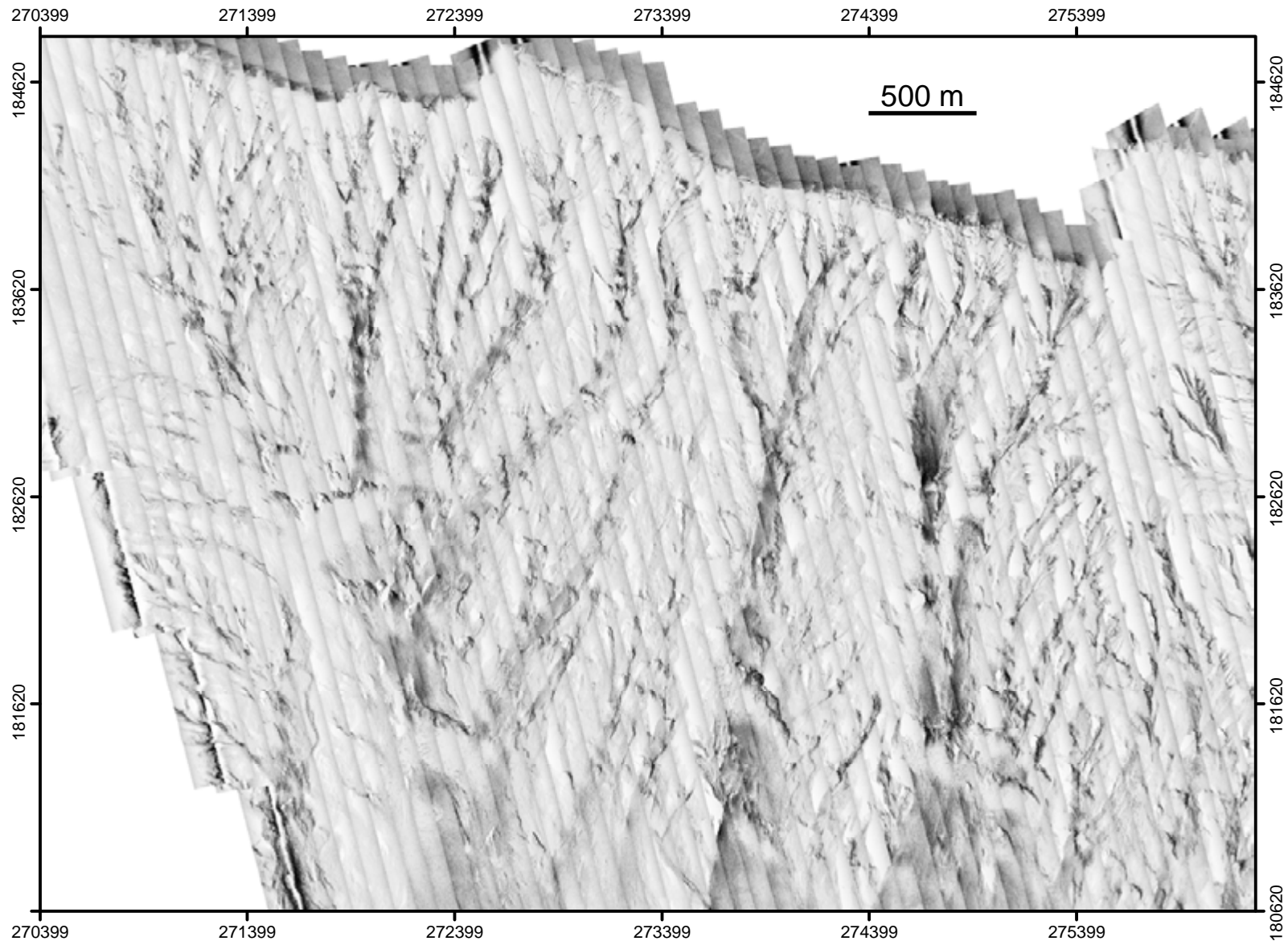


Figure 26. Sidescan sonar image of dendritic gully systems on the upper Russian slope. For location see figure 23.

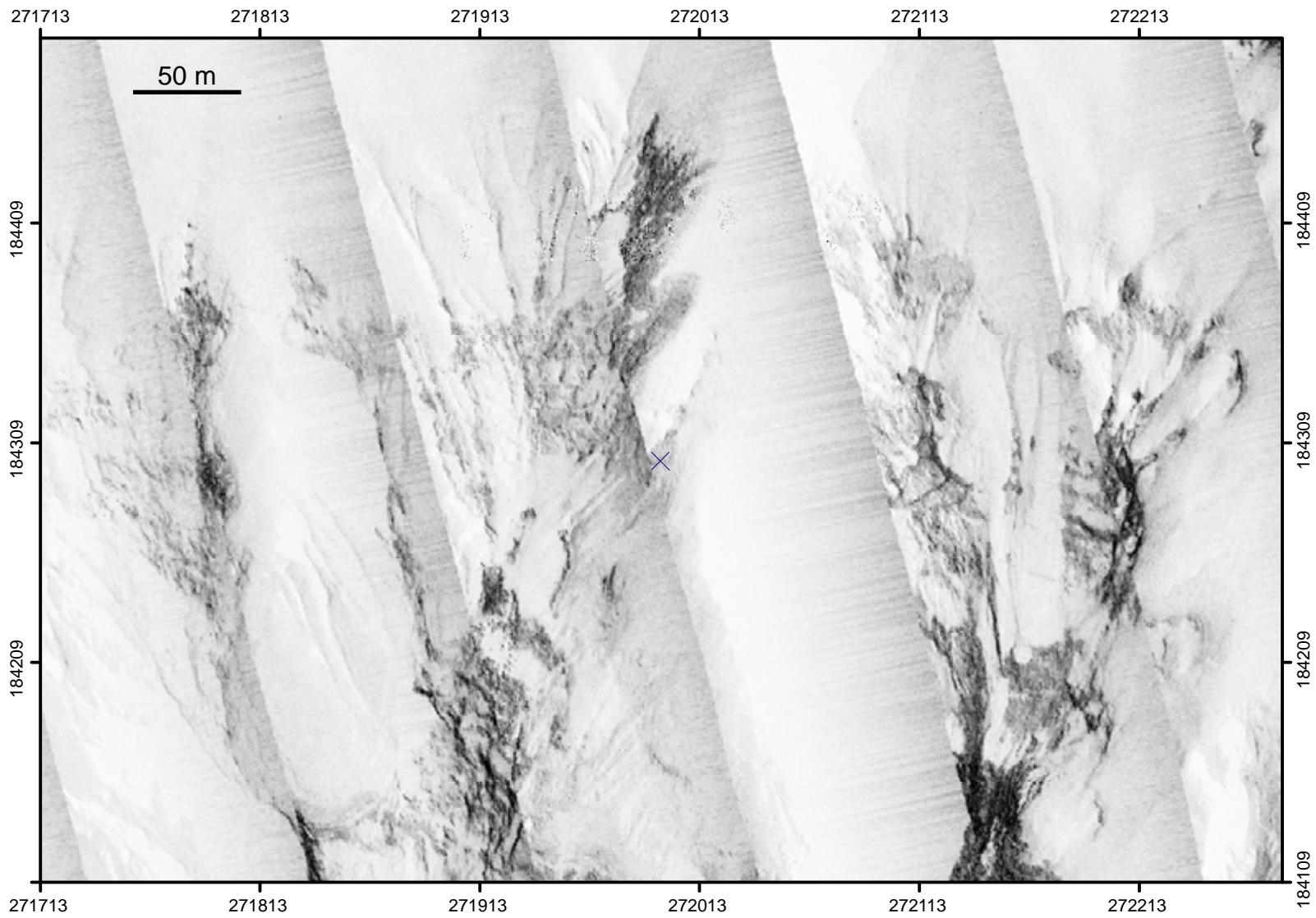


Figure 27. Detail of sidescan sonar data from the upper Russian slope showing the upslope part of a dendritic gully system. Note high backscatter in the gully axis, indicating coarse sediment. Gullies either terminate upslope in a distinct headwall, indicating headward erosion, or simply fade out, suggesting a stable system. For location see figure 23.

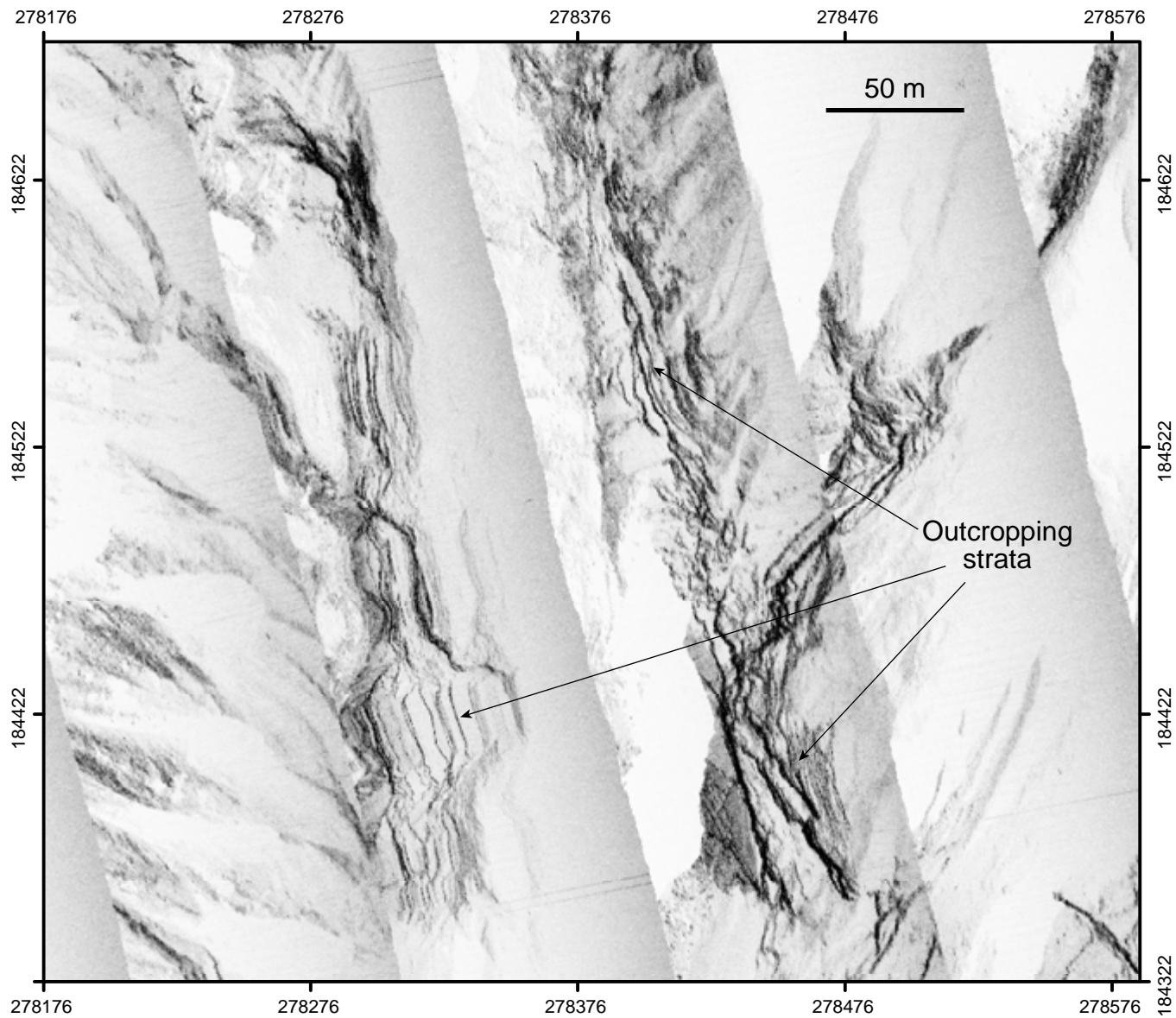


Figure 28. Sidescan sonar image showing outcropping strata along gully walls on the upper Russian slope. For location see Figure 23.



Figure 29. (a) and (b). Still images derived from ROV videos of large angular boulders on the upper Russian slope. (c) image showing the edge of an upper slope gully. Water depth and location are given on each image.

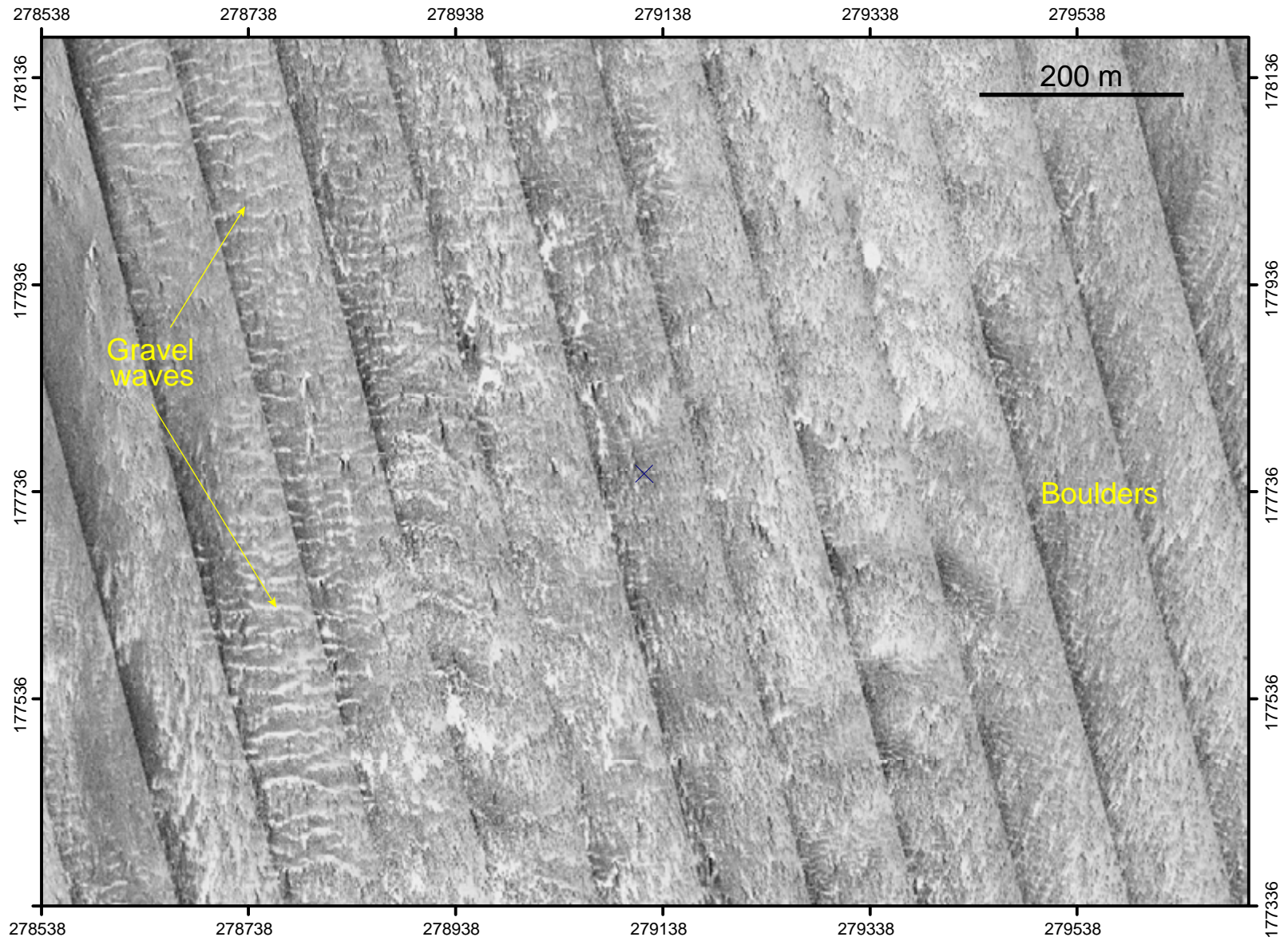


Figure 30. Sidescan sonar image showing gravel waves and boulders on the surface of the talus slope on the upper Russian slope. For location see Figure 23.



Figure 31. Still images derived from ROV video of metre sized boulders on the talus slope on the upper Russian slope. These are large enough to be visible on sidescan sonar data (Figure 30). Depth and location are given on

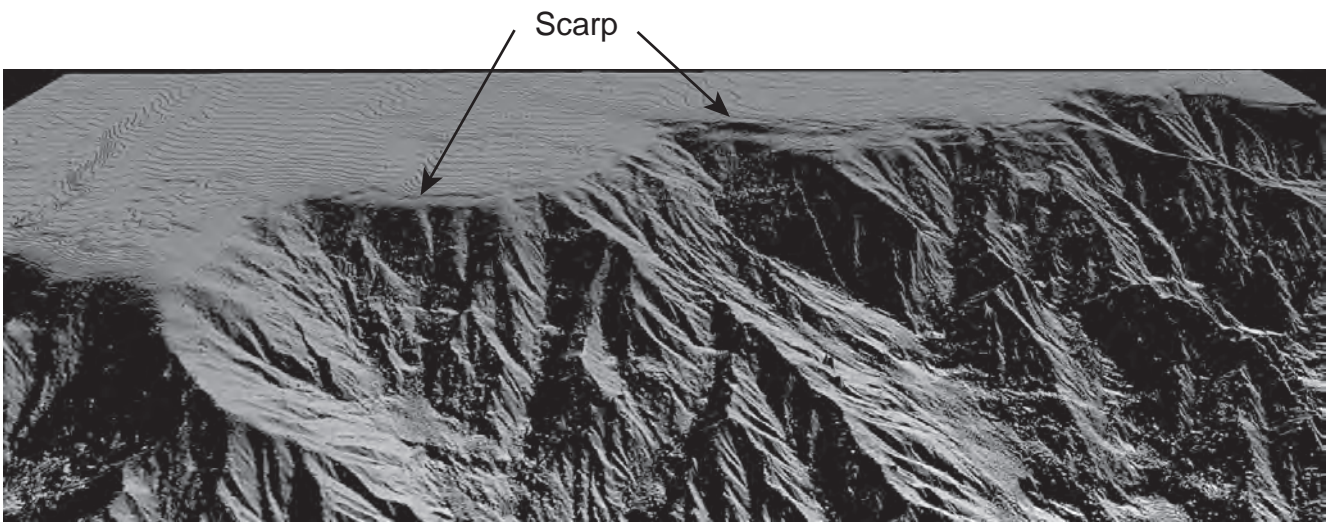


Figure 32. 3D bathymetric image showing a small intermittent escarpment that extends along the edge of the Russian shelf.

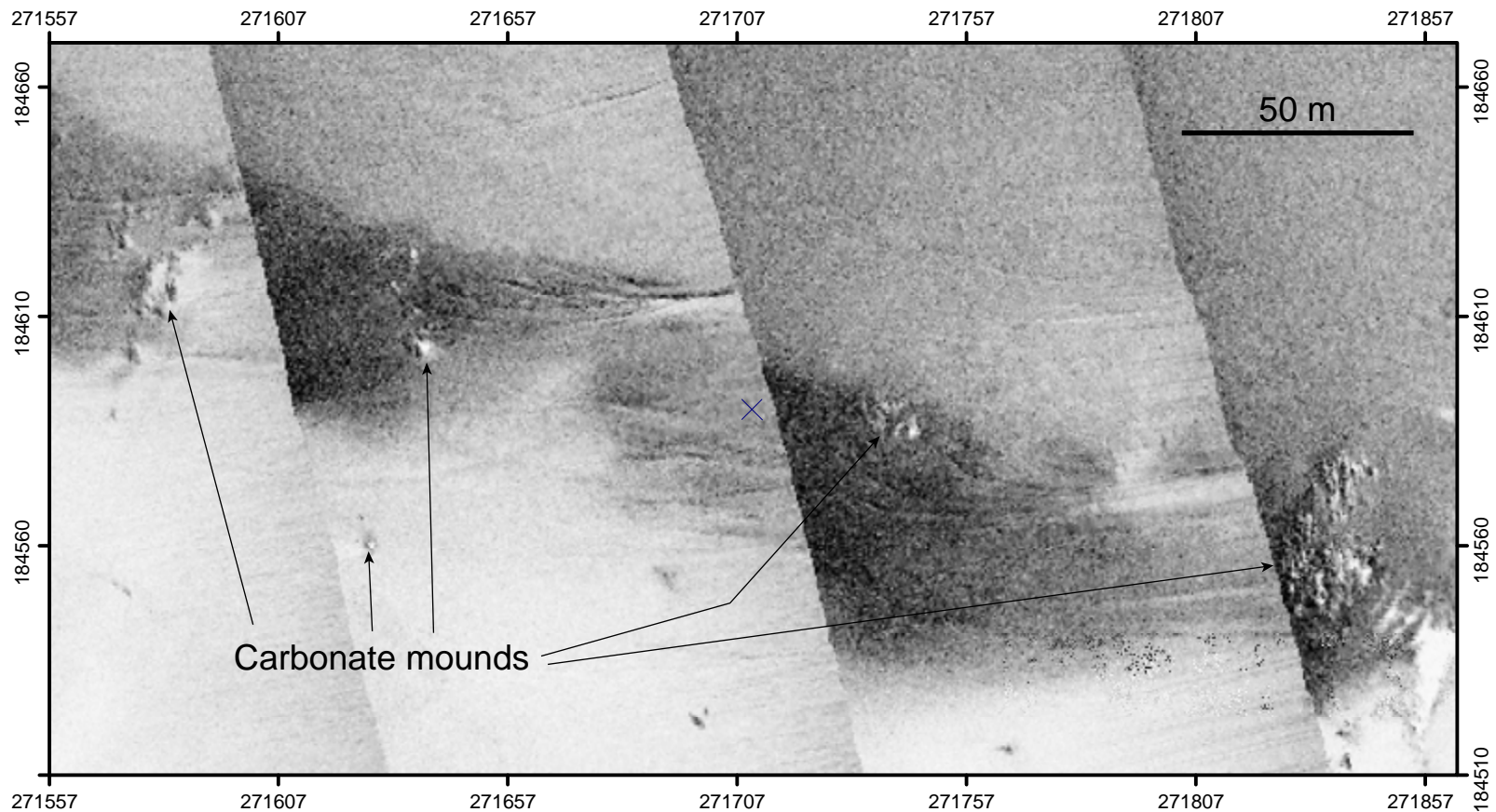


Figure 33. Sidescan sonar image of small carbonate mounds on the uppermost Russian slope. Water depth around 120 m. Video data has not been obtained from these features, but they are identified by comparison with similar features on the Bulgarian slope, where video evidence confirms the identification. For location see figure 23.

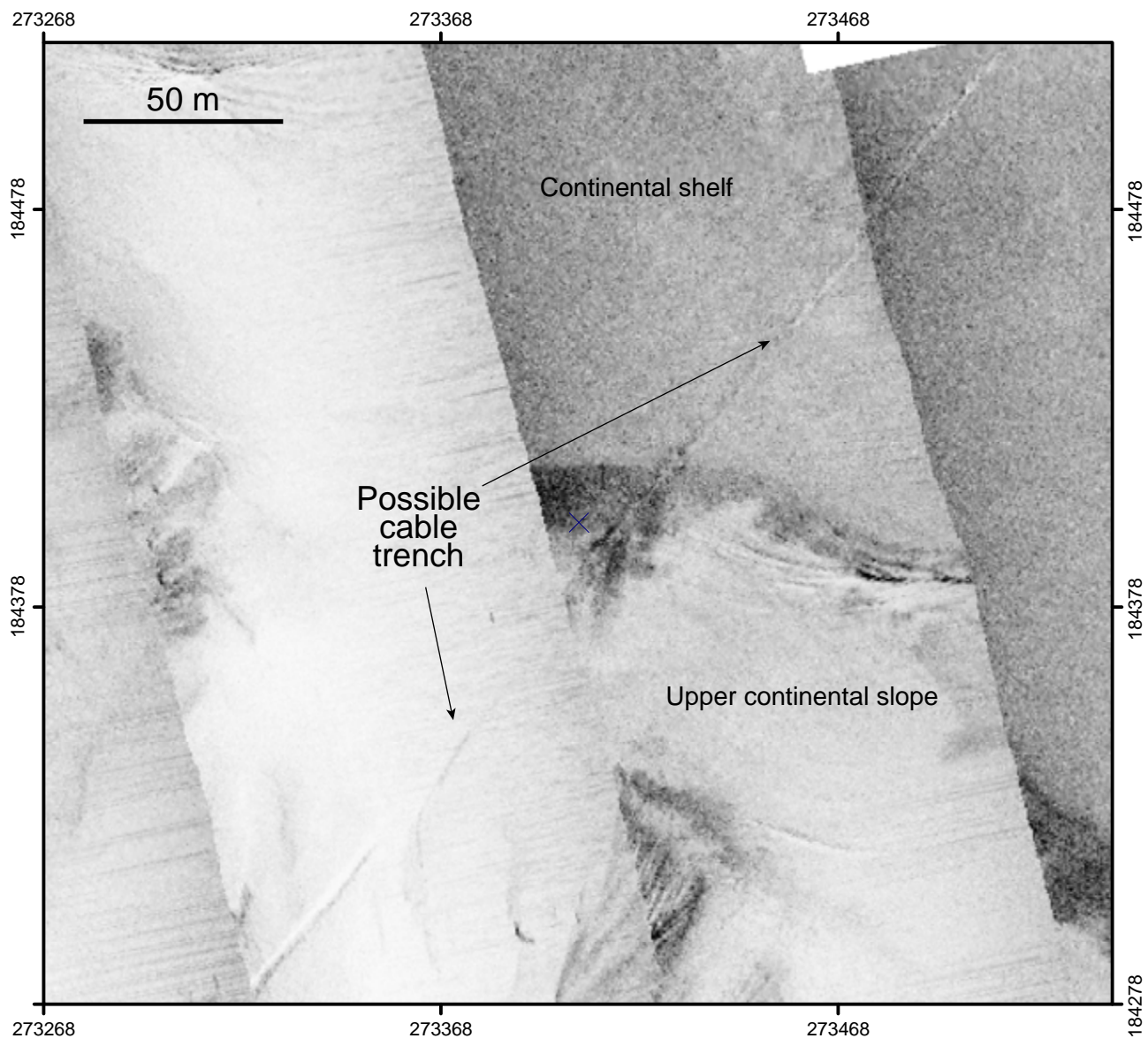


Figure 34. Sidescan sonar image of probable cable trench crossing the Russian shelf edge. For location see figure 23.



(a)



(b)



(c)

Figure 35. Photographs of submarine cables, derived from ROV video, on the Russian slope. (a) and (b). Intact cable suspended above the seabed due to the rough topography. (c) contorted cable wrapped around large boulder. It is not known whether this is the result of cable destruction by a landslide, or whether it is a discarded piece of old cable dumped on the seabed.

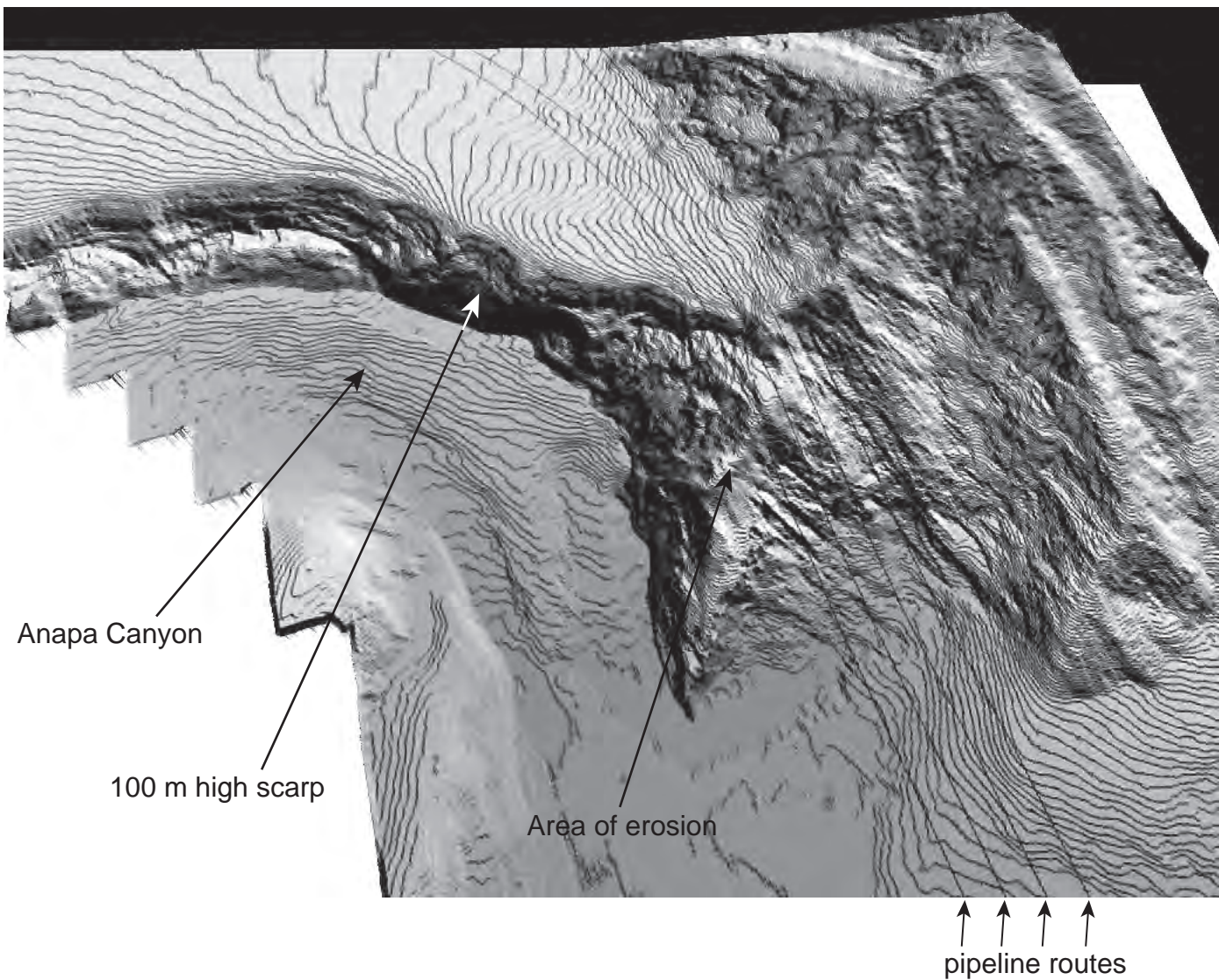


Figure 36. 3D perspective view of bathymetry data from the area where the Anapa Canyon intersects the pipeline route. Note the area of erosion probably caused by flows overtopping the canyon wall at the sharp bend in the canyon pathway.

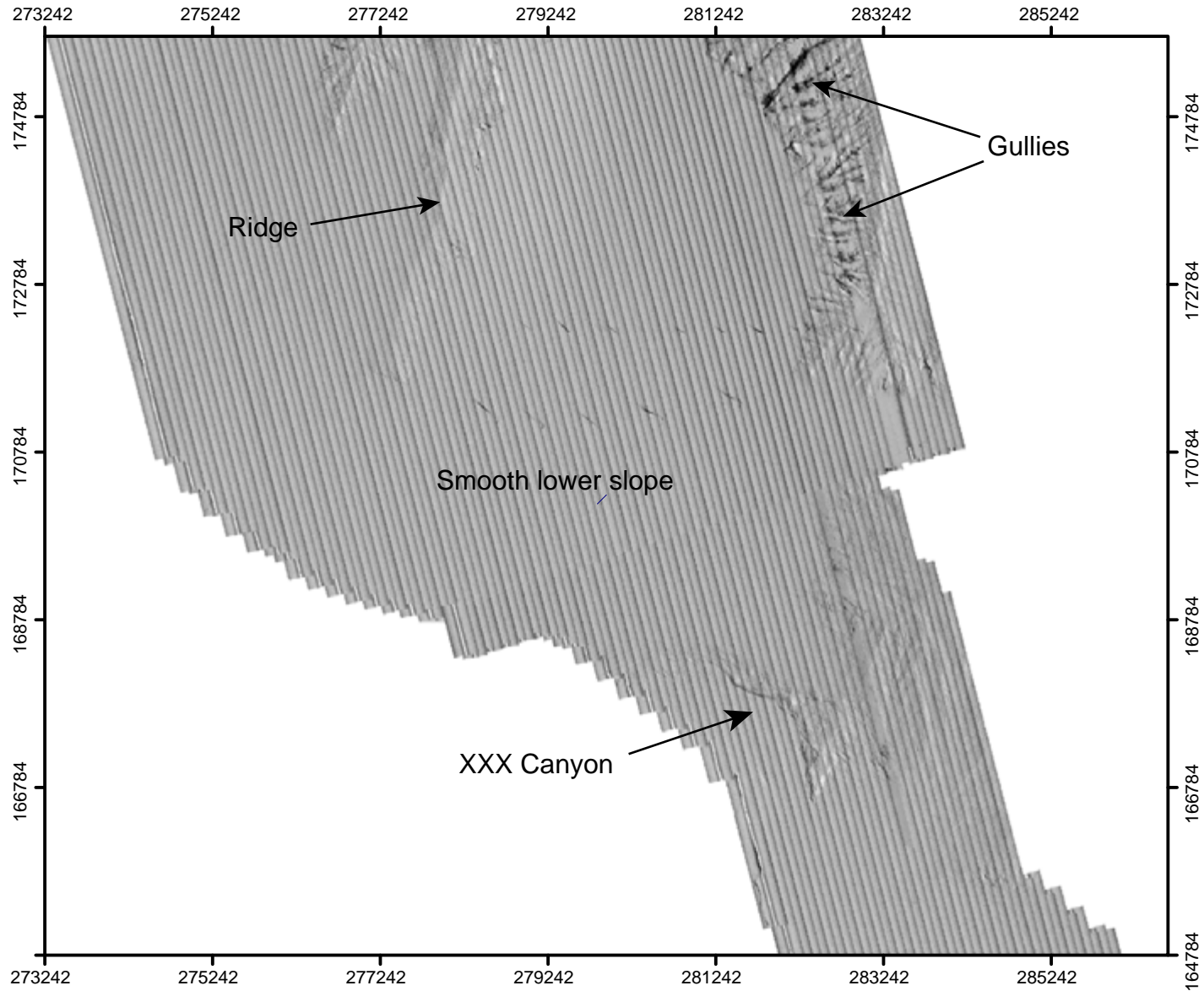


Figure 37. Overview of sidescan sonar data from the middle part of the Russian slope. Limited backscatter contrasts suggest that most of this area is draped by a uniform sediment later. For location see figure 23.

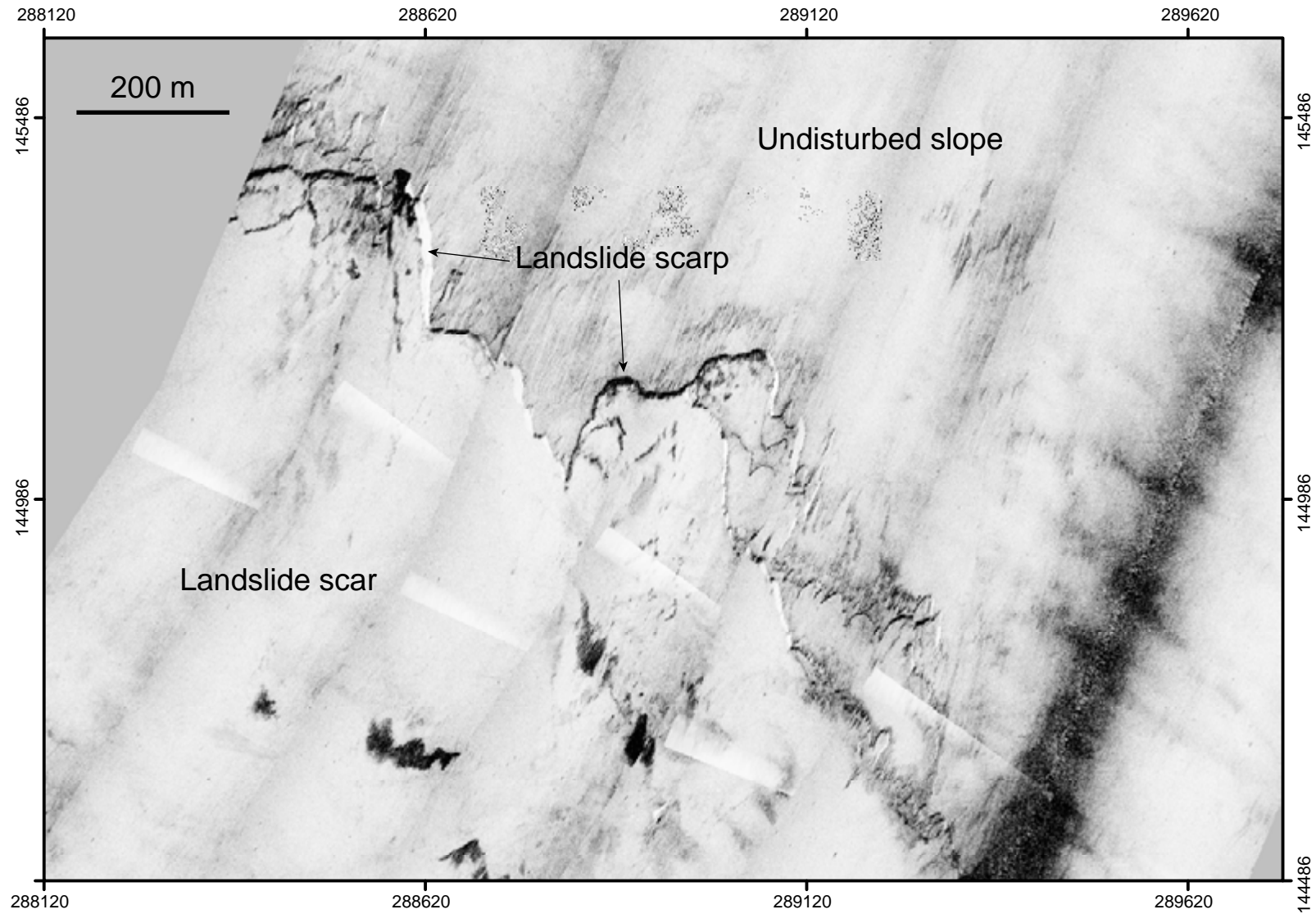


Figure 38. Sidescan sonar image of landslide scarp on the lower Russian slope. Scarp is 2-4 m high. The landslide scar has a slightly lower backscatter than the undisturbed seafloor, suggesting it may be partly infilled by post-landslide sediments. For location see figure 22.

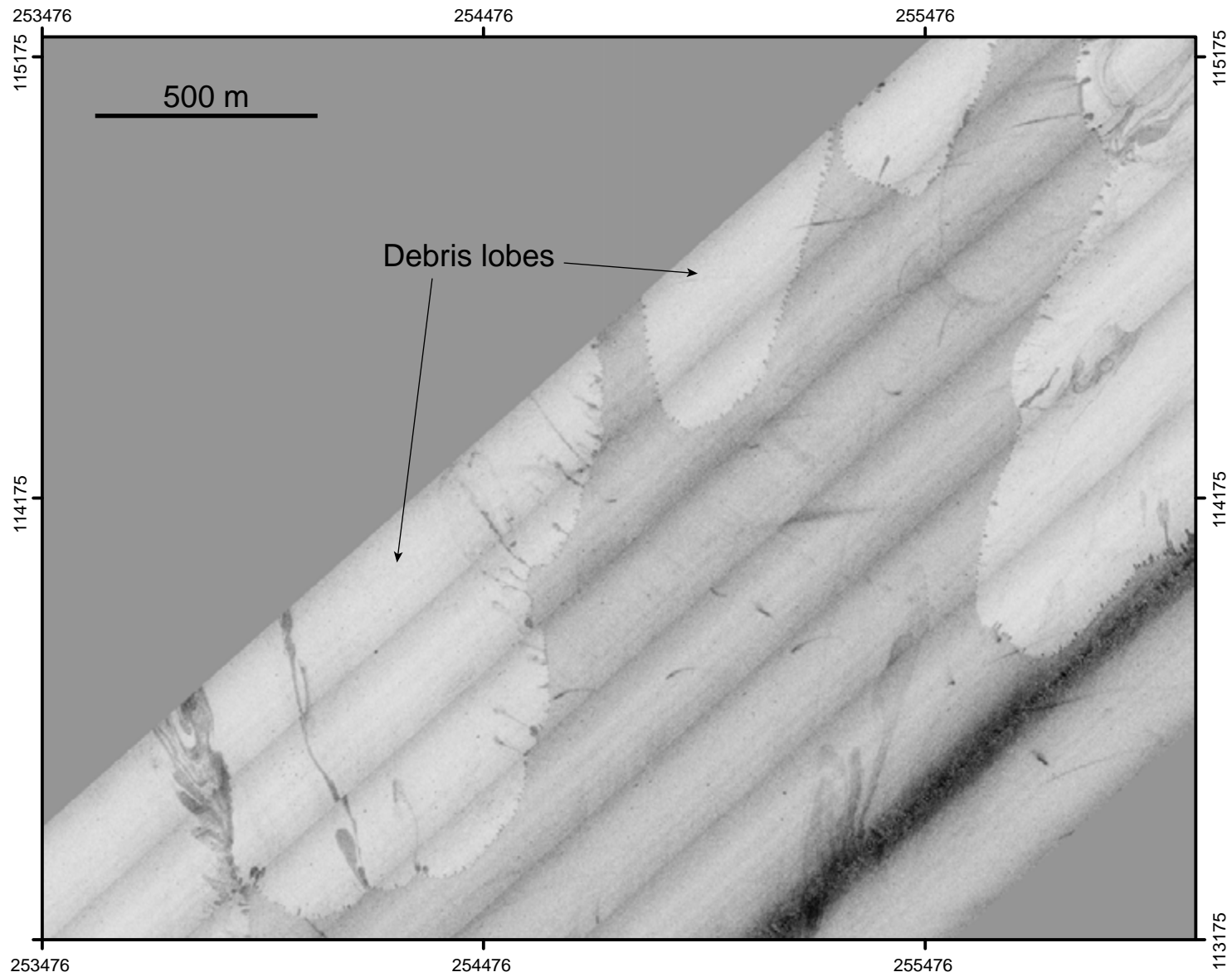


Figure 39. Sidescan sonar image of debris lobes on the lower Russian slope. Note the typical frond like patterns that characterise lobe edges. For location see figure 22.

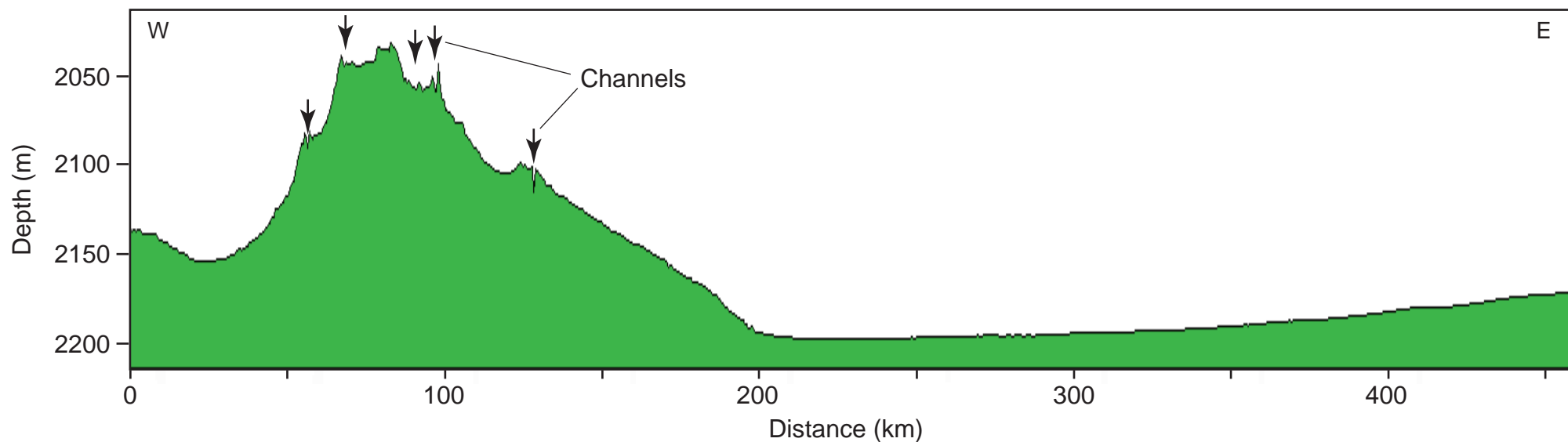


Figure 40. Highly exaggerated bathymetric profile along the entire 460 km of the proposed pipeline route across the Turkish Abyssal Plain. This shows that the plain consists of two distinct geomorphological provinces, a true flat abyssal plain the east and a channel levee complex in the west. The channel levee complex is part of the inactive distal Danube Fan. The locations of five channels crossing the pipeline route in the Turkish sector are marked by arrows. A sixth channel also occurs to the west, in the Bulgarian sector.

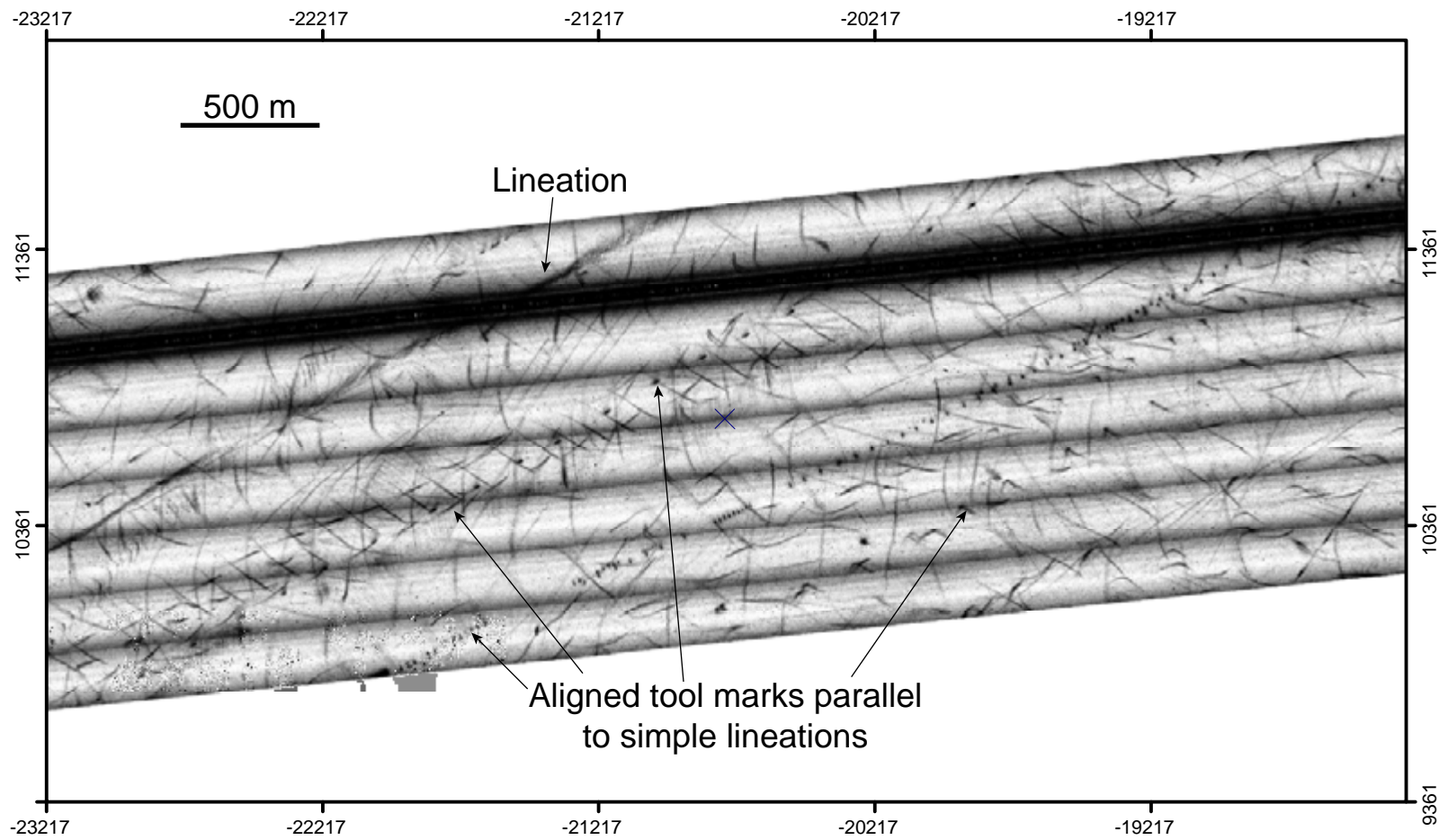


Figure 41. Sidescan sonar image of fine-scale lineations and irregular marks interpreted as tool marks, probably caused by objects such as trees carried along by bottom currents and gouging the seafloor. Note that these features have no bathymetric expression, suggesting that they are relatively old features buried by later sedimentation. For location see figure 19.

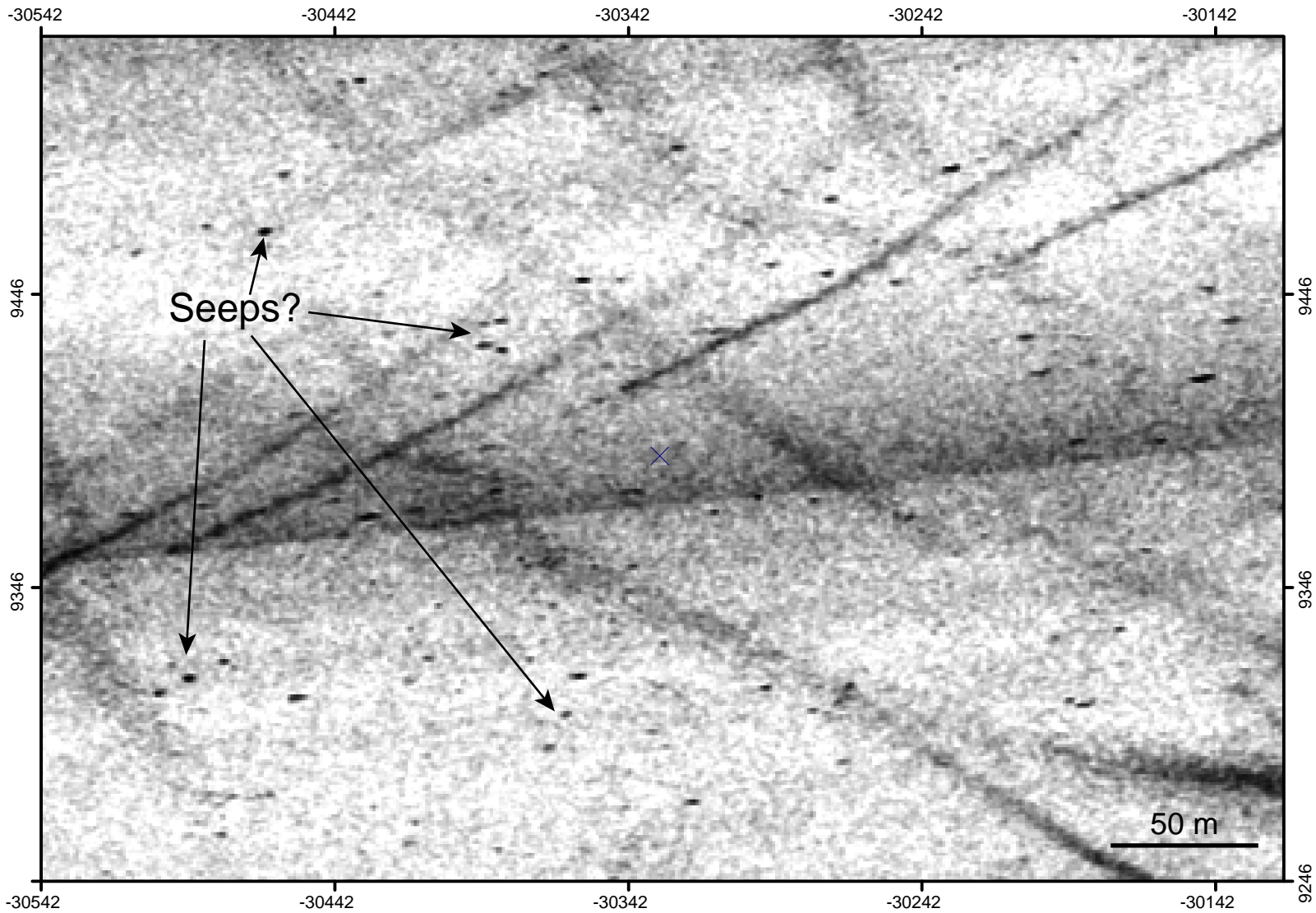


Figure 42. Sidescan sonar image showing small, randomly scattered but relatively strong targets. These could possibly be related to fluid seepage from the seafloor. None have been identified on video footage, suggesting that they may be buried features, hidden by a layer of soft organic-rich sediment. For location see figure 19.

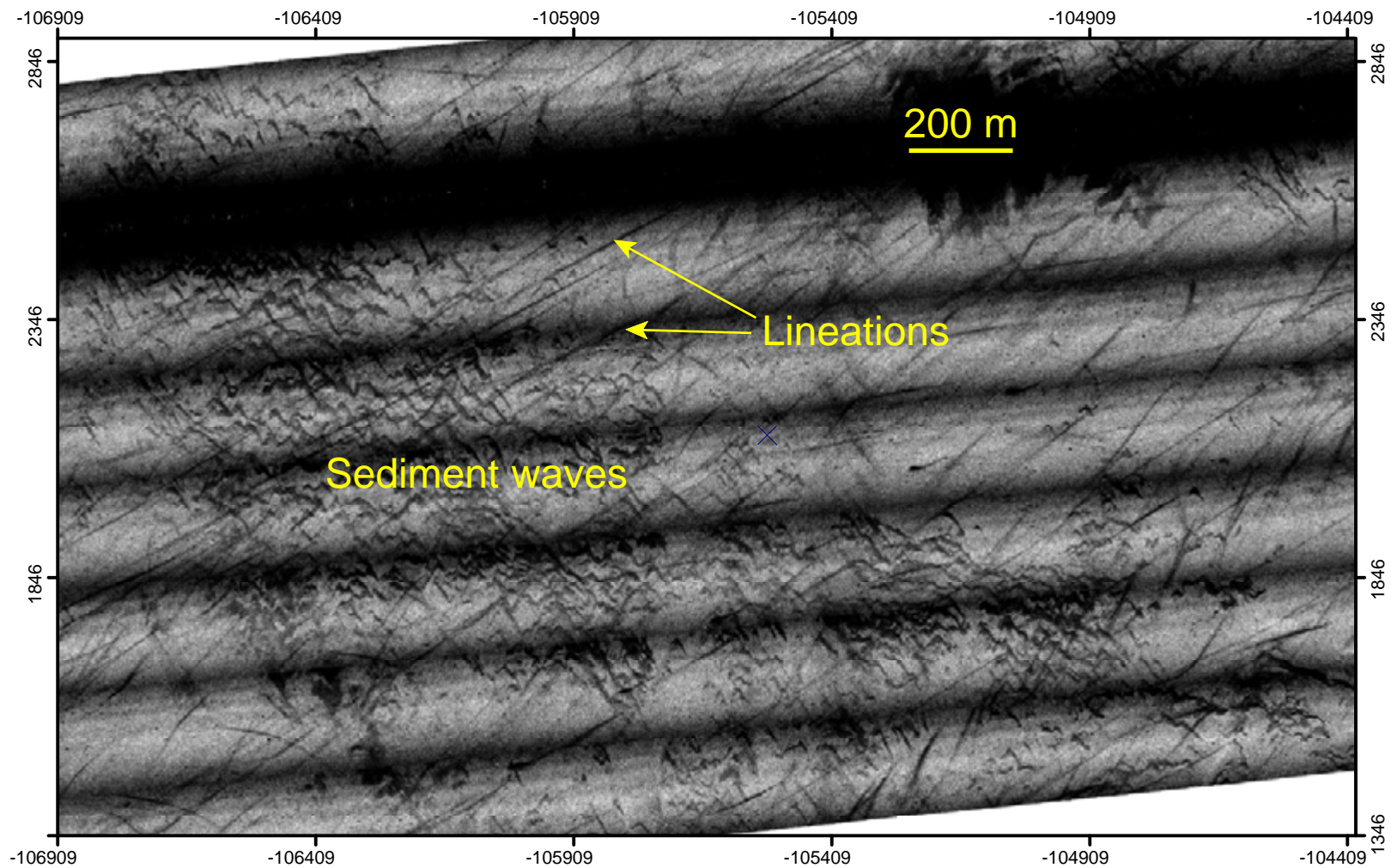


Figure 43. Sediment waves on the flank of the Danube Fan channel levee complex. Waves are produced as a consequence of turbidity current deposition and indicate that currents flowed from north to south. Sediment waves are overprinted by fine-scale lineations and are thus older than the lineations. For location see figure 18.

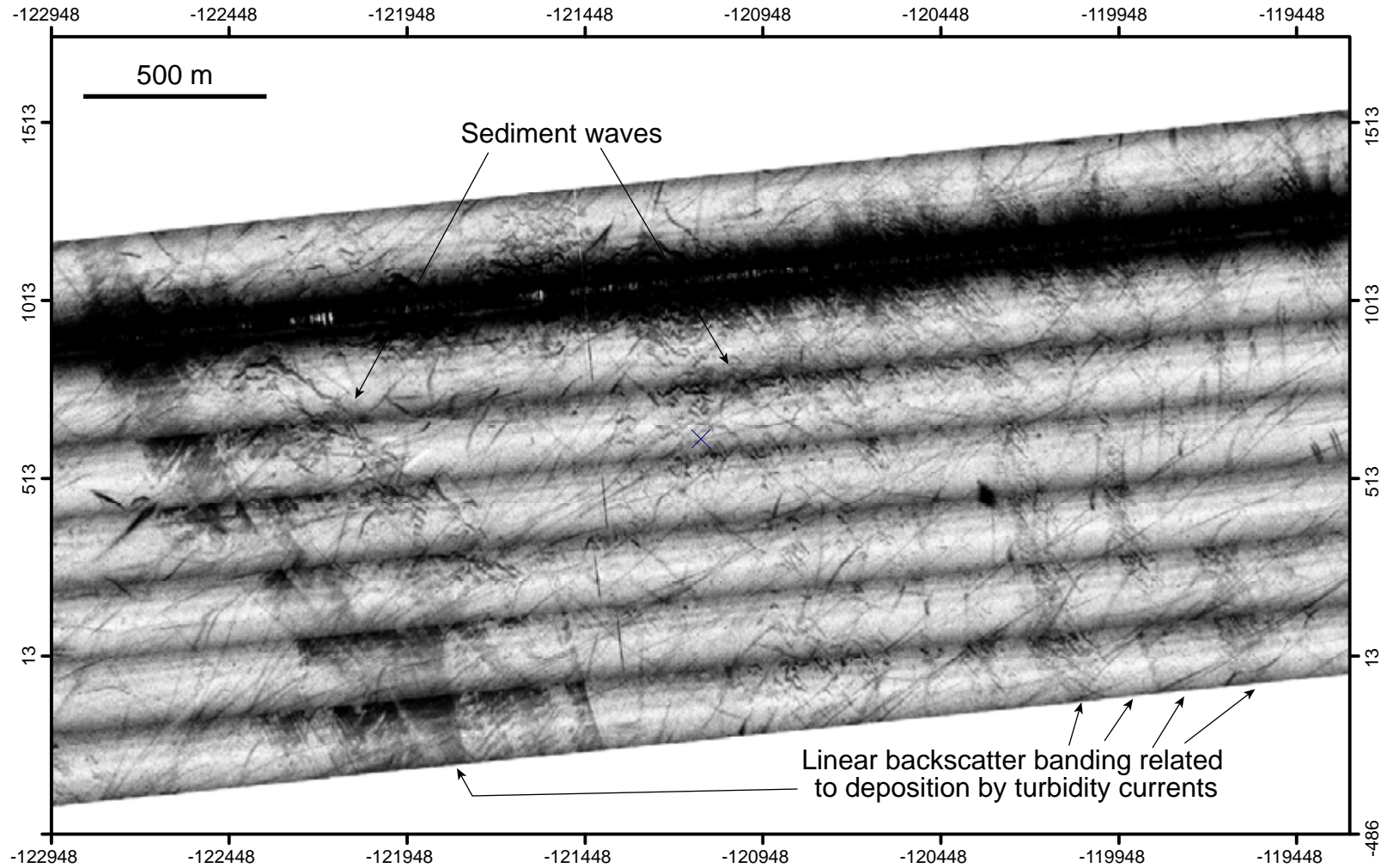


Figure 44. Linear backscatter banding, characteristic of sediments deposited by turbidity currents, on the flanks of the Danube Fan channel levee complex. Banding is oriented at 330-340°, indicating flow from the NNW. For location see figure 18.

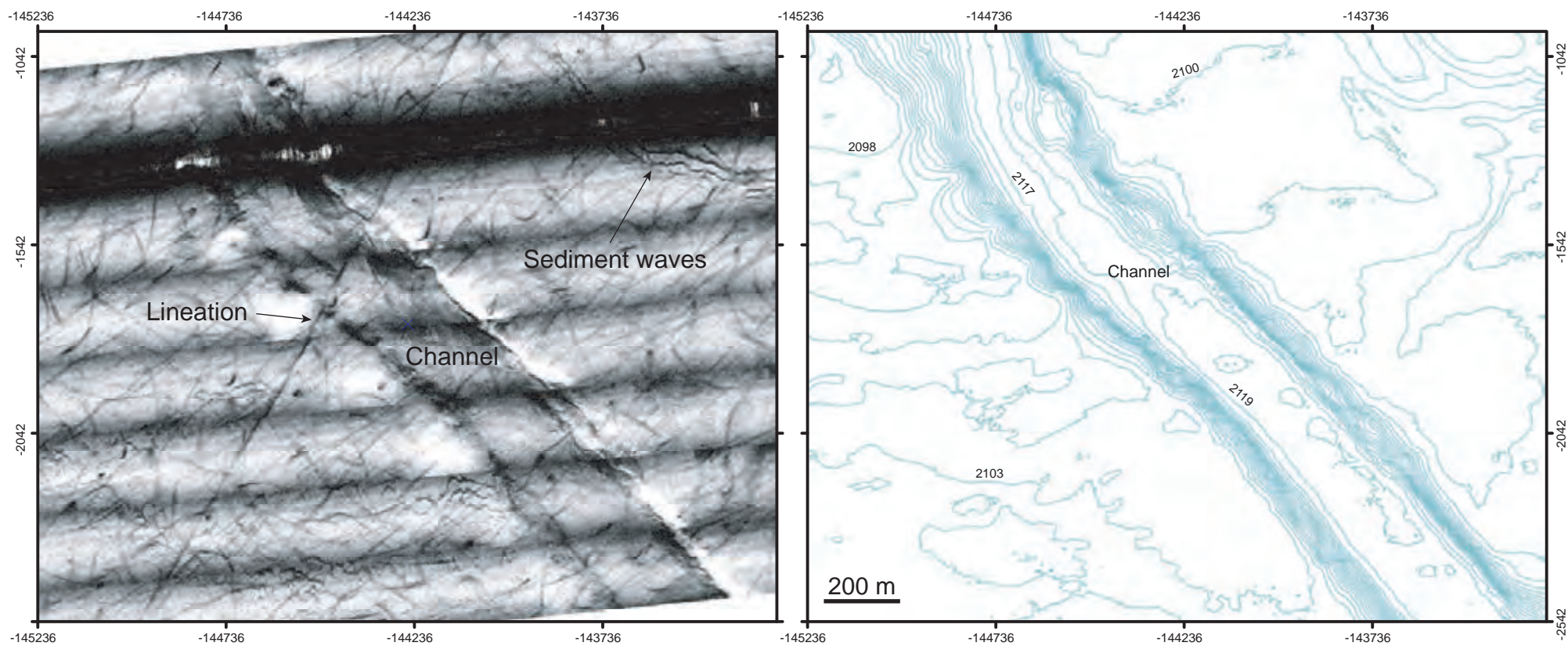


Figure 45. Sidescan sonar image (left) and bathymetry (right) showing part of a channel on the distal Danube fan. The channel is about 20 m deep. There is little backscatter contrast between the channel floor and surrounding seafloor, suggesting that both are draped with a layer of younger sediment. This is consistent with the age of the Danube fan, which became inactive about 9000 years ago. Lineations cross-cut the channel are clearly younger than it. For location see figure 18.

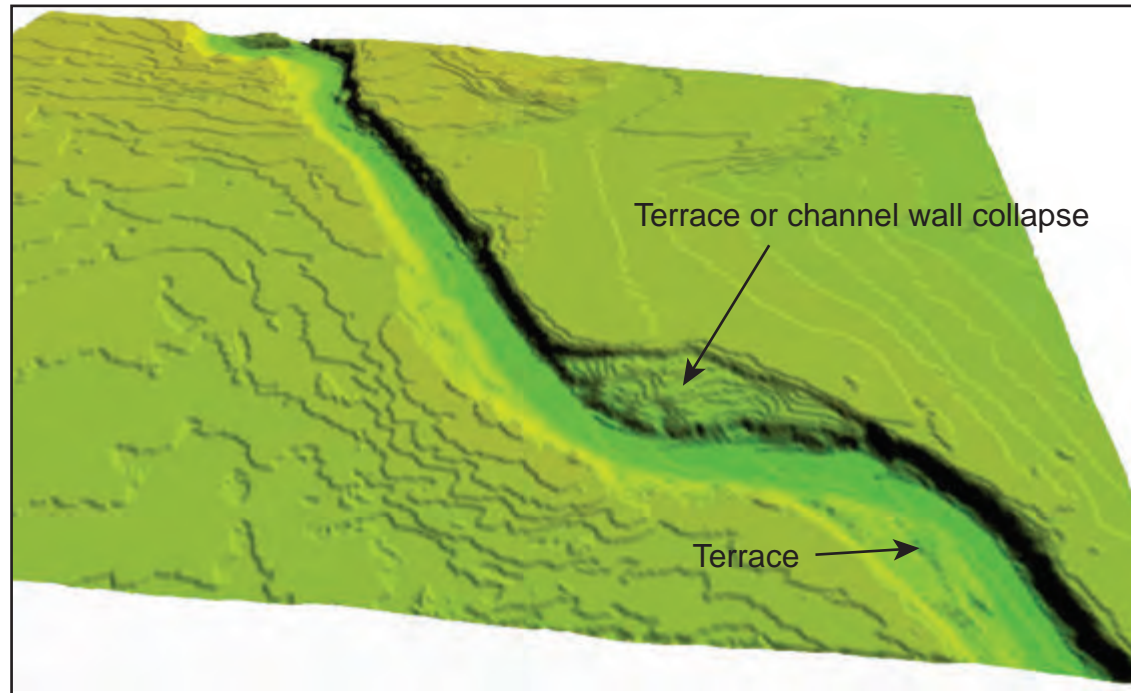


Figure 46. 3D bathymetric representation of the channel shown in figure 45. The image shows terraces or areas of channel wall collapse. Position of the features relative to channel meander bends supports a terrace interpretation.

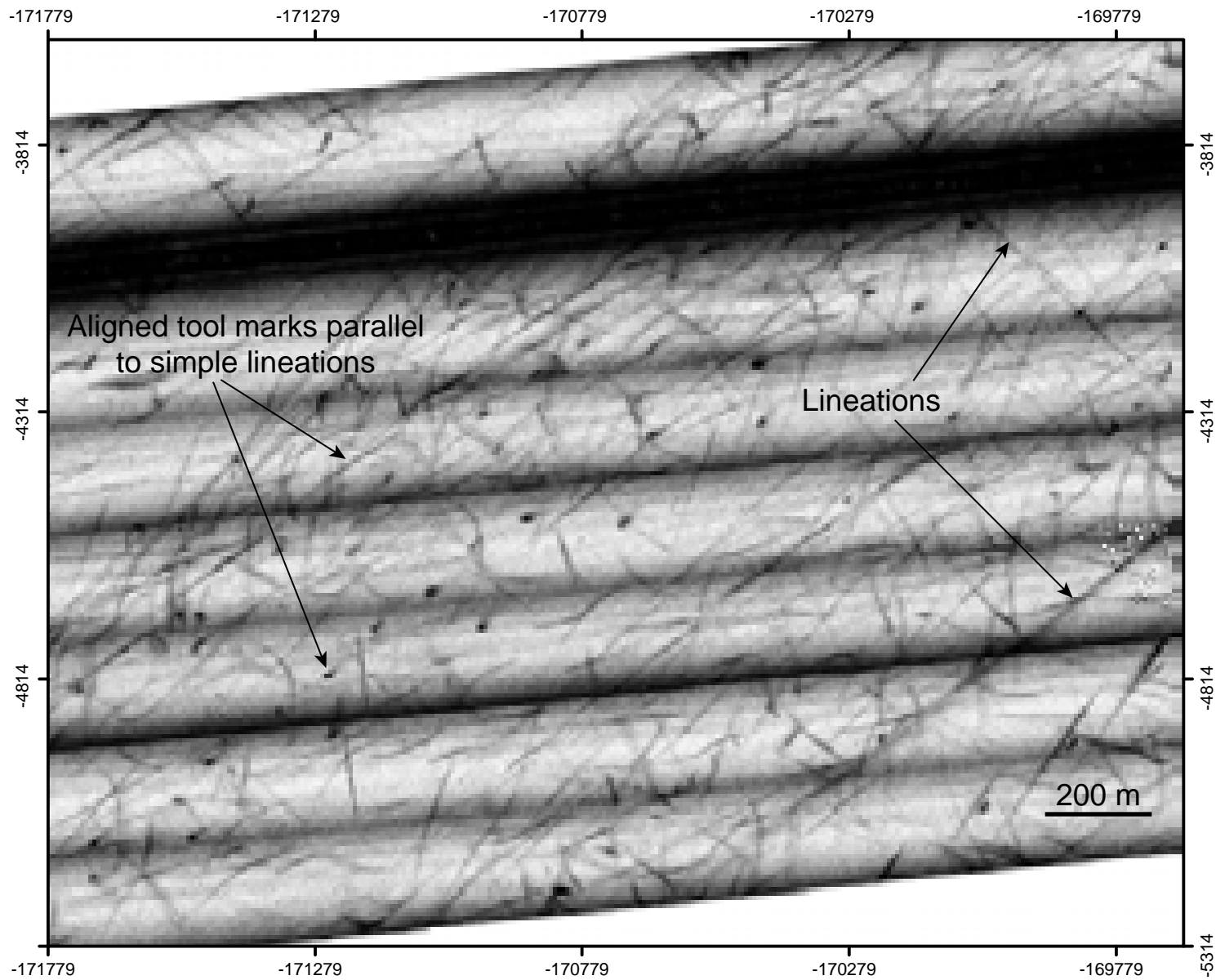


Figure 47. Fine-scale lineations and irregular markings seen in sidescan sonar data from the central Turkish Abyssal Plain. Trend of linear features is approximately NE-SW. For location see figure 18.

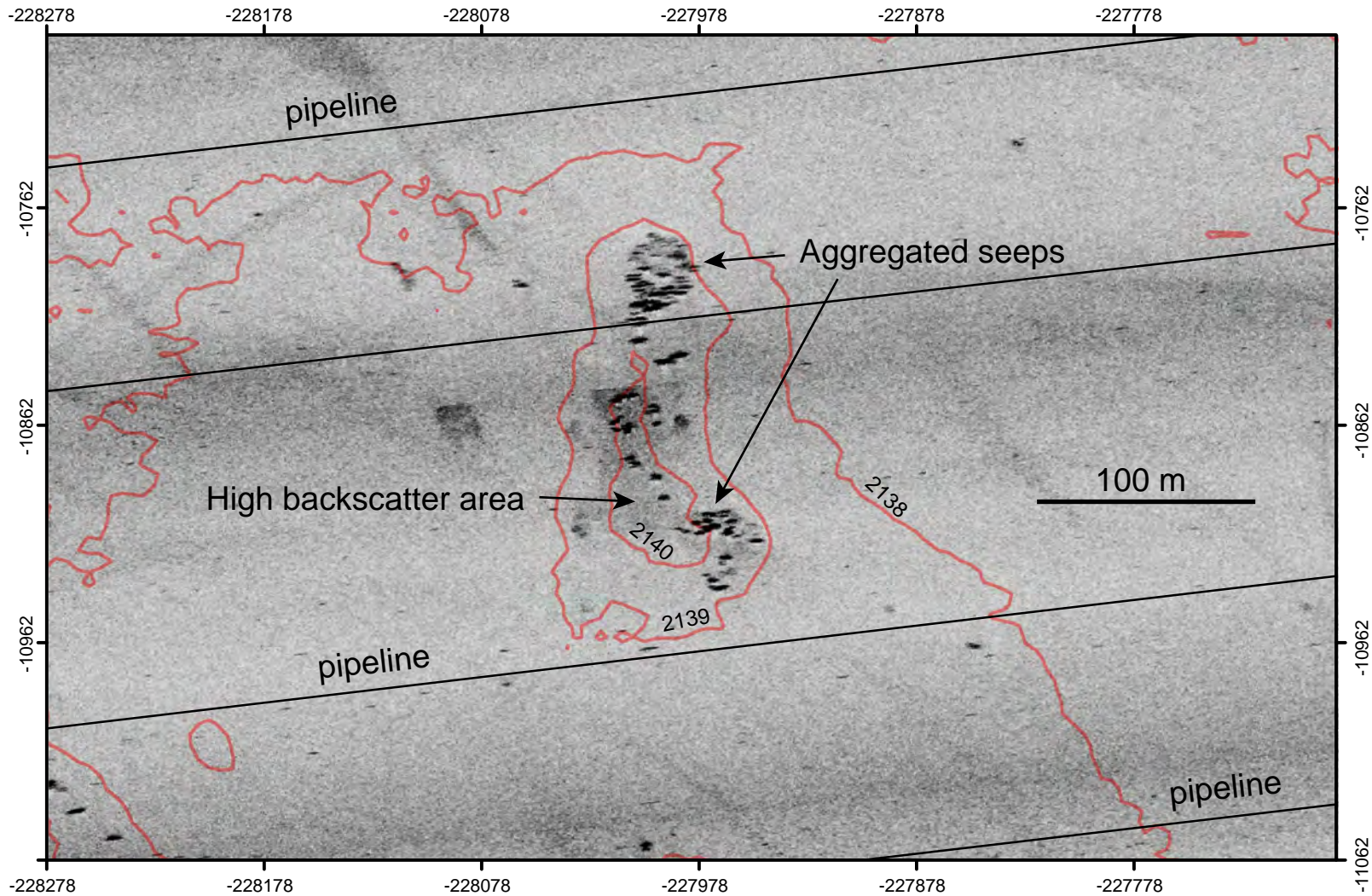


Figure 48. Cluster of small strong sidescan sonar targets contained within a shallow seafloor depression in the Turkish Abyssal Plain. Note that the area around the targets is characterised by slightly higher backscatter (dark). The origin of this feature is uncertain, but a pockmark containing small carbonate buildups is one possible interpretation. For location see figure 17.

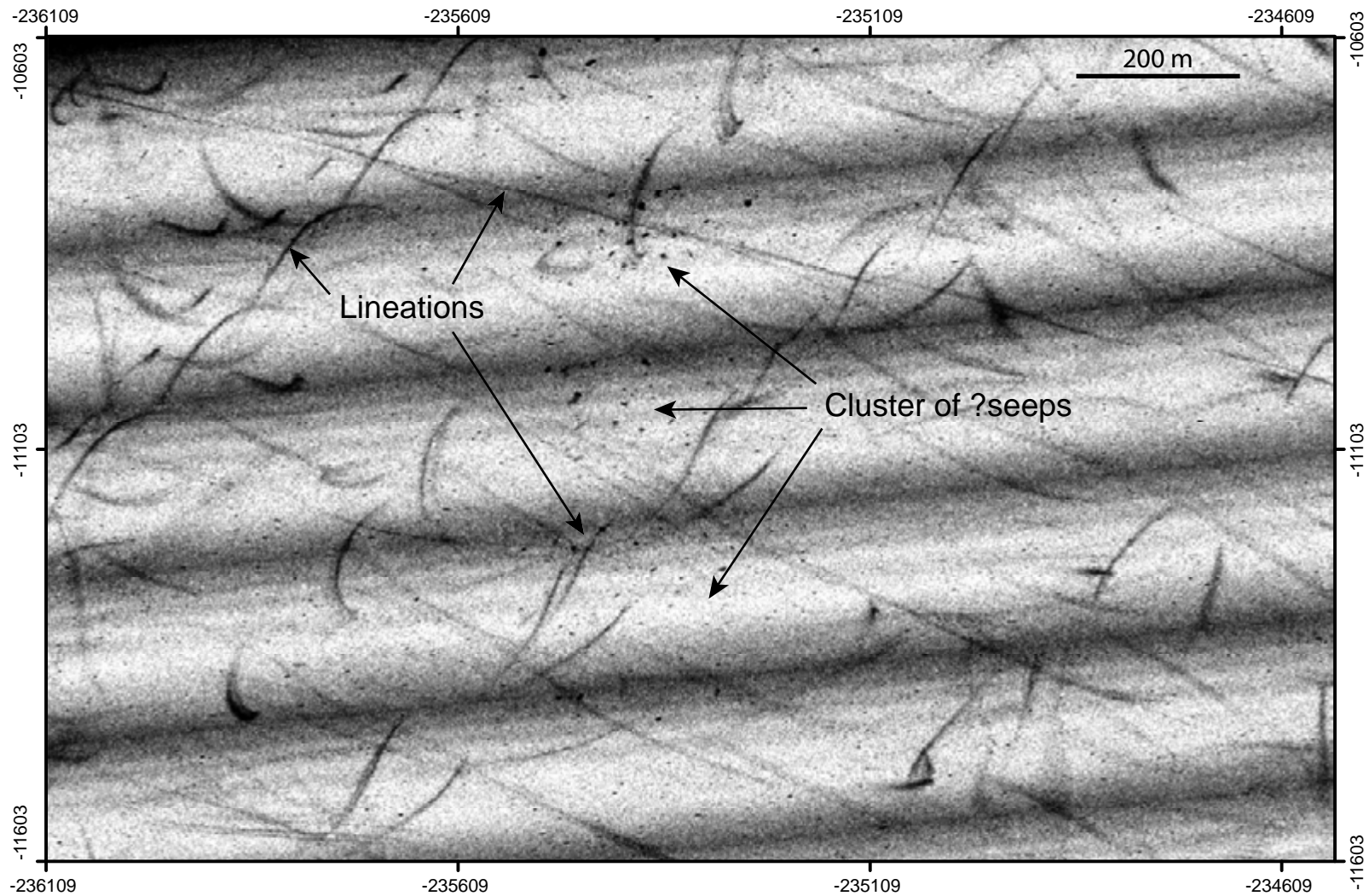


Figure 49. Loose cluster of small sidescan sonar targets. Origin unknown but possibly related to fluid seepage from seafloor. For location see figure 17.

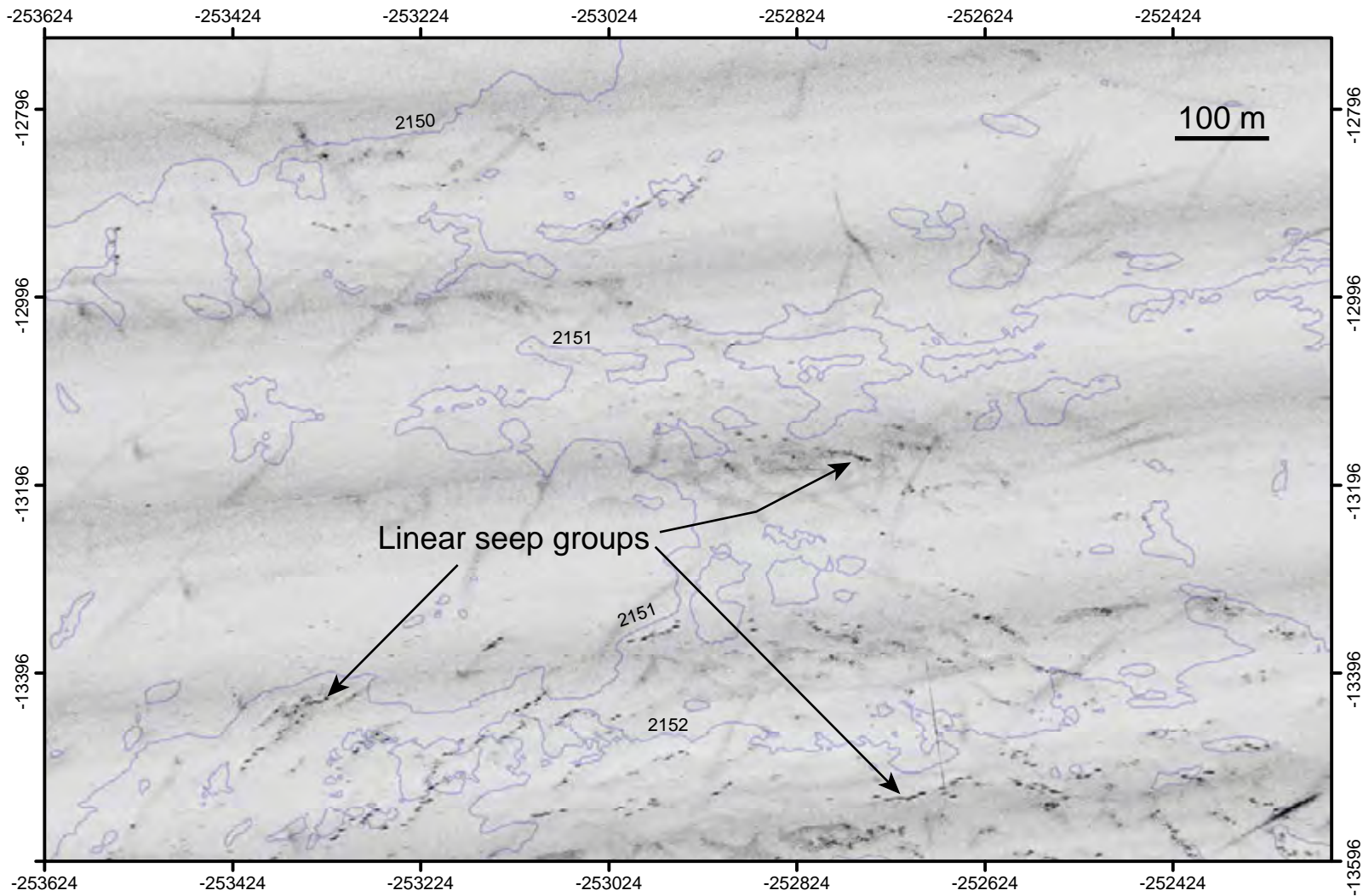


Figure 50. Clusters of small sidescan targets arranged in linear groups. A local high backscatter halo surrounds most seeps clusters. In this example, there is no clear relationship between targets and bathymetric lows or highs. For location see figure 17. The origin of these targets is uncertain, but small carbonate buildups related to fluid seepage from the seafloor is one possible interpretation.

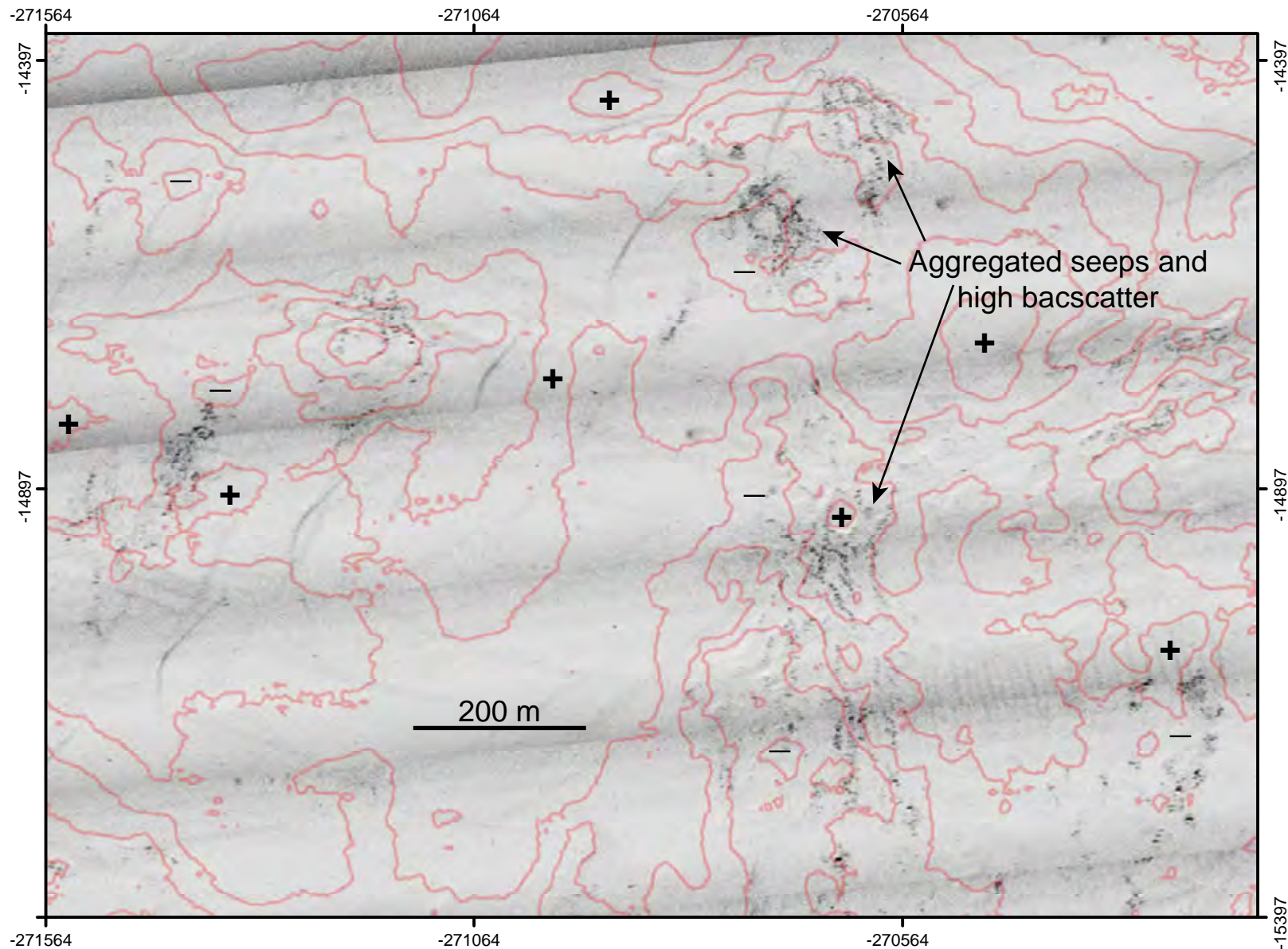


Figure 51. Clusters of small sidescan sonar targets associated with patches of high backscatter (dark). Most are located in subtle bathymetric lows. The origin of these feature is uncertain, but irregular pockmarks containing small carbonate buildups is one possible interpretation. For location see figure 17.

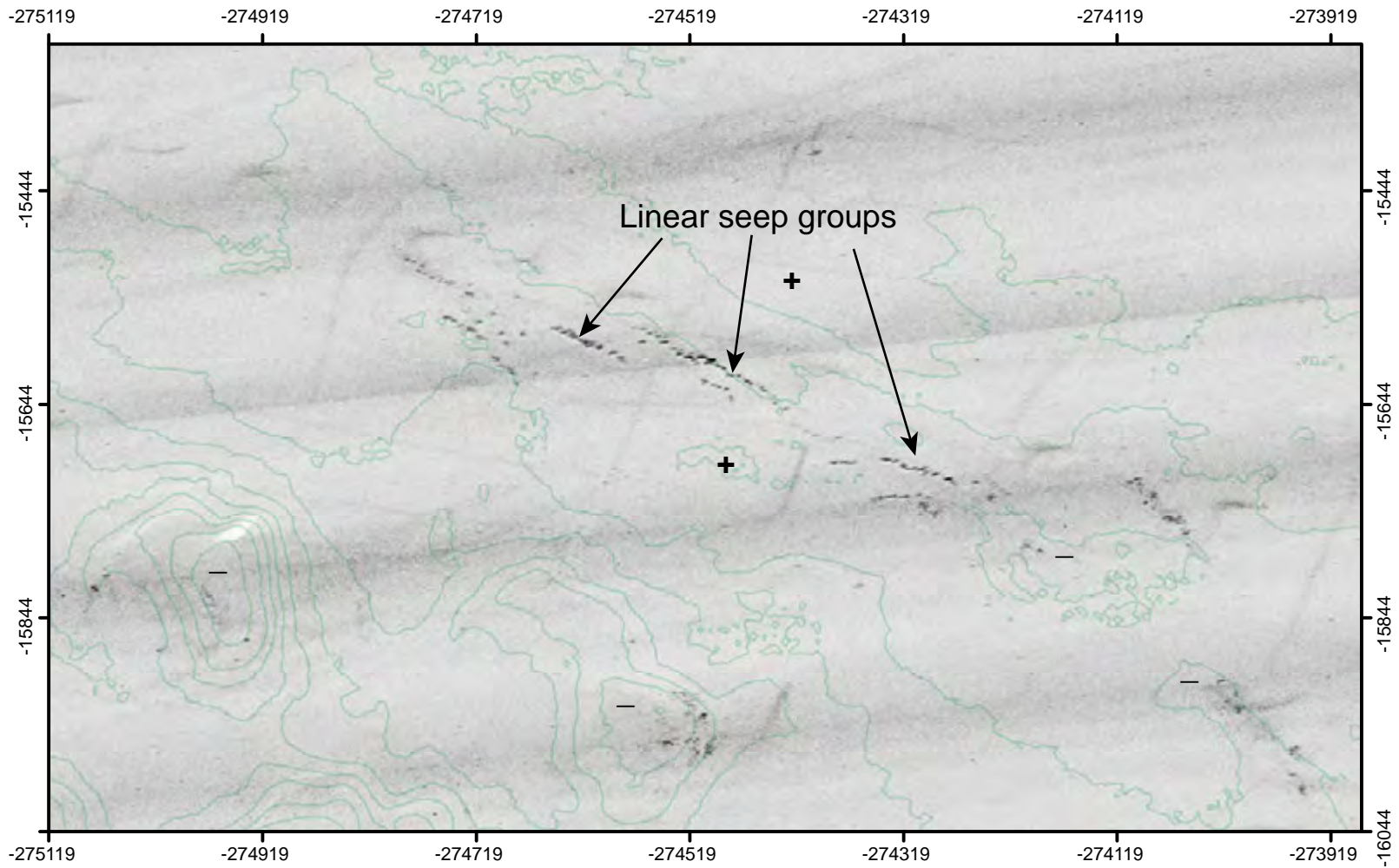


Figure 52. Linear clusters of small sidescan sonar targets located in a subtle bathymetric low. The origin of these targets is uncertain, but small carbonate buildups related to fluid seepage from the seafloor is one possible interpretation. For location see figure 17.

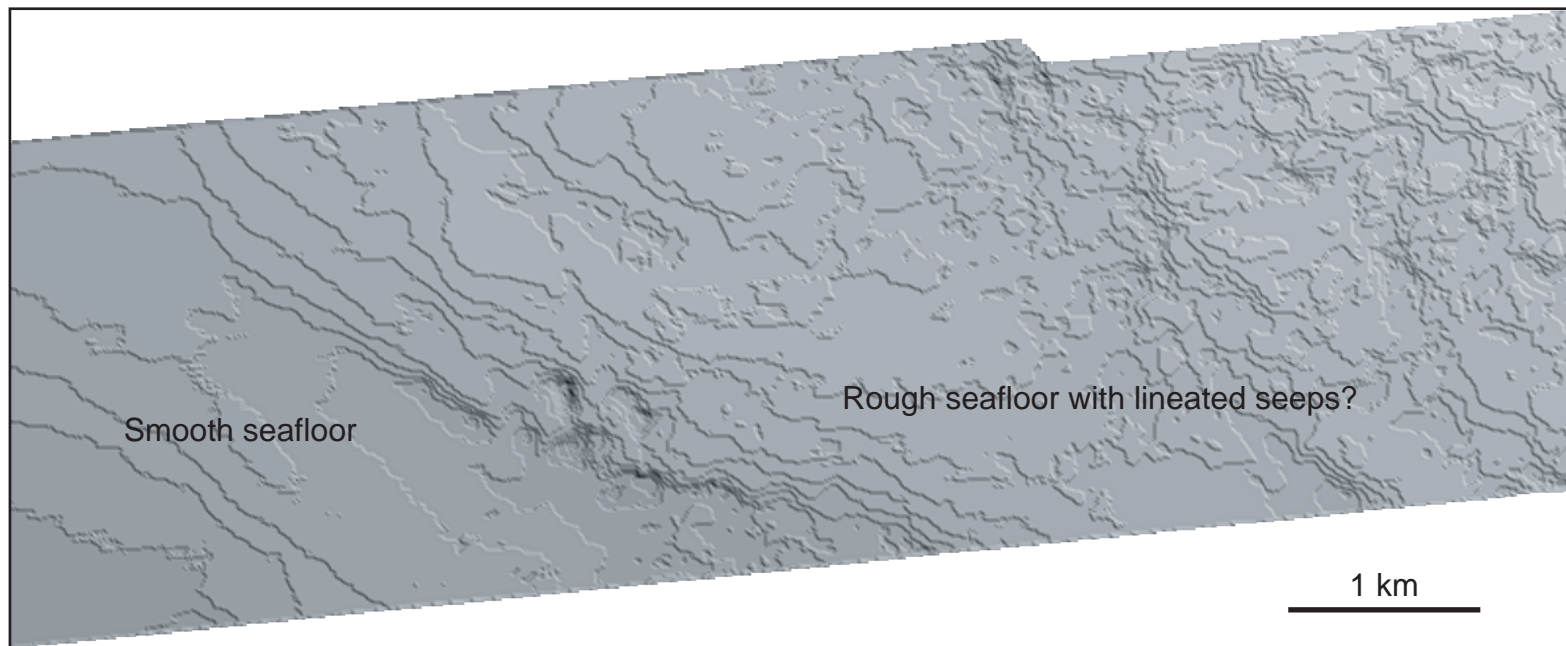


Figure 53. 3D bathymetric image of the western boundary between the area of rough seafloor characterised by numerous possible seep-related features (see figures 48-52) and the smoother seafloor to the west. Note that the rough area is a few metres shallower than the smooth area.

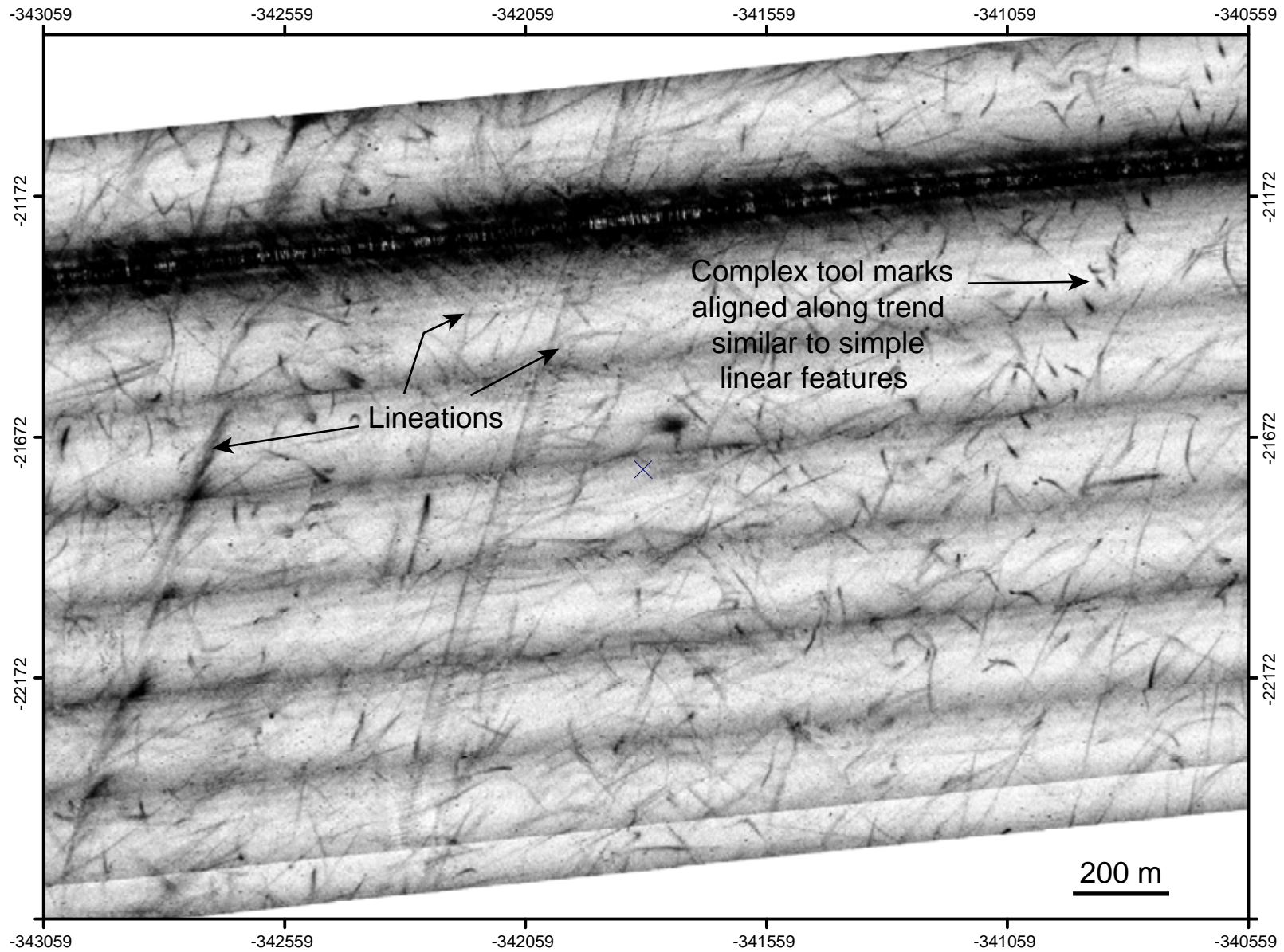


Figure 54. Fine-scale lineations and irregular tool marks on the Bulgarian abyssal plain. Note that the tool marks are also often arranged in groups that, overall, parallel the more linear features. The main trend is NNE-SSW. For location see figure 16.

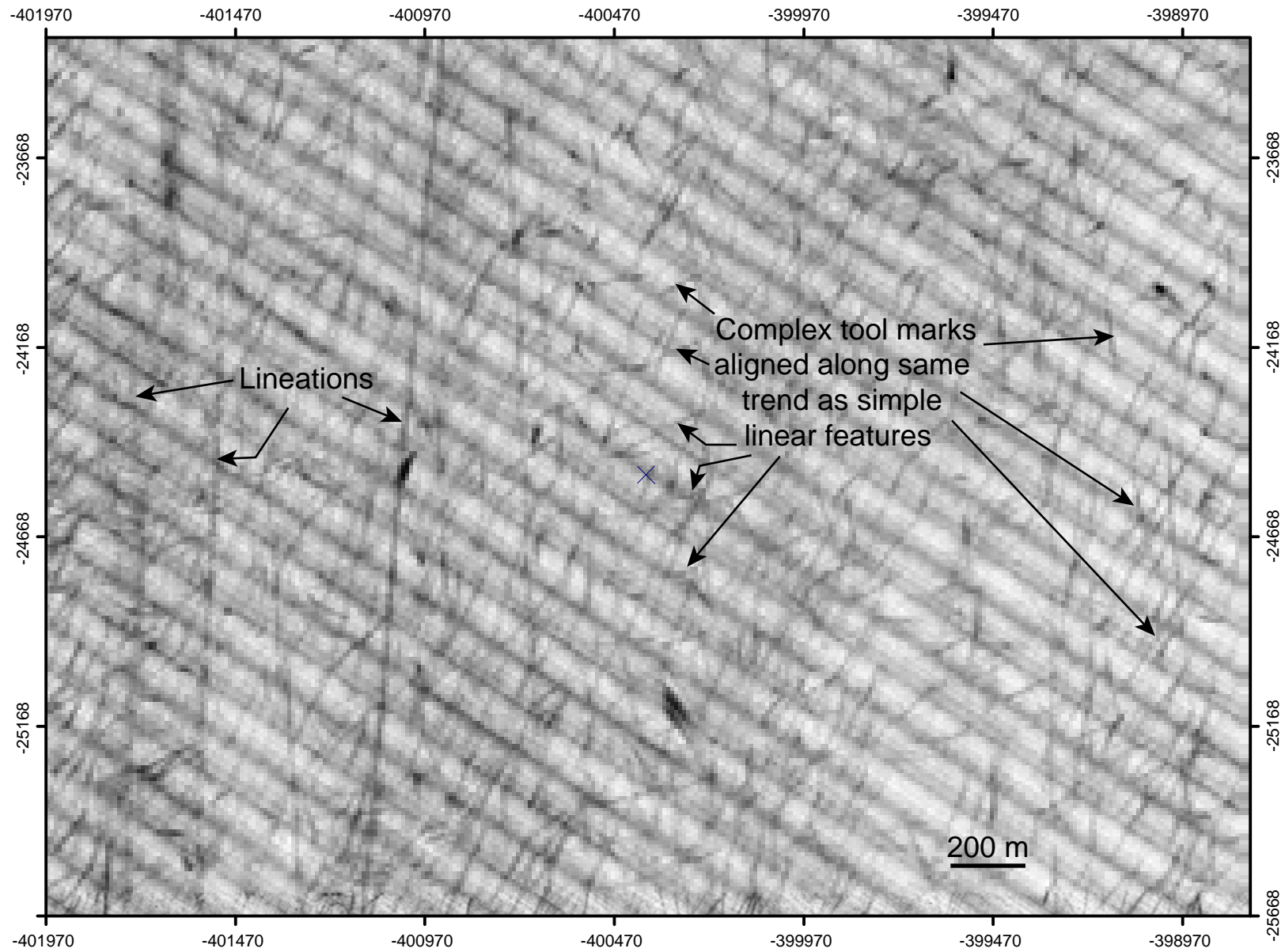


Figure 55. Fine-scale lineations and irregular tool marks on the lower Bulgarian slope. Note that the tool marks are also often arranged in groups that, overall, parallel the more linear features. The main trend is approximately N-S. For location see figure 15.

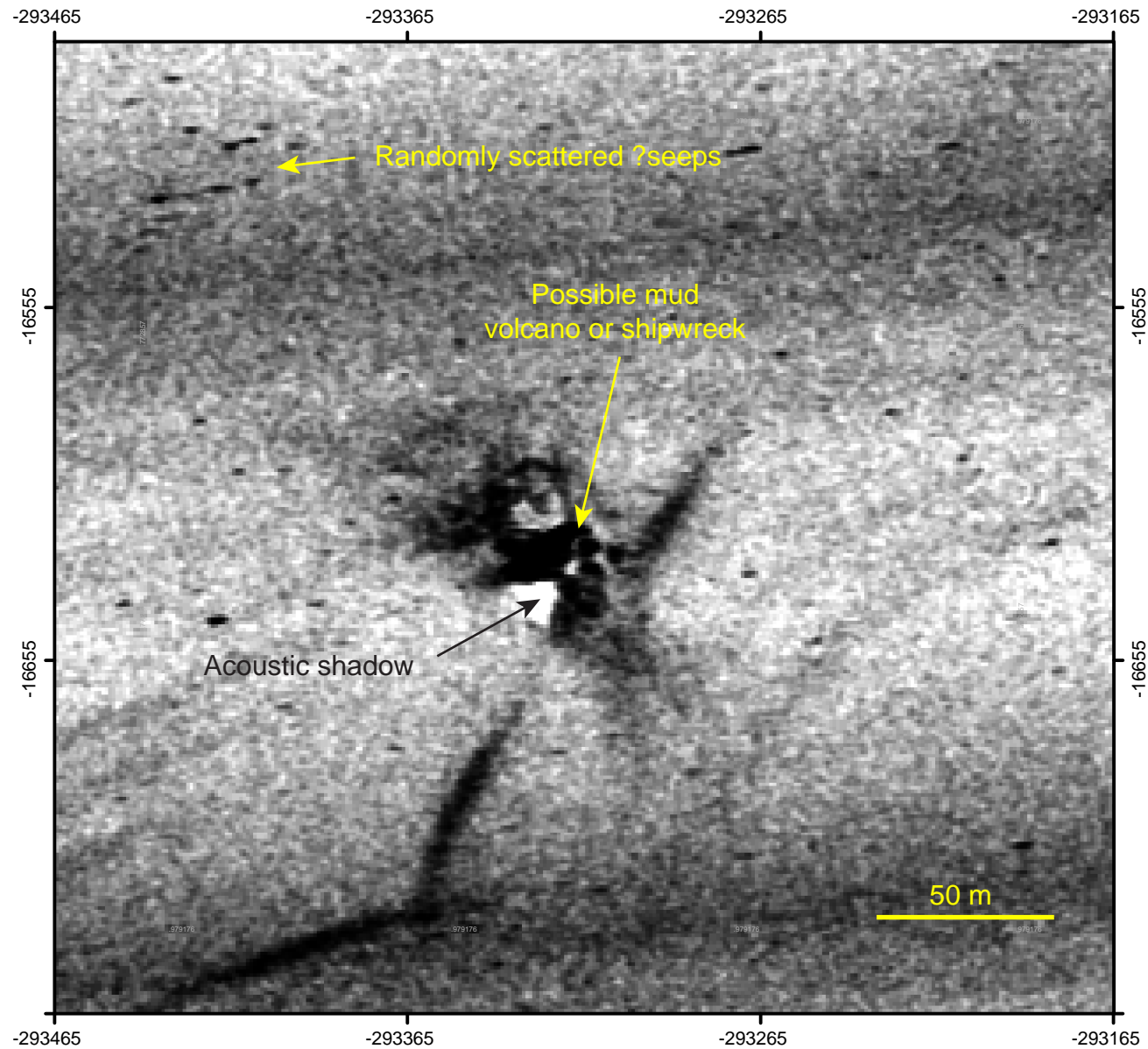


Figure 56. Strong sidescan sonar target in the Bulgarian Abyssal Plain. The acoustic shadow suggests a target that extends significantly above the seafloor. Target dimensions are in the region of 25 x 50 m. possible interpretations include a ship or a mud volcano For location see figure 16.

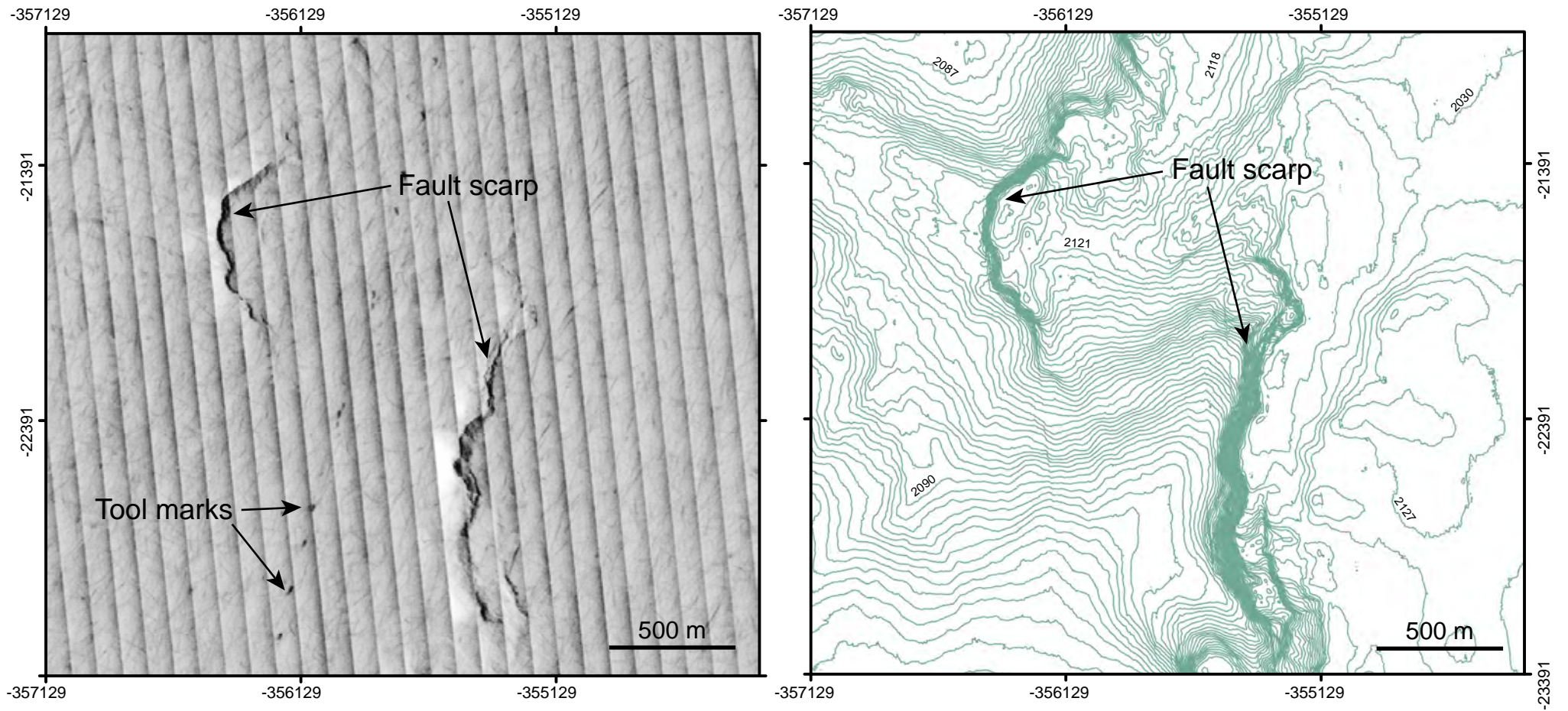


Figure 57. Sidescan sonar image (left) and bathymetry (right) of part of a strike-slip or oblique-slip fault zone in the Bulgarian Abyssal Plain. Fault zone consists of multiple, discontinuous, discrete en echelon segments. Sidescan sonar imagery suggests that some segments with sharp outlines may have experienced relatively recent movement. For location see figure 16.



Figure 58. Images derived from ROV video along the route of the 'Caucasus' cable. (a) cable exposed at the seabed in the centre of a seabed depression interpreted as a possible pockmark. Cable may be visible because active fluid flow keeps the area from being covered by layer of flocs. (b) Edge of the possible pockmark showing eroded edge of floc layer. (c) part of pockmark interior showing broken partially consolidated floc layers.

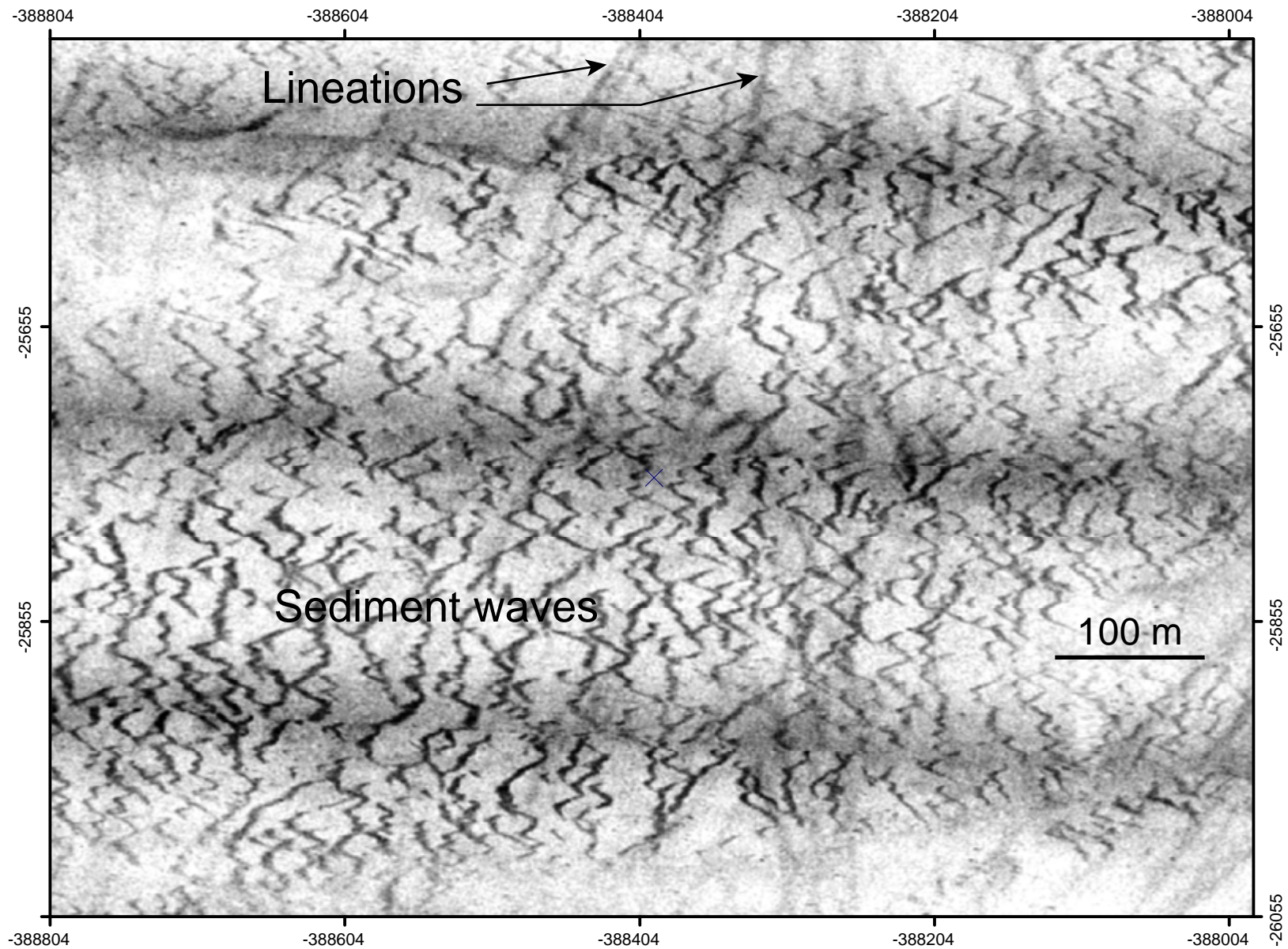


Figure 59. Sidescan sonar image of sediment waves on the western Bulgarian Abyssal Plain. Wave orientation indicates that waves are the result of turbidity current deposition with the flows derived from the Bulgarian slope immediately to the west. Note that sediment waves overprint the fine-scale lineations and are thus younger than the lineations. Figure located on figure 15.

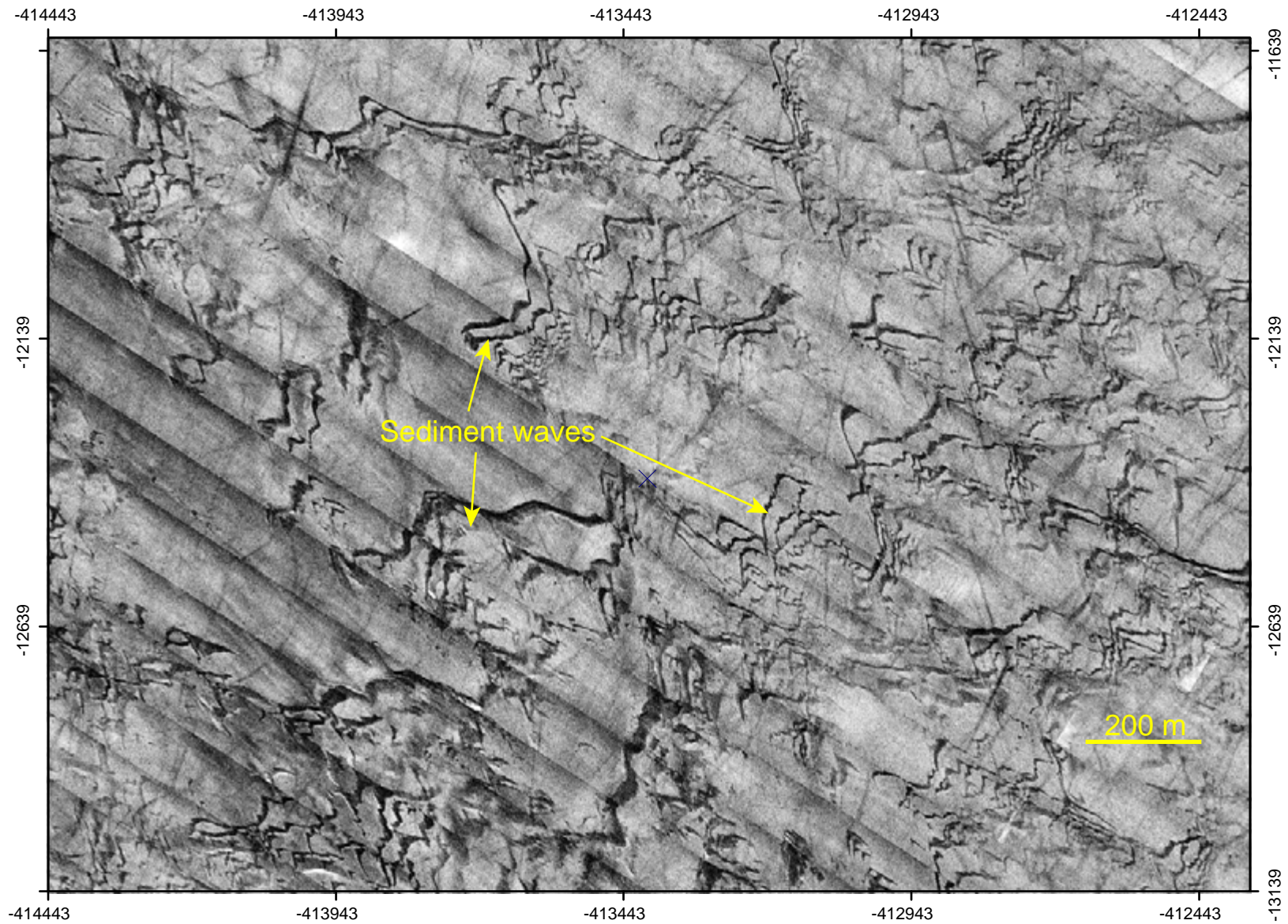


Figure 60. Sidescan sonar image of sediment waves within the large landslide scar on the Bulgarian slope. Wave orientation indicates that waves were built by downslope turbidity currents confined within the landslide scar. For location see figure 15.

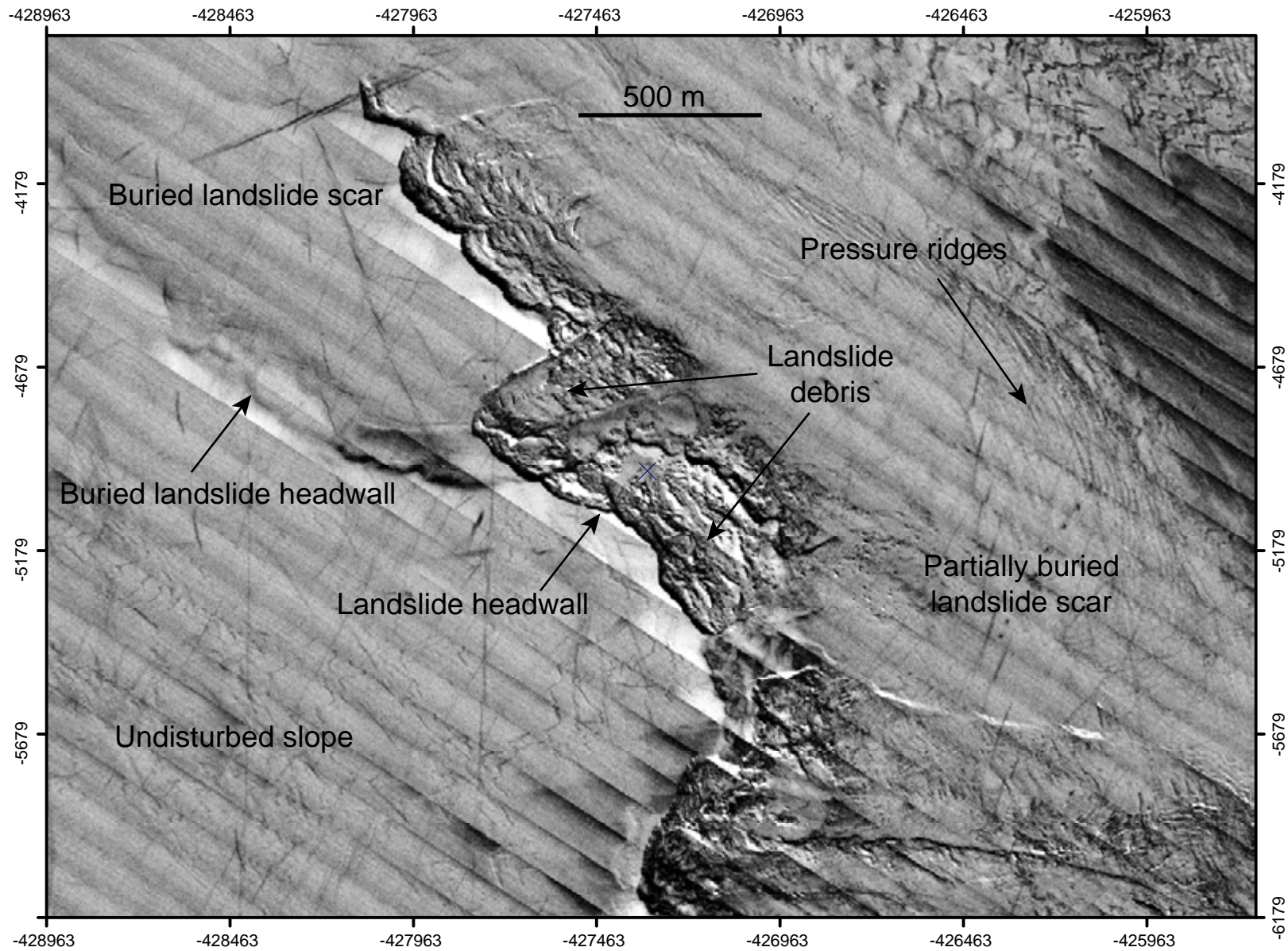


Figure 61. Sidescan sonar image of a part of the large complex landslide scar on the Bulgarian slope. Note that some parts of the landslide headwall are clear and sharp, while others are diffuse and largely buried by later sediments, indicating different failure ages. Similarly, landslide debris within the scar shows different degrees of burial. For location see figure 15.

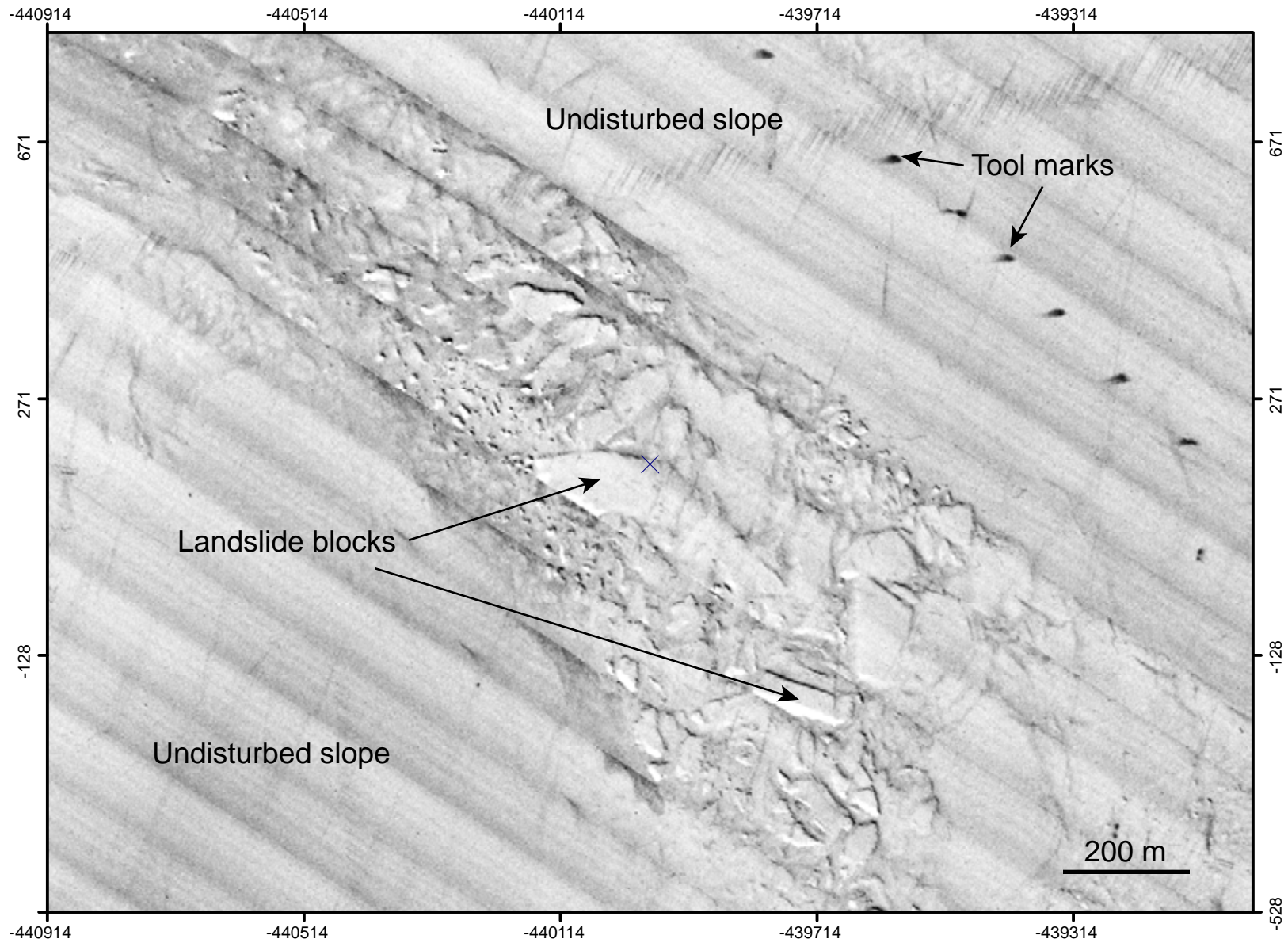


Figure 62. Sidescan sonar image of landslide blocks on the Bulgarian slope. Individual coherent blocks are up to 200 m across. These blocks are derived from a landslide headwall only a few hundred metres upslope of this image. For location see figure 15.

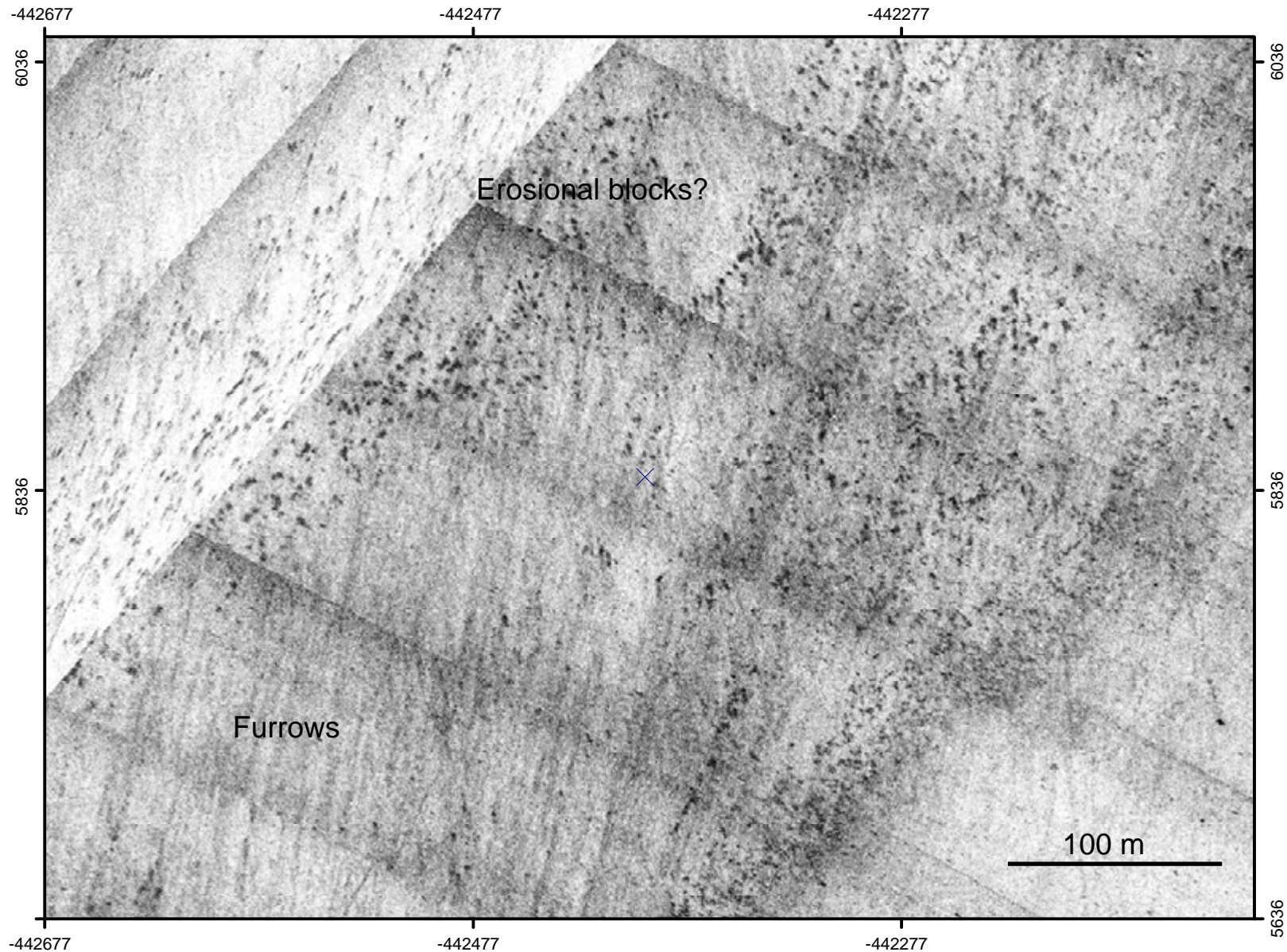


Figure 63. Sidescan sonar image of erosional furrows and blocks, caused by alongslope currents, on the upper Bulgarian slope. Video data indicate that these are apparently covered by a layer of organic rich floes, so they are unlikely to be active at the present day. For location see figure 15.

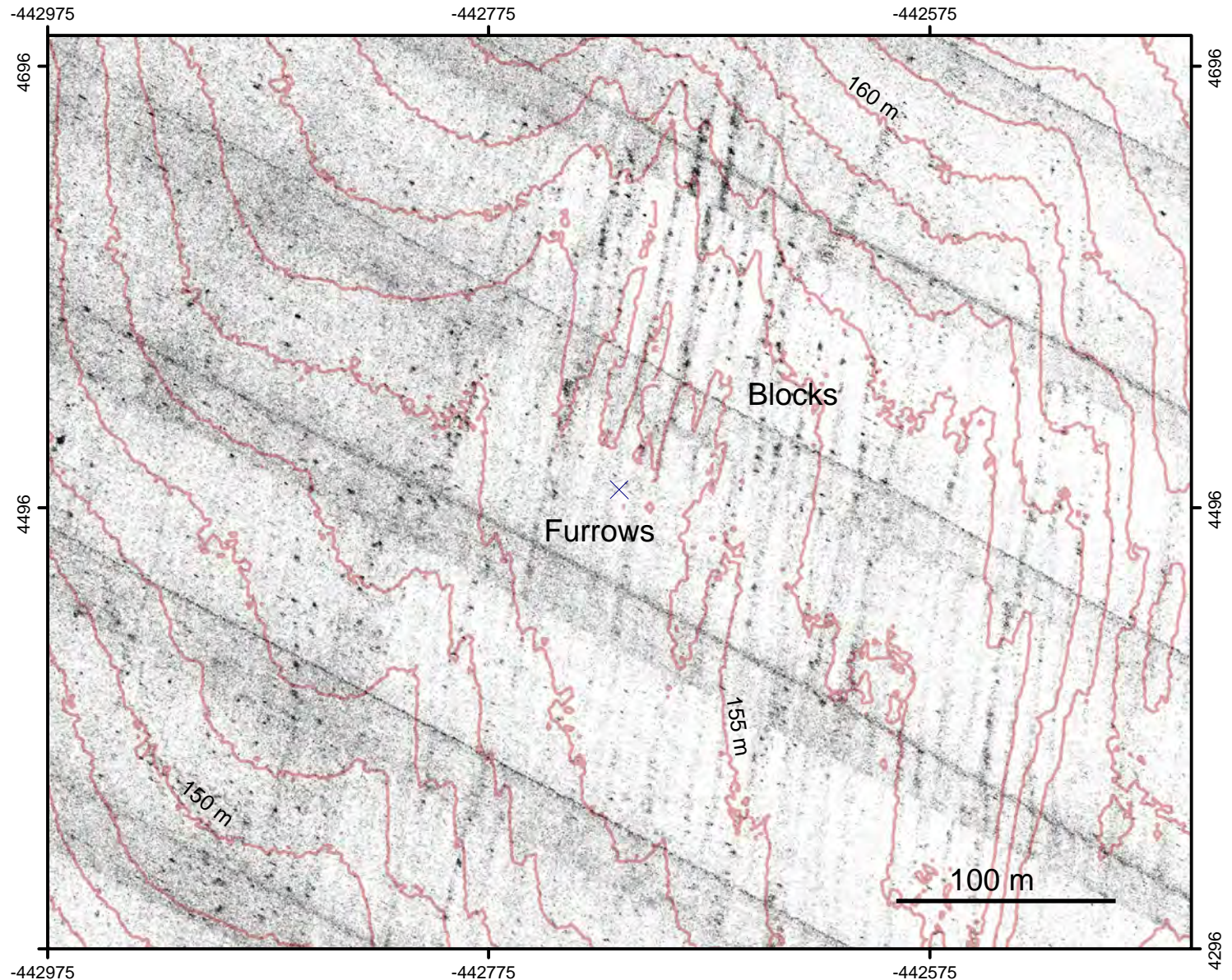


Figure 64. Sidescan sonar image of erosional furrows and blocks, caused by alongslope currents, on the upper Bulgarian slope. Bathymetric data (1 m contours) show that furrows can be up to 1 m deep. Video data indicate that furrows are apparently covered by a layer of organic rich flocs, so are unlikely to be active at the present day. For location see figure 15.

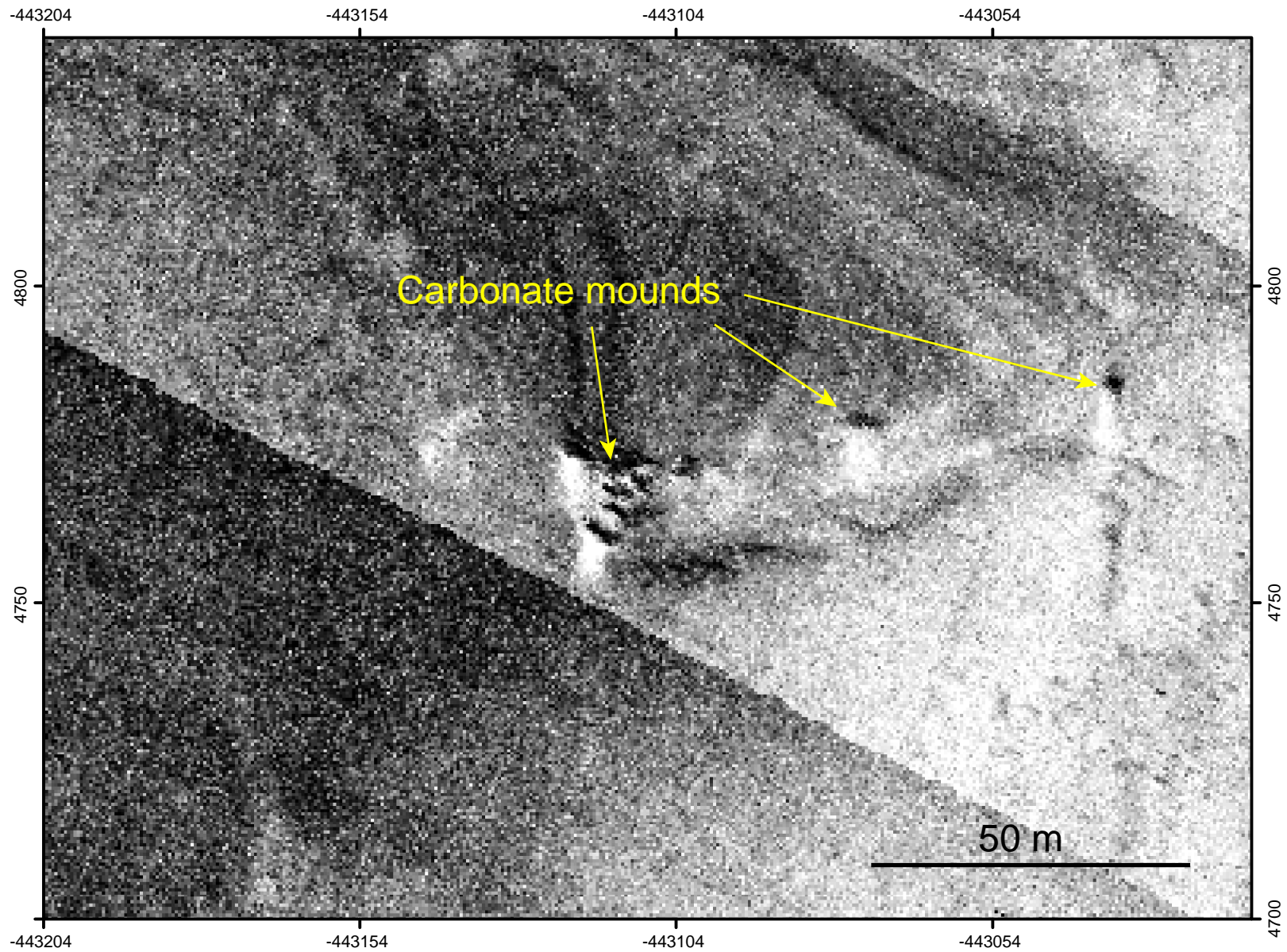


Figure 65. Sidescan sonar image of carbonate mounds between 130 and 140 m water depth on the upper Bulgarian slope. Interpretation is confirmed by ROV video data (Figure 68-69). For location see figure 15.

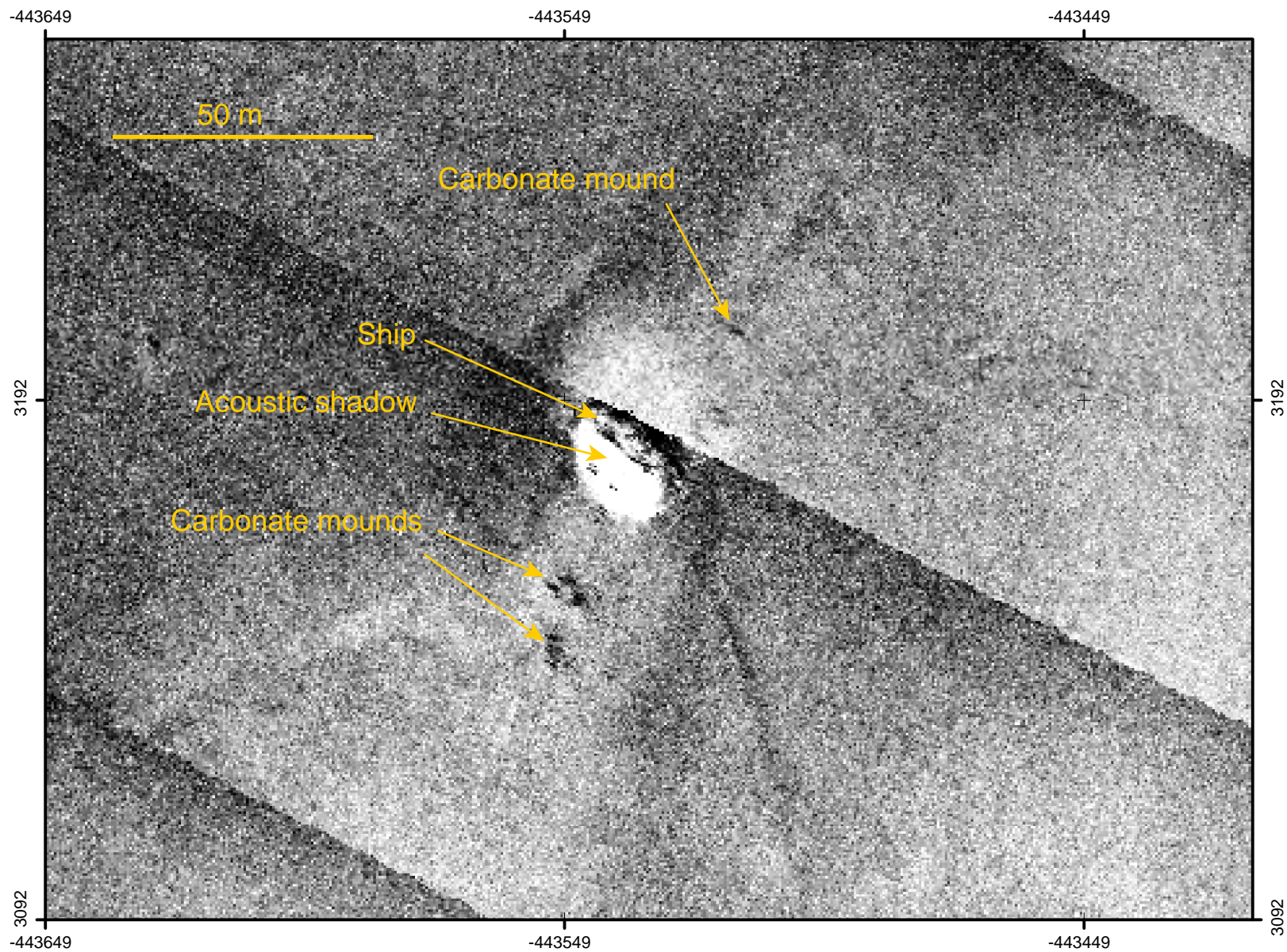


Figure 66. Sidescan sonar image of carbonate mounds and a shipwreck between 130 and 140 m water depth on the upper Bulgarian slope. Interpretation is confirmed by ROV video data (Figure 68-69). For location see figure 15.



Figure 67. Still images derived from ROV video data showing typical carbonate mounds related to fluid seepage on the upper Bulgarian slope. Discoloured, predominantly dark grey, seabed areas indicate areas of active seepage.

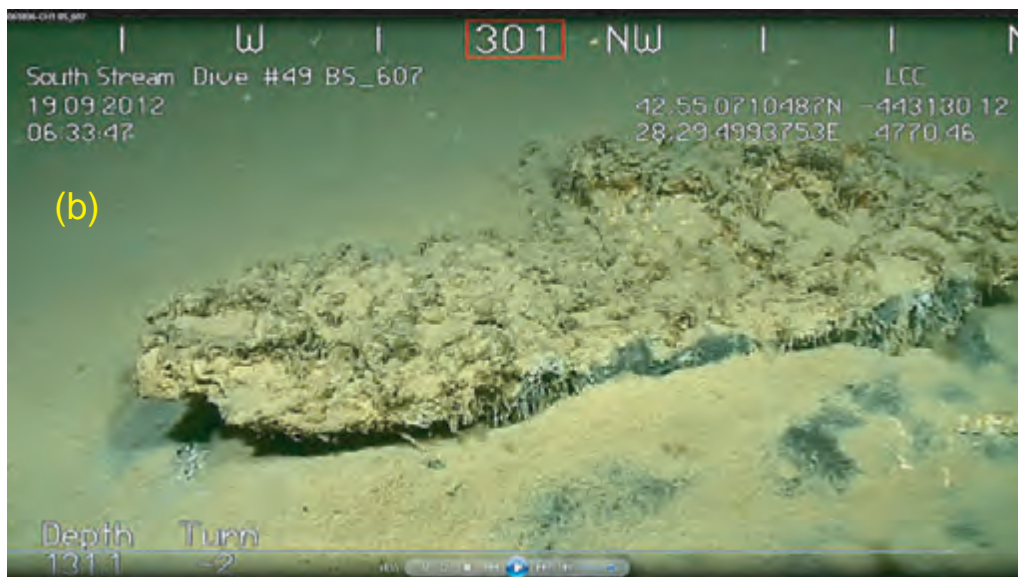


Figure 68. (a) and (b). Still images derived from ROV video data showing typical carbonate mounds related to fluid seepage on the upper Bulgarian slope. Discoloured, predominantly dark grey, seabed areas indicate areas of active seepage. (c) Possible carbonate block on the abyssal seafloor. Thick drape of flocs hinders interpretation of this feature.

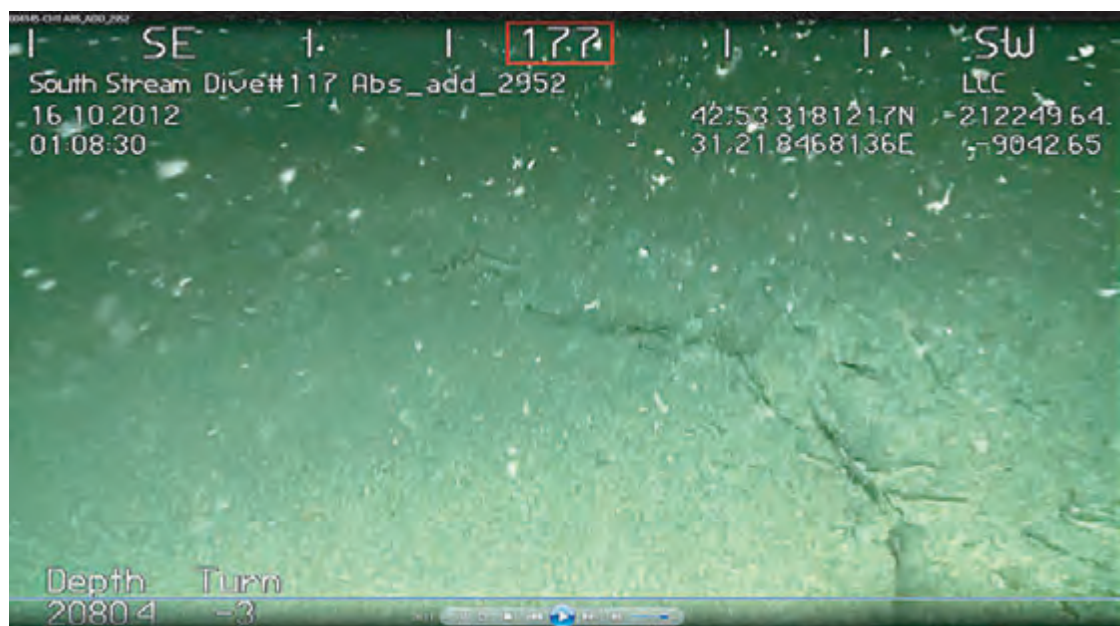


Figure 69. Still images derived from ROV video data showing shallow depressions, a few metres in diameter, surrounded by rims of apparently broken layered floc-rich sediment. These are interpreted as pockmarks. The absence of floc deposits in the depressions indicates that they may be active.



Figure 70. Still images derived from ROV video data showing shallow depressions, a few metres in diameter, surrounded by rims of apparently broken layered floc-rich sediment. These are interpreted as pockmarks. The absence of floc deposits in the depressions indicates that they may be active.



Figure 71. Still images derived from ROV video data showing patches of discoloured seafloor that indicate active seepage on the Bulgarian shelf. Some colours may be due to bacterial activity within the sediment.

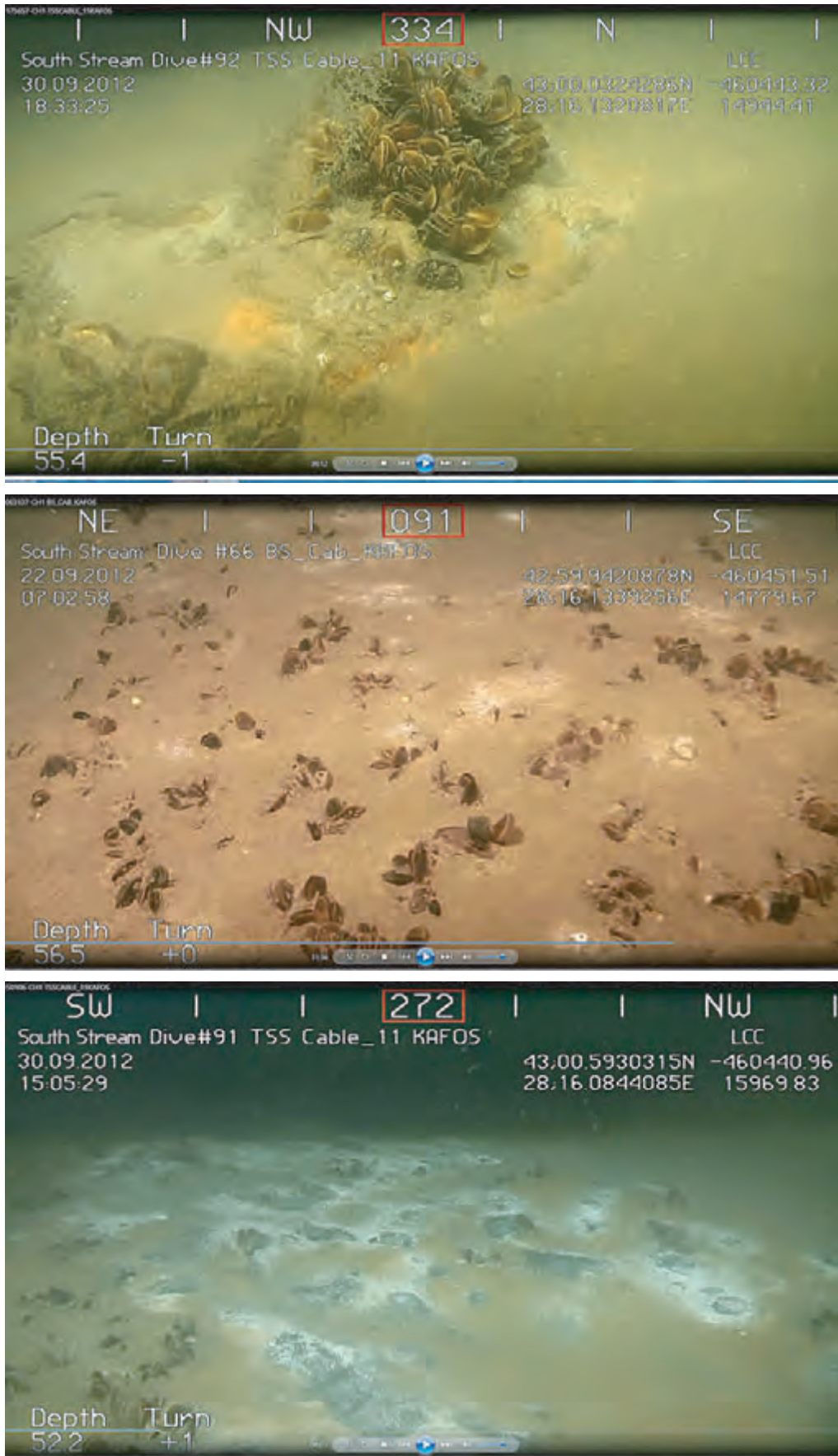


Figure 72. Still images derived from ROV video data showing patches of mussels on the Bulgarian shelf. Mussels occur adjacent to, but not within, areas of apparently active seepage, suggesting that they exploit hard substrates generated by seep-related carbonate cementation of the seafloor.



Figure 73. Still images derived from ROV video data. (a) a modern tool mark on the abyssal seabed. A gentle grooved slope indicates where a floating object impacted and slid along the seabed, pushing up an elevated sediment ridge ahead of it. (b) gentle seabed ridges on the lower Bulgarian slope. These could be partially buried sediment waves or tool marks.

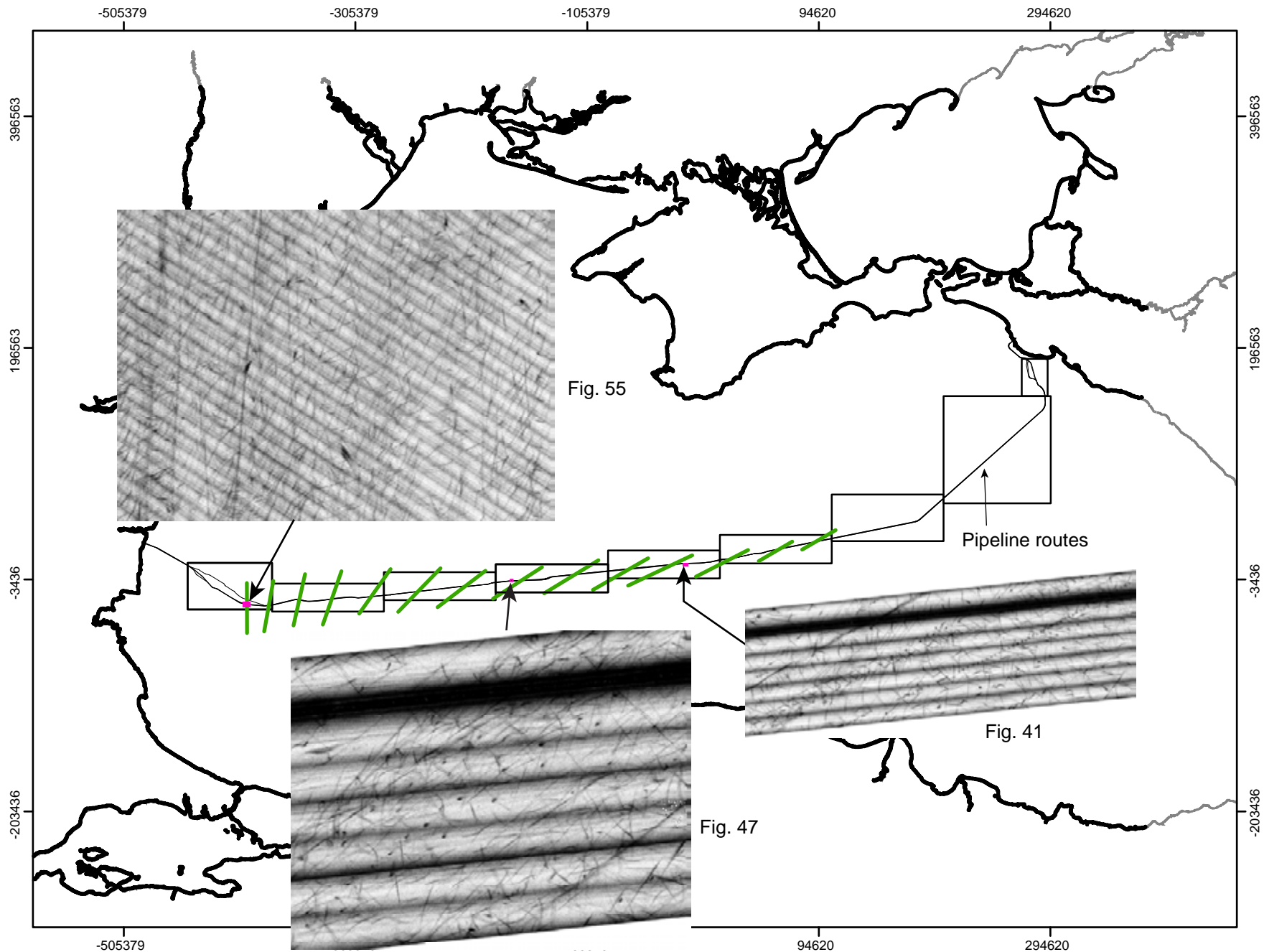


Figure 74. Summary of fine-scale lineation trends on the abyssal seafloor. Trends, shown schematically by green lines, define a fan-shaped pattern with the apex of the fan at the mouth of the Bosphorus. This indicates that these features are a consequence of bottom currents related to flow of dense Mediterranean water into the Black Sea and its subsequent sinking and dispersal across the abyssal basin. Inset sidescan sonar panels are examples of lineation patterns shown in more detail in other figures.



Figure 75. Still images derived from ROV video showing trees on the abyssal Black Sea seafloor.



Figure 76. Still images derived from ROV video showing trees on the abyssal Black Sea seafloor.



Figure 77. Still images derived from ROV video showing linear trails of pits and grooves cut into the soft seafloor flocculent layer by pieces of discarded plastic carried across the seafloor by bottom currents. This is a modern analogy for the much larger tool marks summarised in figure 75.



Figure 78. Still images derived from ROV video showing linear trails of furrows, pits and grooves cut into the modern soft seafloor floc layer by objects carried across the seafloor by bottom currents.



Figure 79. Still images derived from ROV video showing wooden shipwrecks on the seabed.



Figure 80. Still images derived from ROV video showing a wooden shipwreck, a small boat or lifeboat and some discarded rubbish on the seabed.



Figure 81. Still images derived from ROV video showing various pieces of discarded rubbish on the seafloor.



Figure 82. Still images derived from ROV video showing various pieces of discarded rubbish on the seafloor.



Figure 83. Still images derived from ROV video showing dark patches of flocculated organic detritus on the abyssal plain floor. White rims, probably consisting of coccoliths, are commonly seen around the dark patches.



Figure 84. Still images derived from ROV video showing dark patches of flocculated organic detritus on the abyssal plain floor. White rims, probably consisting of coccoliths, are commonly seen around the dark patches.



Figure 85. Still images derived from ROV video showing dark patches of flocculated organic detritus on the Bulgarian slope at 477 m water depth. The dark floc patches seen at deeper water locations are here overlain by more recent loose aggregations of olive brown flocs.



Figure 86. Still images derived from ROV video of a 'groove' cut through the surficial floc layers by a submarine telephone cable. This surficial material can be seen to have a jelly-like consistency when observed on the video. The floc layer appears to have a thickness of perhaps 20 cm at this location on the Bulgarian Abyssal Plain.

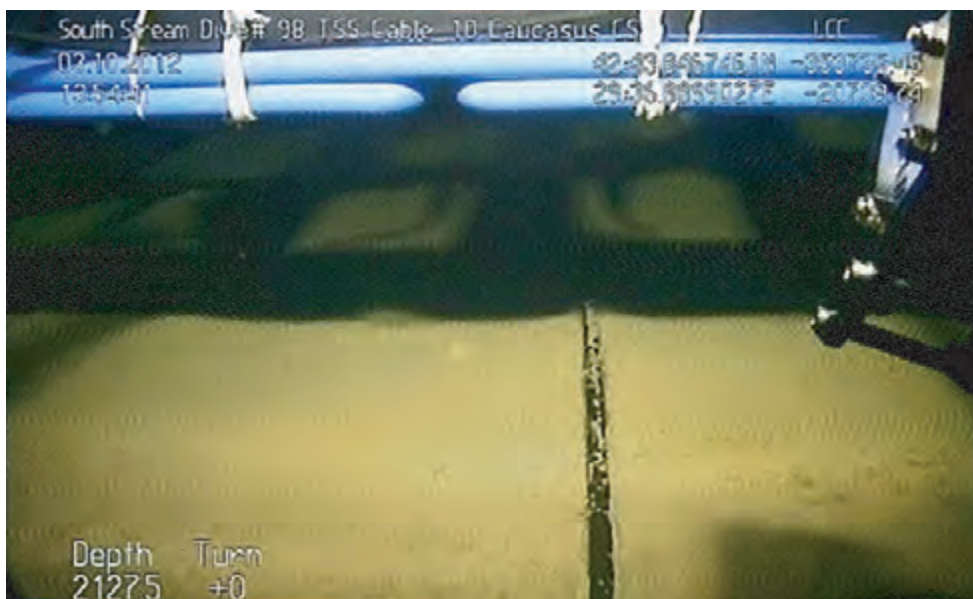


Figure 87. Still images derived from ROV video of a telephone cable exposed at the seabed.

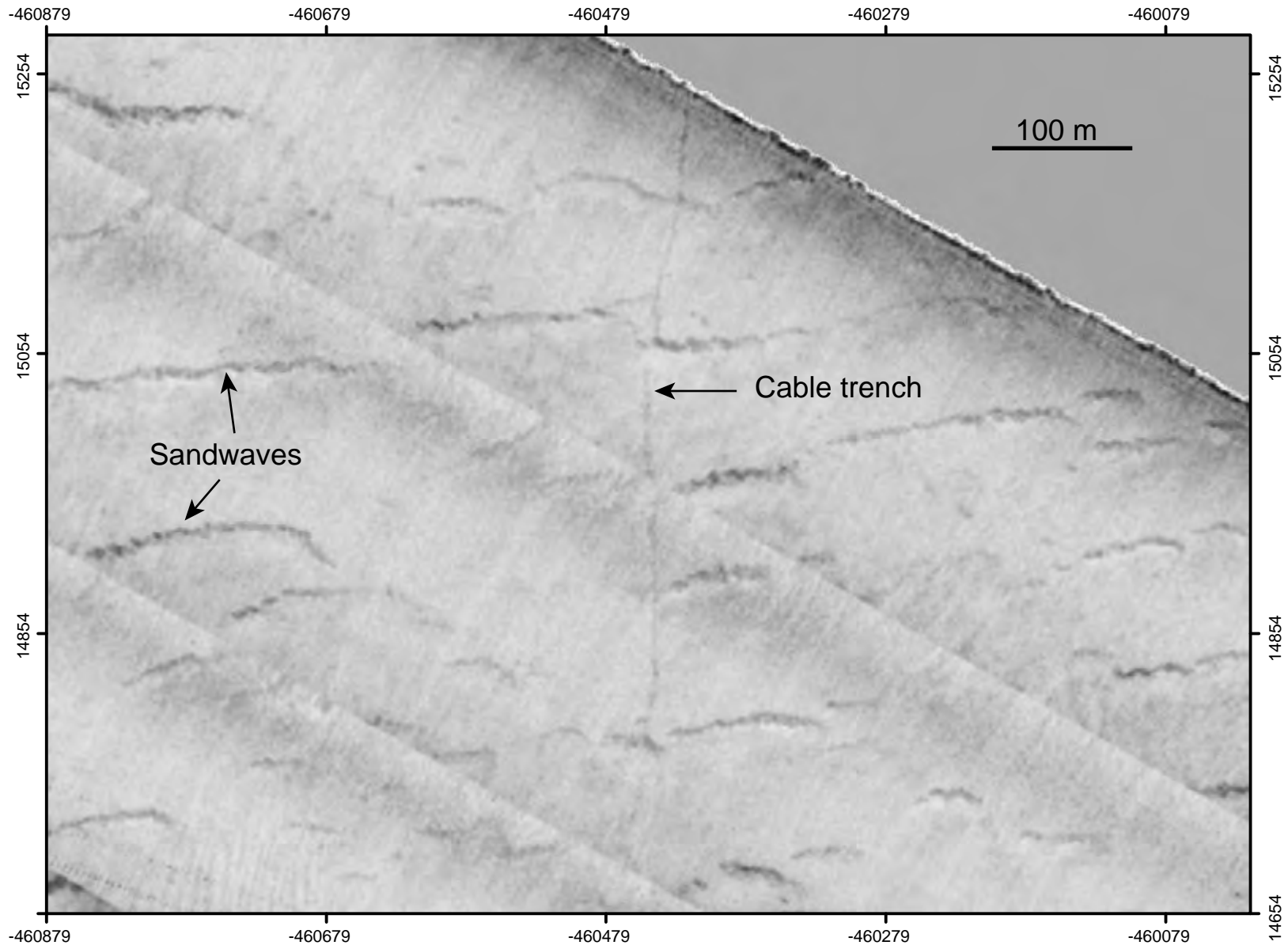


Figure 88. Sidescan sonar image of a submarine cable trench and sediment waves on the Bulgarian continental shelf.